Computer Vision for Additive Manufacturing.

Eiríksson, Eyþór Rúnar

Publication date:
2018

Document Version
Publisher's PDF, also known as Version of record

Computer Vision for Additive Manufacturing

Eyþór Rúnar Eiríksson

Kongens Lyngby 2017
PhD-2017-447

Technical University of Denmark
Department of Applied Mathematics and Computer Science
Richard Petersens Plads, building 324,
2800 Kongens Lyngby, Denmark
Phone +45 4525 3031
compute@compute.dtu.dk
www.compute.dtu.dk

PhD-2017-447
ISSN: 0909-3192

Summary (English)

Ever since the commercialization of additive manufacturing in the late 80's, it has been clear what enormous potential the technology could have, potentially disrupting several industries. However, we have yet to see the technology fully adopted by the manufacturing industry. One of the issues that has prevented widespread adoption of 3D printing for use within manufacturing is the apparent lack of quality control during and after the printing process.

This thesis demonstrates how computer vision may be applied in beneficial ways within additive manufacturing. The main contributions aim at solving part of the challenges required for the technology to reach its full envisioned potential, and to reach widerspread industry adoption as a de-facto manufacturing modality. Quality control has been a major milestone to overcome in this regard. As a result, a core part of the contributions revolves around this central topic.

The work is separated into three main categories: The first two concerning process and quality control of appearance and geometry. The third category concerns machine interaction paradigms within additive manufacturing. Here, challenges are addressed within the 3D ecosystem, aiming towards facilitating a fluid integration of additive manufacturing within the factory of tomorrow.

Summary (Danish)

Siden additiv fremstilling, eller 3D-print, blev kommercialiseret i slutningen af 80'erne, har det stået klart, at teknologien har et kæmpe potentiale, der med stor sandsynlighed vil disrupte adskillige industrier. Her ca. 30 år senere har vi stadig til gode, at se denne teknologi blive adapteret af fremstillingsindustrien. En af hovedårsagerne til dette manglende indpas, er tilsyneladende, en mangel på kvalitetskontrol under og efter denne additive fremstillingsproces.

Denne afhandling demonstrerer hvordan computer vision kan have en relevant anvendelse i forbindelse med additiv fremstilling. Specifik er der bidrag der imødekommer mange af de hindringer der er for at 3D print kan opnå sit fulde potentiale, herunder især kvalitetskontrol og -sikring.

Arbejdet der ligger til grund for denne afhandling falder primært i tre kategorier. De første to omhandler proces- og kvalitetskontrol af henholdsvis 3D geometri og udseende (farve). Den tredje kategori omhandler menneske-maskine interaktion i relation til adaptiv fremstilling, hvor der er fremsat metoder til at styrke en flydende integration af additiv fremstilling i morgendagens fabrik.

Preface

This thesis was prepared at the Department of Applied Mathematics and Computer Science at the Technical University of Denmark (DTU). It is done in fulfilment of the requirements for obtaining a doctor of philosophy degree (Ph.D.) in applied mathematics with an emphasis on computer vision.

This project is a cross-department collaboration effort between DTU Compute and DTU Mechanical Engineering, fully funded by the Technical University of Denmark and operated in collaboration with the Manufacturing Academy of Denmark (MADE).

The work performed in this thesis is a step towards solving a part of the challenges required for additive manufacturing to reach its full envisioned potential. The thesis consists of an introductory motivation, brief overview of the core technologies used and a summary of the relevant literature and prior art. Finalizing, by presenting a total of 11 publications that contribute to the field.

The project was supervised by Associate Professor Henrik Aanæs and co-supervised by Scientist David Bue Pedersen. The research has been conducted at DTU in the Section of Image Analysis and Computer Graphics and the Section of Manufacturing Engineering. External research was conducted at the Massachusetts Institute of Technology, under the supervision of Professor Pattie Maes in the Fluid Interfaces group at the MIT Media Lab.

Lyngby, 13-March-2017

Eyþór Rúnar Eiríksson

Acknowledgements

First of all I would like to thank my supervisors, Henrik Aanæs and David Bue Pedersen, for all the laughs, academic and non-academic guidance, and most importantly our friendship for the past three years. It has been an absolute pleasure working with the two of you. Furthermore, I would like to thank Prof. Hans Nørgaard Hansen and Provost Rasmus Larsen for assembling this cross-department team.

Thanks to all of the friendly individuals over at DTU Mechanics, especially Jannick Schultz for all the printing and Jakob Skov Nielsen for everything else. Thanks are also due to my collaborators in the Manufacturing Academy of Denmark (MADE) and the SPIR Work Package 9 team. Special thanks to the academy for honouring me with the first Alexander Foss Made Award.

Warmest thanks to Professor Pattie Maes at the MIT Media Lab, for the collaboration and welcoming me as one of your own in the Fluid Interfaces group. Special thanks to Valentin Heun for our past and future collaborations, as well as Jan Gugenheimer and the rest of the Fluid Interfaces group.

Thanks to all my friends, colleagues and collaborators in the Image Analysis and Computer Graphics group. In particular, my office mates J^3 = Jakob Wilm, Jannik Boll Nielsen and Jonathan Dyssel Stets. Many thanks to Jeppe Revall Frisvad for your insights and collaboration. Special thanks to Hildur Einarsdóttir and Guðmundur Einarsson for the proof-reading and feedback on the thesis.

I would like to thank my parents and family for the never ending love and support. *Takk fyrir allt mamma og pabbi.*

Last but not least, I would like to thank my fiancée Hildur Einarsdóttir and our son Arnar Eyþórsson, whom without, I would never have made this document. *Þið gerið mig að betri manni.*

List of Contributions

Included Thesis Contributions

The contributions included in this thesis are listed below in the order of appearance. For benefiting the reader they are segmented into the three fundamental categories relevant to this thesis: *Appearance and Color*, *Geometry* and *Human Machine Interaction*. The full text documents are found in Appendices A−K as indicated by the list. Contributions G and H are are not included in the public version of this thesis.

Appearance and Color

[A] Nielsen, J. B., **Eiríksson, E. R.**, Kristensen, R. L., Wilm, J., Frisvad, J. R., Conradsen, K., & Aanæs, H. (2015). *Quality Assurance Based on Descriptive and Parsimonious Appearance Models.* In MAM2015: Eurographics Workshop on Material Appearance Modeling: Issues and Acquisition. Eurographics. DOI: 10.2312/mam.20151199 [NEK+15]

[B] Pedersen, D. B., Hansen, H. N., & **Eiríksson, E. R.** (2015). *Spatial Accuracy of Embedded Surface Coloring in Color 3D Printing.* In Proceedings of Achieving Precision Tolerances in Additive Manufacturing: ASPE Spring Topical Meeting. (Vol. 60, pp. 147-150). ASPE – The American Society for Precision Engineering. [PHE15]

[C] **Eiríksson, E. R.**, Pedersen, D. B., & Aanæs, H. (2015). *Predicting Color Output of Additive Manufactured Parts.* In Proceedings of Achieving Precision Tolerances in Additive Manufacturing: ASPE Spring Topical Meeting. (Vol. 60, pp. 95-99). ASPE – The American Society for Precision Engineering. [EPA15]

[D] **Eiríksson, E. R.**, Luongo, A., Frisvad, J. R., Pedersen, D. B., & Aanæs, H. (2016). *Designing for Color in Additive Manufacturing.* In Proceedings of the ASPE/euspen 2016 Summer Topical Meeting on Dimensional Accuracy and Surface Finish in Additive Manufacturing. (pp. 98-102). ASPE – The American Society for Precision Engineering. [ELF+16]

Geometry

[E] Pedersen, D. B., **Eiríksson, E. R.**, Aanæs, H., & Hansen, H. N. (2016). *In-Situ Monitoring in Additive Manufacturing Using Contact Image Sensors.* In Proceedings of the ASPE/euspen 2016 Summer Topical Meeting on Dimensional Accuracy and Surface Finish in Additive Manufacturing. (pp. 114-118). ASPE – The American Society for Precision Engineering. [PEAH16]

[F] **Eiríksson, E. R.**, Wilm, J., Pedersen, D. B., & Aanæs, H. (2016). *Precision and Accuracy Parameters in Structured Light 3-D Scanning.* International Archives of the Photogrammetry, Remote Sensing and Spatial Information Sciences, Volume XL-5/W8, 7-15. DOI: 10.5194/isprs-archives-XL-5-W8-7-2016 [EWPA16]

[G] **Eiríksson, E. R.**, Pedersen, D. B., Hadar R., Hansen, H. N. & Aanæs, H. (2017). *Additive Manufacturing Apparatus.* Patent Pending.

[H] **Eiríksson, E. R.**, Pedersen, D. B., Hansen, H. N. & Aanæs, H. (2017). *Technical Note: Additive Manufacturing Apparatus.* Internal Technical Note.

Human Machine Interaction

[I] Dal Corso, A., Olsen, M. D., Steenstrup, K. H., Wilm, J., Jensen, S. H. N., Paulsen, R. R., **Eiríksson, E. R.**, Nielsen, J. B., Frisvad, J. R., Einarsson, G. & Kjer, H. M. (2015). *VirtualTable: a projection augmented reality*

game. In Proceedings of SIGGRAPH Asia 2015 Posters. [40] Association for Computing Machinery. DOI: 10.1145/2820926.2820950 [DOS+15]

[J] Gugenheimer, J., Wolf, D., **Eiríksson, E. R.**, Maes, P., & Rukzio, E. (2016). *GyroVR: Simulating Inertia in Virtual Reality using Head Worn Flywheels.* In Proceedings of the 29th Annual Symposium on User Interface Software and Technology (UIST '16). (pp. 227-232). Association for Computing Machinery. DOI: 10.1145/2984511.2984535 [GWE+16]

[K] **Eiríksson, E. R.**, Pedersen, D. B., & Aanæs, H. (2017). *Augmented Reality Interfaces for Additive Manufacturing.* In review at Scandinavian Conference on Image Analysis, SCIA 2017.

Other Contributions

Below are contributions that have *not been included* in the thesis, although they are considered relevant to the topic. The work is not included in the appendix and will only be cited, when mentioned.

Appearance and Color

- Stets, J. D. , Dal Corso, A., Nielsen, J. B., Lyngby, R. A., Jensen, S. H. N., Wilm, J., Doest, M. E. B., Gundlach, C., **Eiríksson, E. R.**, Conradsen, K., Dahl, A. B., Bærentzen, J. A., Frisvad, J. R. & Aanæs, H. (2017). *Digitizing Heterogeneous Scenes and Evaluating the Pipeline Using Photorealistic Rendering.* In review SIGGRAPH 2017. [SDO+17]

Geometry

- Messer, D. Wilm, J., **Eiríksson, E. R.**, Dahl, V. A. & Dahl, A. B. (2017). *Image-Based Alignment of 3D Scans.* In review at Scandinavian Conference on Image Analysis, SCIA 2017. [MWE+17]

- Pedersen, D. B., **Eiríksson, E. R.**, Hansen, H. N., & Nielsen, J. S. (2016). *A self-calibrating robot based upon a virtual machine model of parallel kinematics.* Virtual and Physical Prototyping (Online), 11(3), 227-234. DOI: 10.1080/17452759.2016.1208363 [PEHN16]

Human Machine Interaction

- Heun, V., **Eiríksson, E. R.**, & Maes, P. (2017). *HRQR: A Human and Machine Decodable Matrix Code.* Submitted to the 16th IEEE International Symposium on Mixed and Augmented Reality (ISMAR). [HEM17]

Acronyms

Here, an overview of the acronyms used throughout the thesis are given:

AM Additive Manufacturing

AMF Additive Manufacturing File Format

AR Augmented Reality

CAD Computer-Aided Design

CMM Coordinate Measuring Machine

CNC Computer Numerical Control

CT Computed Tomography

DLP Digital Light Processing

DMD Digital Micromirror Device

FDM Fused Deposition Modeling

ICC International Color Consortium

JND Just Noticable Difference

LED Light Emitting Diode

LUT Look-Up Table

MOEMS Micro-Opto-Electromechanical System

OBJ Wavefront Object file

QR Quick Response

RGB Red, Green, Blue

SL Structured Light

SLA Stereolithography Apparatus

STL Stereolithography

SLM Selective Laser Melting

SLR Single-Lens Reflex

SLS Selective Laser Sintering

UV Ultra Violet

VRML Virtual Reality Modeling Language

Contents

Summary (English) i

Summary (Danish) iii

Preface v

Acknowledgements vii

List of Contributions ix

Acronyms xiii

1 Introduction 1
- 1.1 Industrial Applications . . . 2
- 1.2 Challenges . . . 5
- 1.3 Scope . . . 6
- 1.4 Thesis Objectives . . . 7
- 1.5 Thesis Outline . . . 8

2 Background and Related Work 9
- 2.1 Additive Manufacturing . . . 10
  - 2.1.1 Stereolithography . . . 13
  - 2.1.2 Digital Light Processing SLA . . . 15
  - 2.1.3 Color 3D Printing . . . 16
- 2.2 Color and Appearance . . . 18
  - 2.2.1 Consumer Perception and Quality Control . . . 19
  - 2.2.2 Visual Perception . . . 20
  - 2.2.3 Additive and Subtractive Colors . . . 20
  - 2.2.4 Color Spaces . . . 21

2.2.5 Color Difference . . . 22
2.2.6 Color Calibration . . . 23
2.3 Acquisition of Geometry . . . 25
2.3.1 Structured Light 3D Scanning . . . 25
2.3.2 Coordinate Measurement Machine . . . 30
2.3.3 Computed Tomography . . . 30
2.4 AM System Monitoring . . . 31
2.4.1 In-Line Geometric Metrology of 3D Print . . . 31
2.4.2 Metrology of 3D Printed Color . . . 33
2.5 The Digital Ecosystem . . . 34
2.5.1 Augmented Reality . . . 34

3 Contributions **39**
3.1 Appearance and Color . . . 40
3.2 Geometry . . . 42
3.3 Human Machine Interaction . . . 45
3.4 Other Work . . . 47

4 Conclusion **49**

A Quality Assurance Based on Descriptive and Parsimonious Appearance Models **53**

B Spatial Accuracy of Embedded Surface Coloring in Color 3D Printing **59**

C Predicting Color Output of Additive Manufactured Parts **65**

D Designing for Color in Additive Manufacturing **71**

E In-Situ Monitoring in Additive Manufacturing Using Contact Image Sensors **77**

F Precision and Accuracy Parameters in Structured Light 3-D Scanning **83**

G Technical Note: Additive Manufacturing Apparatus **93**

H Additive Manufacturing Apparatus **109**

I VirtualTable: A Projection Augmented Reality Game **141**

J GyroVR: Simulating Inertia in Virtual Reality using Head Worn Flywheels **143**

K Augmented Reality Interfaces for Additive Manufacturing **151**

Bibliography 165

Chapter 1

Introduction

Ever since Additive Manufacturing (AM), or 3D printing, was first commercialized in the late 80's, it has been clear what enormous potential the technology could have, potentially disrupting several industries. With specific applications ranging from medical, aerospace and even personal factories in your home, one of the biggest impacts lies within industrial production. With AM, it has become possible to print geometries in a large range of materials with near complete geometric design freedom. Producing forms and shapes that would otherwise be impossible to manufacture with traditional processes such as milling, turning or injection moulding.

In the last decades, conventional production processes have been developed with speed and cost in mind. Many of these are focused towards mass manufacturing, and have limited flexibility when it comes to producing complex geometrical forms. As a result, our modern world has become square and somewhat dull, with diminishing cultural elements, demoted to shapes that are easy, quick and cheap to manufacture. With the design freedom offered by AM, it is possible to re-enter an era of design aesthetics, artistry, and craftsmanship, at a fraction of the previous cost.

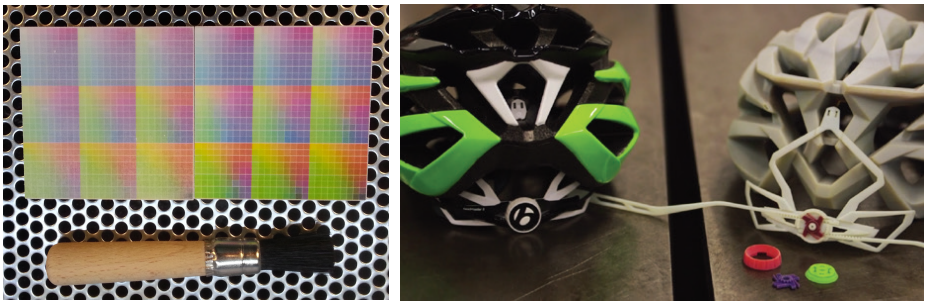

Figure 1.1: Examples of full-color concept and functional prototyping. (Left) 3D printed color plates for color calibration. From [Contribution C]. (Right) A bicycle helmet prototype (Trek) using multi-color and material technology [Str17b].

1.1 Industrial Applications

Several industrial applications are considered relevant to the content of this thesis, all of which are applicable today. Although not exhaustive, the following sections give a brief description on the major industrial applications, where AM has a substantial benefit. The four areas discussed are *Rapid prototyping*, *Mass customization*, *Soft tooling* and *Topology optimization*, the two first being the most commonly used [Woh16].

Rapid Prototyping

Traditionally, prototyping can both be a time consuming and costly process. This dictates the number of design iterations a product can go through until a business case is no longer viable. The fewer the design iterations, the higher the financial risk, particularly for high volume production with associated tooling costs. To overcome this, designers and engineers frequently use prototyping materials such as wood, paper, cardboard or even clay for visualizing the general feel and aesthetics of the product [Obe05]. However, these classical methods only mimic form, not function. Examples of rapid prototyping are shown in Figure 1.1.

The impact AM has had on rapid prototyping is substantial [HLMH13, CBG12], although much work remains in that regard. AM has made it possible to print physical prototypes, in form, color and function, in a relatively short amount of time and at a low cost [Woh16]. This allows for an increased number of


Figure 1.2: Examples of mass customization applications. (Left) 3D printed hearing aids [Wid17]. (Right) 3D printed orthodontics [Str17a].

shorter development iterations, where potential design risks have a higher potential of being minimized, before committing to machine tools for production. Ultimately, resulting in a better end product. As a result, utilization of AM in the design process significantly reduces time to market.

Mass Customization

Additive manufacturing makes it possible to print one-off custom made products with unique characteristics. This opens up possibilities for a concept known as mass customization, where each product is tailored uniquely to the end consumer while being produced at a competitive price. Some industries are obvious candidates for mass customization and a few have already adopted the technology. As an example closely linked to Danish industry, AM is already being used in final part production, as half of the worlds custom fitted hearing aids have been produced via AM [Woh16]. This has been an ongoing trend since the year 2000. As no two ear canals are the same, this makes for an ideal use case of AM. Other industries, such as the dental industry, are also adopting the technology, see Figure 1.2.

Additionally, *"Industry 4.0"*, or similar digitalization efforts within manufacturing, envision stock or inventory to be a thing of the past [KPH14, Ber12]. As AM converges towards a print-on-demand paradigm, there is potential for significantly reducing such internal investments. This would give companies the possibility of a strong global presence, as replacement parts for customers may be printed near the local markets or on-site in remote places. Additionally, businesses are given a competitive advantage as they can be more flexible in their manufacturing and quickly address changes in production or markets.

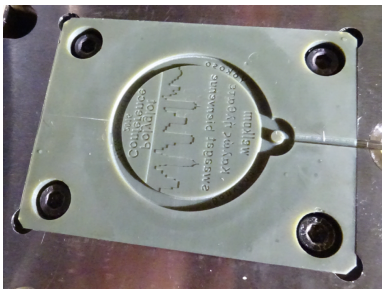

Figure 1.3: 3D printed polymer injection moulding inserts for small series production, developed at the Technical University of Denmark [MTN+17].

Soft Tooling

One of the biggest potentials for AM lies in the fact that unique parts can be printed without any tooling costs. This is a limitation in the injection moulding industry, where moulds have to be manufactured and machined for a production run. Such machined moulds are both very time consuming and costly to make. The latter is somewhat more acceptable, especially given a large volume production run, where the initial tooling cost is spread over millions of products [HH12]. However, as a result, conventional injection moulding is not suitable for low volume production or prototyping. With 3D printer technology, this becomes a thing of the past, as it is possible to print injection moulds or inserts, as shown in Figure 1.3. Significant work remains in maturing soft tooling AM processes [MTN+17]. However, if successful, the low cost of the printed tool would open up viable business cases for low volume manufacturing. Thus, leveraging all the benefits of injection moulding whilst reducing tooling cost and time to market.

Topology Optimization

Due to the geometrical freedom additive manufacturing enables, it is possible to manufacture features that are traditionally impossible to produce. If the design calls for a square hole or hollow interior cavities, AM will embrace them with ease. More importantly, the geometrical freedom allows for better topology optimized parts as shown in Figure 1.4, where object properties can be optimized i.e in a lighter form factor [BAH11, BS13]. As an example, this enables significant cost reduction within the aerospace industry [TM11], as lighter components save fuel, which directly affects environmental impact. Furthermore, complex

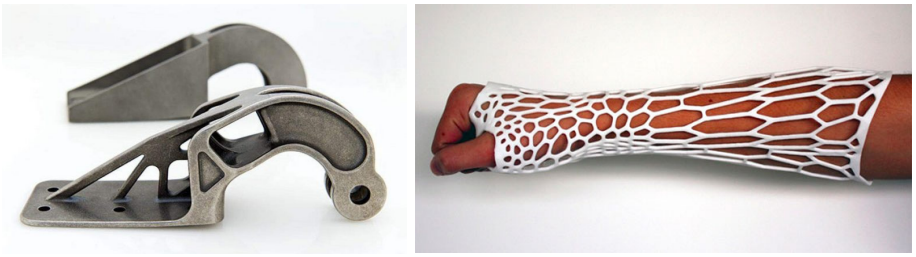

Figure 1.4: Examples of topology optimization. (Left) Optimized and printed hinge bracket from an Airbus A320 [Enl12]. (Right) A designers take on a printed and topology optimized cast for a broken arm [Evi13].

geometries can allow for efficient and optimized internal conformal cooling channels, enabling manufacturing of injection moulds where parts are quickly and uniformly cooled [RGG07]. This will improve part tolerances and reduce production time which may have a substantial financial impact.

1.2 Challenges

Despite all the benefits previously described, and given the fact that it has been 30 years since the first AM system was commercialized, we have yet to see it fully adopted by the manufacturing industry. Furthermore, we have yet to see the disruption that potentially could help us enter the next industrial revolution. Here, some major challenges AM has been facing, and currently is facing, will be discussed.

Initially the technology was quite expensive, and thus only available to larger corporations. Now, that key patents have recently expired, [GZR+15], we have new printer manufacturers entering the market with more competitive price points, making part of the technology now accessible to medium or small sized companies [Woh16].

A hindrance to widespread adoption of 3D printing for use within manufacturing is the apparent lack of quality control during and after the printing process [PDH13]. Applied industrial metrology, which serves an important role at the heart of any production, has not been easily transferable to the new manufacturing medium. As of now, 3D printing lacks the measurement principles and standards such that part quality control can be enforced. Given the complexity of these free-form artefacts, traceable measurements of geometric features are

challenging, and in many cases impossible with traditional metrology instruments such as a coordinate measurement machine [PDH13]. When dealing with internal structures, one must result to technologies such as metrological grade Computed Tomography (CT) scanners [KBC+11]. The technology is however, expensive, time-consuming and requires significant operator expertise. Additionally, with a manufacturing process where each produced part can be unique, every part needs to be measured in order to guarantee its part tolerances and specifications. No longer will it be feasible to measure only a subset of the manufactured parts in order to make statistical assumptions about the rest, as no two parts are the same. These challenges call for new methods and measurement practices tailored toward AM that are inspired by tried and true methods from applied metrology and computer science.

As mentioned before, despite having existed for over 30 years, AM is still in its early stages. In order for it to reach its full envisioned potential, more work remains ahead. There exist many individual focused efforts improving subproblems in the AM pipeline. However, given the broad range of technologies and processes available, the problems must be approached from an interdisciplinary systems perspective. Such oversight is only present at the printer manufacturers themselves, however the proprietary nature of the industry has inhibited progress.

1.3 Scope

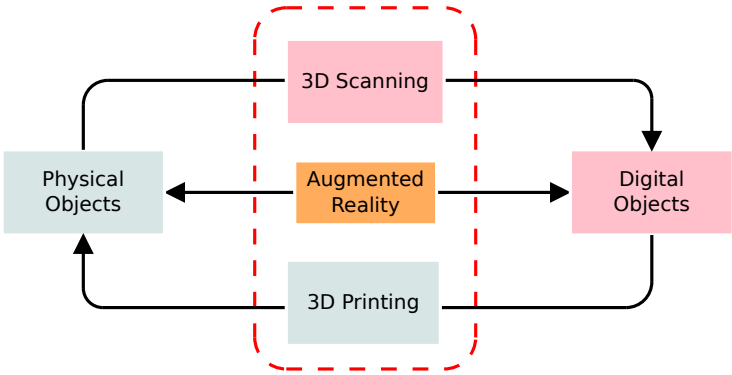

Figure 1.5: Illustration of the thesis scope. Focus is placed on applying computer vision within 3D printing, however the boundary between physical and digital objects is also explored in that context.

The work performed in this thesis is a step towards solving a part of the challenges required for additive manufacturing to reach its full envisioned potential. Quality control is a major milestone to overcome in this regard. As a result, a core part of the contributions revolves around this central topic. However, there are several aspects that influence the successful adoption of AM in the industry. One in particular, is related to its integration within digital manufacturing or industry 4.0.

With rapidly increasing amounts of complex data produced by modern machine tools, it is important that advanced manufacturing processes and process chains can be interacted with, in a simple and intuitive manner. More importantly, the scalability and flexibility of such interactions are crucial in order to rapidly adapt to changes in production and bring products to market faster.

Therefore a part of the thesis contribution takes a step back and addresses challenges within the 3D ecosystem as a whole. An interdisciplinary exploration is performed on the potential for old and upcoming technologies and how they might play a role in the factory of tomorrow, where the boundary between digital and physical becomes more intimate. An illustration highlighting the focus area of the thesis can be seen in Figure 1.5.

1.4 Thesis Objectives

The thesis has three main focus areas: The first two concern appearance and geometry of process and quality control in AM. The third category, concerns machine interaction paradigms within AM. In all three categories, the common goal is to demonstrate how modern computer science can be applied in beneficial ways within industrial manufacturing. The specific objectives for each category are as follows:

Appearance and Color The objective is to address the lack of color quality control in the domain of AM systems that produce parts in full color and to explore their limitations and ask; Is the printed color correct and in its intended spatial position? and; How can we specify colors as we can with geometry?

Geometry The objective is to take known methods for low cost geometry acquisition and to evaluate their performance and develop new in-line sensor solutions for internal and external part geometry.

Human Machine Interaction The objective is to explore future interaction mechanism for industrial machine tools in order to facilitate fluid integration of AM within digital manufacturing.

1.5 Thesis Outline

The thesis is divided as follows:

Chapter 2 begins by describing the background and related work of the central technologies used throughout the thesis work. A brief review on additive manufacturing technologies is presented, with a more detailed description of the relevant print processes. The fundamentals of color science and acquisition of geometry are presented, followed by a state of the art review of the two in the context of additive manufacturing. Finally a short description on augmented reality, with focus on industrial use, is given.

Chapter 3 describes the contributions performed throughout the thesis work and the motivation behind them. Additionally, discussing the overall contribution to the relevant areas.

In **Chapter 4** a conclusion is given, where the contributions are discussed as a whole in the context of the thesis objectives.

Finally the paper contributions are presented in the appendix of the thesis.

Note: [Contributions G and H] are confidential, and therefore not included in the public version of this thesis.

Chapter 2

Background and Related Work

The aim of this chapter is to give the reader an overview of the central technologies used in this thesis. Due to the multi-disciplinary nature of the work, and therefore the resulting broad scope, only a high level literature overview will be given, followed by a detailed description where relevant. For more in depth information not explicitly provided, the reader will be referred to the relevant literature.

The central focus of this thesis deals with the rapidly growing field of AM. In order to fully convey the pace at which the field is growing, the reader is referred to Figure 2.1, which illustrates the number of scientific publications per year in the field of AM and 3D printing in general. During the 3 years lifetime of the Ph.D project, slightly less than a third of all publications in the field since 1970 were published. Therefore, when presented with the related art, the reader should keep in mind that a large portion of the presented literature took place in parallel to the work conducted in this project. From an academic perspective, this has been quite exhilarating. In the next section, an overview of AM process technologies is presented.

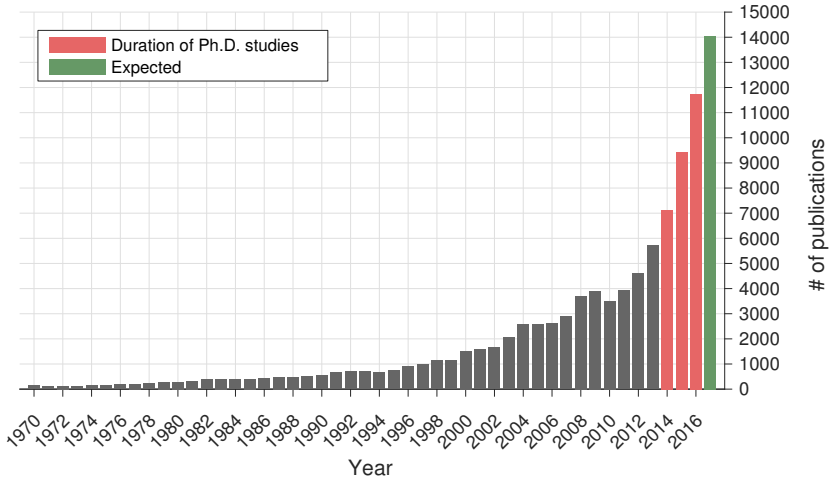

Figure 2.1: Number of 'Web of Science' registered scientific publications on a yearly basis, including *"Additive Manufacturing"* or *"3D Printing"* as a topic or title. A third of all publications in the field has been published during the last 3 years.[1]

2.1 Additive Manufacturing

Additive manufacturing, or 3D printing as referred to by popular media, has been a topic of research for at least 50 years [Woh16]. The technology left the laboratory in the late 1980s, when the first commercial system entered the market [Woh16]. Since then, many different modalities of 3D printers have emerged, having different forms and functions [WG16]. Here, a brief overview of the technology will be given to provide the relevant background and terminology. For further insights into the AM industry, the reader is referred to [WG16, Woh16, PDH13].

The principle of AM differs fundamentally from traditional subtractive manufacturing methods such as milling and turning. There, objects are transformed into its final shape by subtracting or sculpting material away from a block of raw material. With AM, parts are built from the ground up, in an incremental and additive fashion, such that a minimal amount of material is wasted. A typical AM pipeline can be broken down into three steps; *Job Generation*, *Printing* and *Post-Processing*. The following sections give a brief overview of these steps.

[1] Data obtained from the Web of Science [oS].

Print Job Generation

The *Job Generation* process starts with a 3D Computer-Aided Design (CAD) model that is intended to be manufactured. Traditionally, an algorithm takes the geometry and segments the object into a series of cross-sectional slices or layers, with each layer thickness ranging anywhere from microns to millimeters [Woh16]. Thereafter, a planning algorithm analyzes each cross-section and computes the machine instructions required to produce the layer. As the geometry is discretized into slices of finite thickness, a visually unpleasing artifact known as the *staircase artifact* is introduced [HXF14]. The thinner the slices, the less prominent the effect is.

The Printing Process

The *Printing Process* varies between the different print process categories. However, the fundamental principle remains the same. Each cross-sectional slice of the geometry is produced layer by layer until the full part is formed. Wohlers report, on the state of the industry, gives an excellent overview of the different processes and materials [Woh16]. The standardized process categories according to the ISO/ASTM 52900:2015 standard [ISO15] can be seen in Table 2.1. A more complete description on the processes relevant to this thesis is provided in Section 2.1.1. For the remaining process categories the reader is referred to [Woh16, PDH13].

Post-Processing

Post-Processing is often an overlooked part of the AM pipeline in literature [Woh16]. Depending on the printer technology in question and the intended application, post-processing can consist of one or more of the following activities; Support structure removal, machining, sanding, polishing, infiltration, ultrasonic cleaning, chemical cleaning, heat treatment and post curing [Woh16]. The post-processing step can have a substantial effect on the outcome of the final product in terms of geometry and color [SLM+08], and should thus be considered as an equally important part of the AM pipeline. Additionally, as the printer technology becomes faster, this time consuming step of the print pipeline becomes a main bottleneck.

Table 2.1: AM process categories according to the ISO/ASTM 52900 [ISO15].

Material Extrusion	Build material extruded through a heated nozzle or syringe. Popular option in desktop machines for hobbyist and research labs. *Notable systems: Ultimaker 3, RepRap Prusa i3, Makerbot Replicator+, Stratasys FDM series.*
Material Jetting	Deposition of build material droplets using an inkjet print head. Traditionally Ultra Violet (UV) curable liquid photopolymer, supporting full color prints or wax for investment casting. *Notable systems: Stratasys PolyJet series, Solidscape Pro, 3D Systems ProJet 5500X*
Binder Jetting	Deposition of liquid bonding droplets onto a powder bed using an inkjet print head. Full color prints can be obtained using a CMYK inkjet print head. *Notable systems: ZCorp's Zprinter series (3D systems), 3D Systems ProJet 4500, Voxeljet VX series.*
Sheet Lamination	Lamination of cut adhesive sheet material. Materials range from wood laminate or paper to thin metal foils. Full color capability for paper based printers. *Notable systems: Mcor Iris HD, Fabrisonic UAM.*
Vat Photopolymerization	Selective curing of liquid photopolymer using light activated polymerization. See Section 2.1.1 for more information. *Notable systems: Formlabs Form 2, Envisiontec 3SP or Perfactory series, Prodways ProMaker series, 3D Systems ProX 950, Carbon3D M1.*
Powder Bed Fusion	Selective thermal fusion of powder material using laser or electron beam. Includes technologies such as Selective Laser Sintering (SLS) and Selective Laser Melting (SLM), using polymer and metal powder respectively. *Notable systems: EOS M Series, 3D Systems sPro or DMP series, Blueprinter.*
Directed Energy Deposition	Powder or wire material is blown or extruded from a nozzle and simultaneously melted using focused thermal energy such as a laser or electron beam. Traditionally using metal powder. *Notable systems: Optomec LENS, BeAM Easy-CLAD.*

Although AM is associated with rapid prototyping, it is by no means an instantaneous process. Depending on the system at hand, the print process can take up to few hours. In order to achieve results comparable to injection moulding, the process can take several hours or even days. Therefore, a key research goal is to decrease this process time. As previously described, only recently has there been a dramatic increase in AM development. With the expiration of key patents [Dec97, SVM+97, Hul96, RAB+99], new AM machine manufacturers have entered the market, which has positively impacted the industry as a whole [Woh16]. Low cost systems are entering the market, making the technology accessible to hobbyist, research labs and small start-ups.

The fundamental research efforts that have to take place in order for AM to reach widespread adoption have been pointed out by researchers. Huang et al. [HLMD15], specifically mentioned six key areas. A short summary of these areas are as follows:

- Materials: The development of process materials with known and specified properties.
- Design: Focus on design tools throughout the pipeline.
- Modeling: Development of physically based mathematical process models.
- Sensing and Control: Development of sensors for quality and process control.
- Process Innovation: Development of faster and improved AM processes.
- Systems Integration: Development of AM integration from a systems perspective and its place in the cyber-physical factory.

It is clear that current and future research within AM spans several technical fields, including and not limited to, material science, mechanical and electrical engineering, metrology, computer science and design. The following section will give an overview of the key AM process technologies that are relevant to the scope of this thesis.

2.1.1 Stereolithography

A Stereolithography Apparatus (SLA) categorizes as a *vat photopolymerization* process and is one of the earliest form of an additive system [WG16]. Despite being the first patented and commercialized technology, due to advances in material selection, it is still one of the most widely used process to this day. In fact,

in 2015, photopolymers had an estimated 45.5% market share of AM materials sold [Woh16]. It should however be noted that the material consumption is shared with derived processes such as *Material Jetting*.

Traditionally, in a SLA system, a UV laser light source, controlled by an x-y scanning galvanometer mirror system, is projected towards a vat containing liquid photopolymer or resin. The galvanometer system scans the top surface of the liquid resin and selectively cures (solidifies) cross-sectional slices of a 3D CAD geometry. This was the operating principle of the apparatus described in the original patent by Charles W Hull in 1986 [Hul86] and first commercialized by 3D Systems Inc. in 1987 under the name *SLA-1* [WG16]. A schematic of the principle can be found in Figure 2.2.

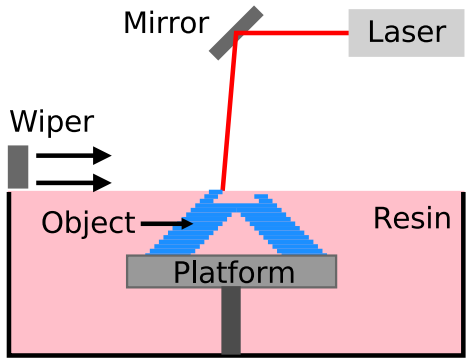

Figure 2.2: A Stereolithography apparatus.

In SLA, each layer is built by the following procedure in order to create a physical object:

1. One layer, representing a cross-sectional slice of the 3D geometry is scanned over the liquid photopolymer resin, using a UV laser source. Thus, solidifying the layer.
2. The printed object is submerged into the liquid by one layer-height, using a motorized elevation stage.
3. The surface of the photopolymer liquid is traversed with a scraper or wiper mechanism in order to distribute and recoat resin over the previous layer. Additionally, this levels the resin surface and minimizes surface tension effects that occur between the liquid resin and the cured layer.
4. The process repeats itself until all layers have been built.

Employing this conventional method yields manufacturing rates that can be measured in micrometers per minute. This is due to the time consuming laser scanning process which is dependent on the surface area of the layer being produced. Additionally, a significant, yet constant time is spent on the re-coating process that occurs in between each layer. Both of these effects depend on the number of layers that are to be produced, and are governed by the layer thickness parameter. Thus, there exists a trade-off between speed and surface finish, as increased layer thickness makes the staircase artifact more prominent. By utilizing a varying and geometry dependent layer thickness throughout the print job, it is possible to reduce print time slightly without compromising surface finish [PZNH16]. Newer SLA systems have emerged that use a 2D UV projection source for curing. This will be described in further detail in the Section 2.1.2.

Two topology variations of the SLA system are available, the first one being the previously described version where the curing light source is projected downward onto a vat of liquid photopolymer. This is known as a *top-down* configuration. Its counterpart is called a *bottom-up* configuration, where the bottom of the vat has a transparent window, through which the curing takes place. In this case the build platform is elevated upward during print, resulting in the object being pulled up out of the liquid resin. In contrast to the top-down approach, where the build platform is submerged into the liquid. As the bottom-up configuration cures through a flat transparent window, the solidified layer will be flat as well. However, the cured layer can stick to the window and as a result, mechanical peeling or de-lamination is required. Due to this, no significant improvement in speed is obtained. To solve this, new processes have recently emerged that use a transparent oxygen permeable window. This special window allows for pressurized oxygen to pass through it, creating a few micrometer dead-zone that inhibits the photopolymer reaction, eliminating the need for mechanical peeling [Car].

2.1.2 Digital Light Processing SLA

Although the galvanometer laser system can support a larger build area without significantly compromising print resolution in the build plane [PDH13], other alternatives have emerged. The technology is know as Digital Light Processing (DLP) SLA, or mask projection, where instead of a single laser spot, a 2D UV mask is projected onto the liquid resin surface. This means that an entire layer is exposed and as such all layers take an equal amount of time to be cured. In comparison to laser scanning systems, this is considerably more time efficient when producing large components.

The projection technology is based on a Micro-Opto-Electromechanical System

(MOEMS) known as a Digital Micromirror Device (DMD). The technology is pioneered by Texas Instruments under the trademarked name DLP and patented in 1991 [Hor91]. The system can contain millions of tiny mirrors that are only a few micrometers in size. Each mirror or 'pixel' can be individually controlled such that two pixel orientations are obtained. A typical DLP projector consist of an illumination source, such as a Light Emitting Diode (LED) or a lamp, and a light engine that guides collimated light towards the DMD. Depending on the orientation of each micromirror, light is either reflected out through the optical path of the projection system or reflected into a heat sink or 'light dump'. Light absorbed in the heat sink has the effect of producing a black pixel, allowing for a high contrast ratio as no light leaves the optical system.

In a mask projection 3D printer, a UV DLP projector is used for generating a 2D curing mask, simultaneously exposing the layer in a discrete fashion using pixels. This places constraints on the printers feature resolution which is dictated by the size of the projected build area and the pixel resolution of the DMD. Nonetheless, a significant improvement in print speed is obtained using a projector instead of a laser point source [Woh16]. Additionally, a projector is less complex and comes at a lower cost than a laser system [PDH13].

2.1.3 Color 3D Printing

A majority of AM systems available on the market utilize single color materials. Only a few AM systems capable of printing in a multitude of colors are commercially available on the market [Woh16]. The definition here of multi-color, or full-color, is when the system is capable of blending a set of primary colors into any combination thereof, ultimately supporting tens of thousands of color combinations. The printers that fall into this category are expensive systems intended for the industrial market. Several of the process categories are capable of supporting multi-color prints, the most prominent being binder jetting, sheet lamination and material jetting.

The combination of colors is obtained in the same manner as in the paper printing industry, by use of subtractive colors. A printer will typically consist of four different colors of material: cyan, magenta, yellow and black, respectively, commonly known as the *CMYK* color representation. The dynamic range of such a print process is governed by the whiteness of the base medium in the absence of the dye and how effectively the blended dye absorbs light. Additive and subtractive colors will be described further in Section 2.2.3, whereas here a brief description on the different AM color processes will be given.

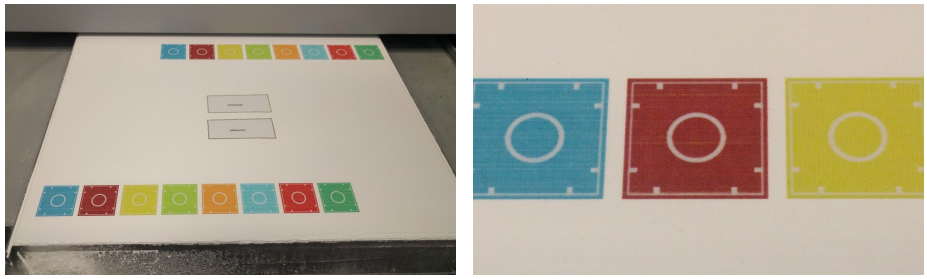

Figure 2.3: Example of a binder jetting system during print. (Left) Colored binder is printed on top of a powder reservoir using an inkjet like printhead. (Right) Close-up of the printed layer.

In binder jetting, as seen in Figure 2.3, a multi color binder is ejected from inkjet-like printheads onto thin layers of white powder material. In fact, the process is quite similar in consumer paper printers. However, instead of the paper feed, a new layer of powder is coated on top of the previous one and the process is repeated until the full object is formed. The process uses CMYK colors with the addition of a clear binder, in order to produce the color white, as it binds the white powder. After the print job, the binder is allowed to dry and the object may then be removed from the print bed. Next, it is brushed clean of any residual powder in a dedicated post processing station, and in some cases lightly sanded to even out any blemishes in the print. After the cleaning process, the colors may appear dull, and the printed part is also quite delicate. Therefore, as a final process, the part is commonly infiltrated with cyanoacrylate, epoxy based hardeners or wax coated. This enhances the colors in the print, as well as provides it with mechanical rigidity and stability. The binder jetting process is mostly intended for concept modelling and not for functional prototypes. This modality is the core focus of [Contribution B, C, D and E].

As an example of the other methods, sheet lamination allows for full color prints and is commonly used for concept modelling. The process is similar to binder jetting, where instead of powder build material, white sheets of papers are used as layers. The paper is then printed on using CMYK inkjet print heads and the contour of the part cut i.e with a cutting tool. In material jetting, liquid photopolymer resin droplets are ejected, in a similar fashion to the inkjet technology. After the photopolymer resin has been printed, a UV curing light source traverses over the printed layer which causes layer solidification. The recent Stratasys J750 [Str16], using the PolyJet technology, is an example of a material jetting system. The printer supports 6 photopolymer materials, and with a combination of CMYK and clear resin, it is possible to reach a combination of 360.000 unique colors, in high detail with varying translucency.

Unlike previous methods, who focused on concept modelling, this technology is claimed to be suitable for functional prototypes as well [Str16]. Furthermore, by supporting semi-translucency of individual printed voxels, complex sub-surface scattering artifacts can be taken advantage of for realistic appearance modelling [BAU15].

Color File Formats

In order to produce the desired product from a computer model, a file format is needed that is supported by the printer manufacturer. The most commonly used AM file format for representing three dimensional geometries is the Stereolithography (STL) format, created by 3D Systems [R+88]. The format was created prior to 3D color printing, and as a result does not support color. Fortunately, many other 3D formats do support color, such as the Virtual Reality Modeling Language (VRML) [CB97] and the Wavefront Object file (OBJ) [MVR05] to name a few. In these formats, color is represented as a Red, Green, Blue (RGB) triplet, as the intended medium for these formats is RGB based devices, such as a computer monitor. The RGB color space spans a region extending the printable range. This is a known problem in the paper printing industry, whose solution was to define a CMYK based file format. Since 3D printers also use CMYK subtractive colors, the RGB file formats are less than ideal, as the conversion from RGB to CMYK is non-trivial [Har01]. As of today, there exist no CMYK formats that are supported by the AM industry. The new ISO/ASTM Additive Manufacturing File Format (AMF) [ISO16] shows potential, being the developing successor of the STL format. The format has however not reached widespread adoption within 3D CAD software or commercial AM hardware. Color management is thus a topic that has not had adequate focus from industry or academia. This serves as a foundation for the work in [Contribution B, C, D and E].

2.2 Color and Appearance

As full-color printing is introduced to manufacturing, the complexity of performing quality assurance and control increases, adding to the dimensionality, as both form and appearance tolerances are introduced. If the technology continues to develop towards a print-to-consumer paradigm, it is crucial that appearance gets an equal amount of attention as form in the AM community. Here, we will discuss quality control of appearance and color from an optical perspective and give a fundamental overview on the science of colorimetry.

2.2.1 Consumer Perception and Quality Control

It has long been known, that the perceived quality of products is heavily dependent on its color and appearance [LH10]. This holds especially true for products such as fruits and vegetables, and other food products in general [Fra95], whose business model depends heavily on these factors. Although these are prime examples, this is also applicable to consumer goods. Quality perception transcends appearance, as humans additionally rely on other senses for quality determination. Textural feel, weight and smell of an object also influences perceived quality [LH10].

Perceived appearance of objects is due to complex interactions of light and the observed material, where a light source of certain spectral characteristics illuminates the object of interest. The light will either be specularly reflected, absorbed, or scattered within the material until it exits the material or is absorbed [NAFC16]. This takes place in a spectral fashion, as these interactions are dependent on wavelength. The geometry of the material also plays a significant role in the appearance, as well as the observers relative position to the illumination source and the material.

In many cases, industrial color quality control consists of a human observer that is trained in comparing the color of a produced sample to nominal. This is a less than ideal solution, as different operators have different interpretations of what determines as within specifications. Additionally, the boolean aspect of the part being either 'good' or 'bad' yields no information on the degree or magnitude of the failure. Such information would be beneficial to obtain, as it might indicate valuable information about the manufacturing process. In particular, this could be useful for monitoring a continuous change or drift in the process parameters, allowing for earlier intervention of change in product properties. Vision systems are to some extent used to solve the problems mentioned above, particularly within the food industry [TDJ+15]. For some applications, it might even be necessary to measure the full spectral reflectance characteristics of a material. This is however a time consuming and complex process, although recent work in both modelling and the rapid acquisition of appearance have emerged [NAFC16, AWL15, RWS+11].

In order to measure color, and say anything quantitative. it is important to have the intended observer defined. With humans, we have somewhat more relaxing tolerances than what is measurable with a vision system. It can easily be argued that it is not necessary to hold stricter tolerances on color than what is observable by humans. Modelling the human observer has been an active topic of research within the field of color science and metrology, where the goal is to establish a quantitative scientific description of color [Har01]. The following

sections highlight the most important topics in this regard.

2.2.2 Visual Perception

Visible light, or light, is an electromagnetic radiation that has wavelengths in the visible spectrum ranging from 400–700 nanometres (nm). Humans are able to distinguish between different wavelengths of light, which the brain conveniently interprets as color. As electromagnetic radiation does not have any specific color associated to it, the color interpretation of its wavelength is thus only a figment of human imagination. The human visual system does not sample wavelengths of light over a continuous region in the visible spectrum. In fact, there are only three general types of cones in the retina which have a sampling distribution around three base wavelengths, referred to as L-, M- and S- cone cells [L+77]. The naming convention relates to long, medium and short wavelengths of the visible spectrum, respectively [L+77]. The brain interprets color from the magnitude or radiant energy from these three wavelength distributions. The colors red, green and blue provide good stimulus to these cones, and depending on their intensities, are interpreted as a wide range of colors in the visible spectrum. As an example, humans are not able to distinguish the difference between yellow light at 580 nm and the equivalent combination of red and green light. This has proven quite useful since any digital display only needs 3 LEDs, red, green, and blue, of controllable intensities to fool the brain into perceiving a wide range of colors. This *visual trivariance* is the basis for human perception of color, and as a result, the basis for colorimetry [Har01].

2.2.3 Additive and Subtractive Colors

Additive colors are obtained when light from two or more wavelengths are added together [Hun67] As stated before, most commonly the primary colors red, green and blue are used in various intensities to create a wide range of colors. When the three primary colors are added, it is perceived by humans as white. As mentioned before, this technique is commonly used in RGB based devices such as televisions, computer monitors and projectors.

The inverse of additive colors is called subtractive colors, which is the process of mixing materials together, such as dyes, ink or paint [Hun67]. The fundamental principle of subtractive colors is that the they usually are blended on top of a white canvas, which ideally reflects all wavelengths of light. Then dyes are added in different color in which the combined absorbance depicts the resulting color. Commonly used subtractive primaries are cyan, magenta and yellow,

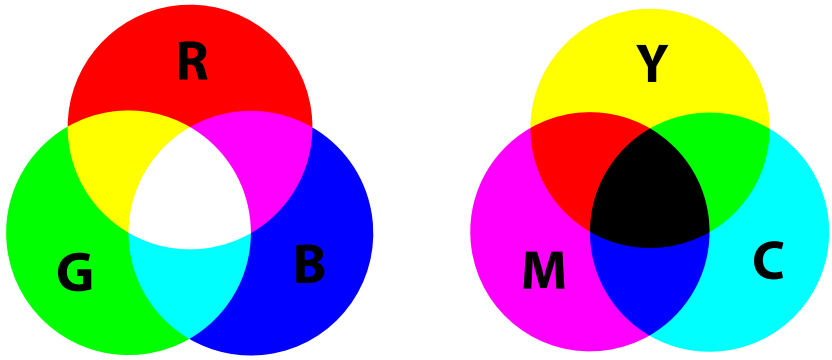

(a) Additive colors. **(b)** Subtractive colors.

Figure 2.4: Illustration depicting additive and subtractive colors.

which in theory when mixed together form a black color. However, in practice this is not the case, thus the color black is often included. This then becomes the color combination known as CMYK. In the absence of a white canvas, white is frequently included in the blend. Both additive and subtractive colors are depicted in Figure 2.4.

2.2.4 Color Spaces

Colorimetry is a field of research and technologies in which color is measured and quantified [WS82]. In order for color to be quantified, a common color space needs to be defined, which maps colors to a quantitative description with respect to a human observer, typically in terms of tristimulus values. In 1931, the International Commission on Illumination (CIE) defined the tristimulus CIE RGB space [SG31], based on color matching experiments using human observers [Wri29, Gui32]. The definition of the CIE XYZ color space followed, which now included an imaginary set of primary colors. However, as human color perception is not linear, it was not possible to accurately compute colorimetric difference between two colors in either RGB or XYZ space. As a result, the perceptually uniform CIE L*a*b* and CIE L*u*v* color spaces were defined in 1976 [McL76, ISO08]. The former has become the industry standard [Har01].

The forward transformation from XYZ to LAB, is defined as follows: [ISO08]

$$L^\star = 116\ f\left(\frac{Y}{Y_\mathrm{n}}\right) - 16 \tag{2.1}$$

$$a^\star = 500\left(f\left(\frac{X}{X_\mathrm{n}}\right) - f\left(\frac{Y}{Y_\mathrm{n}}\right)\right) \tag{2.2}$$

$$b^\star = 200\left(f\left(\frac{Y}{Y_\mathrm{n}}\right) - f\left(\frac{Z}{Z_\mathrm{n}}\right)\right) \tag{2.3}$$

where

$$f(t) = \begin{cases} \sqrt[3]{t} & \text{if } t > \left(\frac{6}{29}\right)^3 \\ \frac{t}{3\left(\frac{6}{29}\right)^2} + \frac{4}{29} & \text{otherwise} \end{cases} \tag{2.4}$$

Here the X_n, Y_n, Z_n is the white point parameter which sets the reference illuminant for the transformation. The standard illuminants defined by CIE are A, B, C which correspond to tungsten filament lighting, direct sunlight and lighting from overcast sky, respectively. Illuminant E represents illumination with equal radiant power for all wavelengths in the visible spectrum. The standard illuminants D_{50}, D_{65} were additionally defined at a color temperature of 5000K and 6500K, representing horizon light (sunset and sunrise) and average daylight at noon, respectively [Har01].

2.2.5 Color Difference

With the perceptually uniform CIELAB color space as defined in 1976, came the benefit of color difference computation. The color difference metric, ΔE^*_{ab}, was simply defined as the euclidean distance between two points. That is, for two $L^*a^*b^*$ colors, (L^*_1, a^*_1, b^*_1) and (L^*_2, a^*_2, b^*_2), their difference is given as

$$\Delta E^*_{ab} = \sqrt{(L^*_2 - L^*_1)^2 + (a^*_2 - a^*_1)^2 + (b^*_2 - b^*_1)^2} \tag{2.5}$$

The ΔE^*_{ab} parameter is a valuable parameter in colorimety, where higher values indicate that colors are less alike. However, the value of which two colors are separable by a human observer remains debated in literature. This value of ΔE^*_{ab} is referred to as the Just Noticable Difference (JND). The value $\Delta E^*_{ab} = 1$ is frequently referred to in literature as JND [HRV97, HP11b], however others have reported a value of 2.3 [MEO94] and even 5.9 [SCB87]. It turns out that the value is quite application specific, and depends significantly on how the colors are visually compared [Har01]. This is an important factor to keep in mind, and special care must be taken when interpreting color difference.

In 1994, the CIE updated the definition to ΔE^*_{94}, [MS95], and further refined it in the year 2000 when the ΔE^*_{00} was presented [LCR01]. The most current definition of a color difference, given the two colors (L^*_1, a^*_1, b^*_1) and (L^*_2, a^*_2, b^*_2) is

$$\Delta E^*_{00} = \sqrt{\left(\frac{\Delta L'}{k_L S_L}\right)^2 + \left(\frac{\Delta C'}{k_C S_C}\right)^2 + \left(\frac{\Delta H'}{k_H S_H}\right)^2 + R_T \frac{\Delta C'}{k_C S_C} \frac{\Delta H'}{k_H S_H}} \tag{2.6}$$

where $\Delta L'$, $\Delta C'$ and $\Delta H'$ represent lightness, chroma and hue differences respectively and S_L, S_C, S_H their respective weighting functions. Furthermore, k_L, k_C and k_h are the respective parametric factors that can be adjusted depending on the measurement application. Their default definition being $k_L = k_C = k_H = 1$. Finally, R_T is a rotation term which improves performance in the blue region. For the complete deriviation of each of these components, the reader is referred to [LCR01, SWD05].

2.2.6 Color Calibration

Most devices that measure color, do so in a device dependent color space. In the case of cameras, different types will have different interpretations and color nuances. Some will discretize light in a linear fashion, whereas others might have some non-linearities associated. Additionally, the range of colors measurable varies between cameras, with some extending beyond the visual spectra. Finally, the illumination in the scene will also dictate the measured color of an object of interest in the image. In colorimetry, it is of key importance that these device dependant color spaces are transformed into device independent color spaces such as the aforementioned CIE XYZ, before anything quantitative can be said about color. This process is known as camera color calibration. It is usually performed by imaging, under defined lighting conditions, a checkerboard of colored patches of precisely known color values in the device independent spaces e.g. CIE XYZ [BP88]. Then a forward transformation from the camera RGB space to the known values is estimated.

When visualizing colors on a computer monitor or a projector, or when printing on a color 3D printer, these devices have a limited range of colors that can be displayed or produced. This color limitation of systems is known as a *color gamut* [Har01]. In a consumer paper printer, the whitest color obtainable would be from the paper itself. Nothing whiter can be obtained. It is clear that the printable gamut is significantly smaller than the color gamut of computer displays, which is the medium where the color design process takes places.

A crucial part in a visual designers pipeline is the process of *color management*, which takes all these limitations into account throughout the color pipeline.

By employing color management, a mapping of gamuts between devices is performed in a device independent space. Several common consumer products supply such a color characterization profile as defined by the International Color Consortium (ICC) [C+10, ISO10]. However, 3D printers have yet to include support for such profiles. With proper color management, a designer can decide to only use colors that fall within the color gamut of the final medium, and at the same time get an accurate representation of the final colors on the computer display. This is the topic of [Contribution C, D].

Color profiles are not supplied with any of the industrial AM systems available. This is due to an industry-wide lack of color-management as discussed in Section 2.1.3. As a result manual profiling needs to be conducted. A solution to this is presented in [Contribution C and D]. In the case of printer profiling, similarly to camera calibration, a colored checkerboard may be printed and each color measured in the device independent CIE XYZ or CIE LAB color space using photospectrometers or calibrated multi-spectral imaging systems [TDJ+15, Har01]. As stated before, the forward or backward transformation from device dependent color spaces to CIE XYZ or LAB need to be modelled. In cases where camera responses or printed outputs are linear, it is often enough to perform a linear regression. That is, for device dependent colors $\boldsymbol{M}_{\text{rgb}} = [\boldsymbol{r}, \boldsymbol{g}, \boldsymbol{b}]$ we wish to find the transformation $\boldsymbol{T}$, that translates these measurements to the measured device independent space $\boldsymbol{M}_{\text{xyz}} = [\boldsymbol{x}, \boldsymbol{y}, \boldsymbol{z}]$ in CIE XYZ with a defined illuminant (white point). This can be formulated as the following least squares minimization problem

$$\arg\min_{\boldsymbol{T}} ||\boldsymbol{M}_{\text{xyz}} - \boldsymbol{M}_{\text{rgb}}\boldsymbol{T}||^2 \tag{2.7}$$

which could be solved in a linear least square sense

$$\boldsymbol{T} = (\boldsymbol{M}_{\text{rgb}}{}^{\top}\boldsymbol{M}_{\text{rgb}})^{-1}\boldsymbol{M}_{\text{rgb}}{}^{\top}\boldsymbol{M}_{\text{xyz}} \tag{2.8}$$

resulting in a 3x3 transformation matrix [GM11]. This method often leads to acceptable results, and has the added benefit that the matrix is invertible. Therefore, a backward transformation can be performed which is required for color calibration. However, it is important that the measurement pairs $\boldsymbol{M}_{\text{rgb}}$ and $\boldsymbol{M}_{\text{xyz}}$ adequately capture the gamut range in several observations. Transformations can additionally be estimated to the CIE LAB space, where the euclidean distance minimization effectively represents the color difference, thus minimizing the perceptual difference. In the case of non-linearities, better results may be obtained by using a higher order polynomial such as

$$\boldsymbol{M}_{\text{rgb}} = [\boldsymbol{r}, \boldsymbol{g}, \boldsymbol{b}, \boldsymbol{rg}, \boldsymbol{rb}, \boldsymbol{bg}, \boldsymbol{r}^2, \boldsymbol{g}^2, \boldsymbol{b^2}] \tag{2.9}$$

or similar of either higher or lower order [FMH15]. In this case, $\boldsymbol{T}$ is no longer squared and thus not invertible. Therefore, the backward transformation must

be obtained using a pseudo-inverse estimator [Tar05]. Finally, the transformation may be obtained by using a three-dimensional Look-Up Table (LUT) [Hun93]. With dense and evenly sampled measurements in the input color space $\boldsymbol{M}_{\mathrm{rgb}}$, intermediate values may be estimated through interpolation such as trilinear interpolation. Its inverse is obtainable by constructing a second LUT and populating it with the observations. In that case, entries in the inverted LUT that fall outside of the color gamut, can either be mapped onto the nearest color or specifically labeled as an out of bound color.

2.3 Acquisition of Geometry

When dealing with geometric metrology within AM, a significant amount of effort is placed on surface texture analysis and characterization within metal based processes [TSB+16]. This is done in efforts to both evaluate part tolerances and to provide better physical understanding of a given AM process [TSB+16]. The small scale surface is not part of the scope of this thesis, as it does not contribute to the overall form of the object. Here, we are concerned with the metrology of the functional shape after the printing process, whereas inline geometric metrology will be covered in Section 2.4.1. Here, a brief overview of current methods and technologies used in free form metrology of AM parts is given. For more detailed information the reader is referred to [SL16].

2.3.1 Structured Light 3D Scanning

Structured Light (SL) scanning, or fringe projection, is a commonly used active 3D scanning modality within industrial metrology [SDCS07]. The technology allows for non-contact, rapid and dense 2.5D shape acquisitions of an object or scene. A known pattern is projected onto the surface, thus encoding the object with features that are observed using one or more cameras. Several different pattern strategies are available [SPB04, SFPL10]. The system is precalibrated in such a way, that it is possible to perform distance measurements to these features via triangulation, by finding point correspondences [Gen11]. It is entirely feasible for a structured light scanner to be capable of producing millions of 3D points in a single scan, at a rate of 10-20 point-clouds per second [WALP16]. Though the hardware is not expensive per se, performance will vary significantly based on its integration, algorithms and operational usage, as a great deal of operator expertise is required. Fortunately, open source algorithms have recently emerged making it possible for researchers and small businesses to build their own high performance systems using commercial off-the shelf

components [WOL14], [Contribution F]. An example of such a system can be found in Figure 2.5, which was built early on during the thesis as a preliminary study.

Structured light systems are commonly found in two types of configurations. These are, systems with a single camera and projector, and systems with two cameras and a projector. In the first, the projector is calibrated and used as if it were a camera in the triangulation. Secondly, the two cameras are used for triangulating and the projector solely used for encoding the scene. The latter is predominately used in industrial systems as cameras can be found in significantly higher resolutions than projectors, resulting in higher triangulation precision. This configuration has been the focus of the work in this thesis, and the next paragraphs will briefly describe the principles involved in structured light 3D scanning.

Camera model A common mathematical description of a camera is the pin-hole model [HZ03]. The model depicts an infinitesimally small aperture separated by a focal distance f to an imaging plane. All rays of light thus travel through the aperture pinhole until intersecting the image plane. The pinhole camera model $\boldsymbol{P}$ has the property of projecting the 3D world point Q into a 2D point q, on the image sensor plane, both in homogeneous coordinates. In mathematical terms this is written as [HZ03]

$$q = \boldsymbol{P}Q \tag{2.10}$$

The pin-hole camera model is then defined as

$$\boldsymbol{P} = \boldsymbol{A}[\boldsymbol{R}|\boldsymbol{t}] \tag{2.11}$$

with $\boldsymbol{A}$ being the intrinsic camera matrix

$$\boldsymbol{A} = \begin{bmatrix} f_x & 0 & c_x \\ 0 & f_y & c_y \\ 0 & 0 & 1 \end{bmatrix} \tag{2.12}$$

where f_x and f_y are focal lengths, c_x and c_y is the intersection between the optical axis and the image plane, commonly known as a principal point, and $[\boldsymbol{R}|\boldsymbol{t}]$ are the extrinsic parameters that define the orientation and position of the camera in the world coordinate space. With modern industrial cameras, $f_x = f_y = f$ and skew distortion compensation is omitted from the equation [HS97, HZ03].

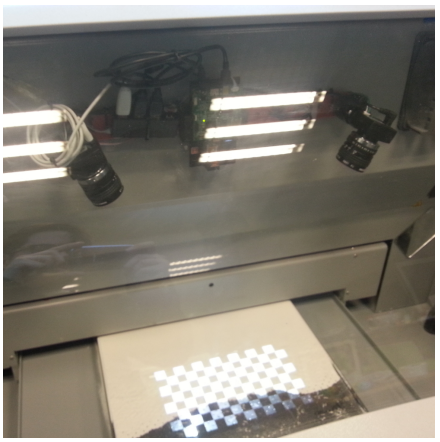

(a) Vision system prototype mounted inside a 3D printer.

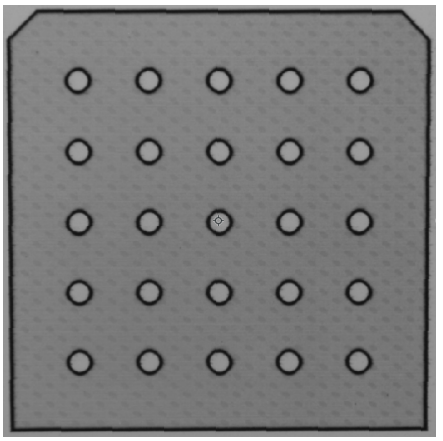

(b) Example slice obtained during print.

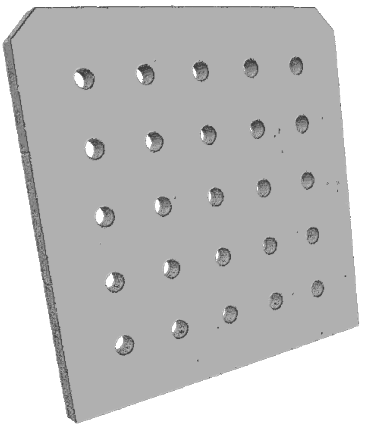

(c) Reconstructed 3D model of the printed object.

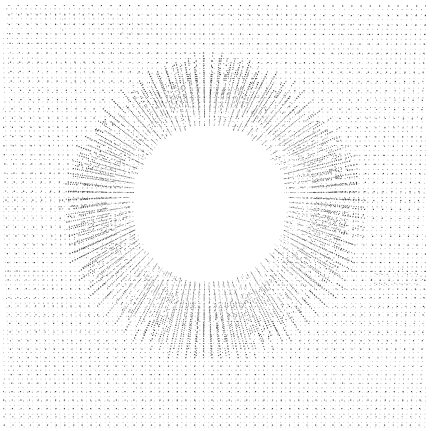

(d) More detailed view of the 3D point cloud obtained, showing a single hole.

Figure 2.5: Pipeline results from a unpublished preliminary study of an in-line structured light vision system that was placed inside a powder-based 3D printer. The powder topography was mapped in-line, each layer segmented and a 3D geometry estimated.

A more accurate description of the camera model is obtained by accounting for lens distortions as proposed by [Dua71]. Radial lens distortion is normally modeled using the polynomial

$$\begin{bmatrix} x' \\ y' \end{bmatrix} = (1 + k_1 r^2 + k_2 r^4 + k_3 r^6) \begin{bmatrix} x \\ y \end{bmatrix} \tag{2.13}$$

where x',y' are the remapped positions on the image plane, $r = \sqrt{x^2 + y^2}$ is the radius from the optical axis, and (k_1,k_2,k_3) are the three distortion coefficients. Additionally, due to misalignments in the optical lens elements, it can be necessary to add compensation for tangential distortion in the model

$$\begin{bmatrix} x' \\ y' \end{bmatrix} = (1 + k_1 r^2 + k_2 r^4 + k_3 r^6) \begin{bmatrix} x \\ y \end{bmatrix} + \begin{bmatrix} 2p_1 xy + p_2(r^2 + 2x^2) \\ 2p_1(r^2 + 2y^2) + 2p_2 xy \end{bmatrix} \tag{2.14}$$

where (p_1, p_2) are the tangential distortion parameters. However, with high quality optics, tangential distortion is often negligible. This is further elaborated in [Contribution F].

Camera Calibration

A camera calibration pipeline deals with the estimation of the intrinsic, extrinsic and lens camera parameters. Although various methods have been presented, the method proposed by Z. Zhang [Zha99] is frequently used and commonly implemented in calibration software [Mat, Bou, B+00]. The method consists of imaging a planar geometry, with optically identifiable features whose relative distances are known. Commonly, a checkerboard is used for this purpose, and the checker corner saddle points used as features. By imaging the checkerboard, pairs of 2D-3D point correspondences are obtained. Initially, parameters are estimated in a closed form solution, thereafter followed by a non-linear optimization, such as using the Levenberg-Marquardt algorithm, that minimizes the re-projection error based on the observations [Zha99].

Stereo Calibration

In structured light and stereo view systems, it is important that the relative rotation $\boldsymbol{R_c}$ and translation $\boldsymbol{t_c}$ between the camera pairs are known, such that triangulation can be performed. The process of determining $\boldsymbol{R_c}$ and $\boldsymbol{t_c}$ is called stereo calibration. In the case of a two camera stereo system, similarly to before, these parameters may be estimated using observations of a checkerboard. This time, the checkerboard should be observable in both cameras and thus mutual

point correspondences are obtained. With the intrinsic and extrinsic parameters for each camera as a priori, it is possible to project the known 3D points and evaluate the stereo reprojection error. The relative $\boldsymbol{R_c}$ and $\boldsymbol{t_c}$ between the two cameras is then estimated such that the re-projection error is minimized, again using non-linear optimization. In some cases, the algorithm is additionally allowed to modify the camera parameters in order to minimize the error even further [HS97, HZ03].

Scanning Performance and Verification

Due to the complex nature of error sources in structured light, quantifying their performance is challenging. This is also applicable for calibrated industrial systems. As the aperture is not infinitely small, cameras will exhibit depth-of-field effects. Due to this, a camera will only be precisely in focus at a particular distance. The focus will gradually become less sharp as objects are placed further or closer to the focusing distance. As a result, feature detection of e.g checkerboard corner will be less precise in these regions. The focus range can be increased by reducing the aperture size as much as possible. However, in order to maintain similar imaging performance one needs to increase the image exposure time or increase the light used to illuminate the sample. The latter being the preferred option, as increasing imaging exposure negatively affects the signal to noise ratio, as well as motion artifacts due to vibration or dynamic changes in the scene become more prominent. Both of these aspects will limit the overall performance.

A significantly large contributor to scanning error is due to optical properties of the material being measured. Radiometric effects, such as transparency, specularity or objects exhibiting sub-surface or volumetric scattering, will affect the scanning result to a varying degree. Although much research on addressing these challenges exists [IKL+08, GAVN13], it is clear that it is not possible to place a single performance metric on a structured light system. The precision and accuracy will always be dependent on the optical properties of the material being measured. A further discussion on this topic is found in [Contribution F].

Efforts have been made to quantify optical 3D scanning performance. The most notable is the German industrial standard VDI/VDE 2634 (Part 2), which focuses on 3D area scanning [VDI00]. The standard describes the scanning procedure of precision calibrated test artifacts, that are to be scanned in different orientations and positions within the scan volume. The standard also provides a set of performance metrics based on these measurements. Thus, it adequately takes into account that scanning accuracy and precision depend on where the sample is placed in the volume, thus accounting for depth-of-field effects. The

Figure 2.6: Calibrated reference artifacts according to VDI/VDE 2634 (Part 2). From [Contribution F].

artifacts used in [Contribution F] are shown in Figure 2.6.

2.3.2 Coordinate Measurement Machine

In the category of tactile measurement devices, there is the Coordinate Measuring Machine (CMM) that is conventionally used within geometric metrology for extremely precise measurements [HCHDC06, SDCS07]. Traditionally, a CMM functions by contact probing the object of interest and recording the probes position, relative to a defined origo, upon contact. Non-contact derivatives using optical probes also exist. Depending on the measurement procedure, it is common to repeat the same measurement such that a statistical analysis may be performed. A limitation of a CMM is that the measurement process is slow compared to optical scanning methods, therefore characterization of every produced part in an AM system is not feasible. Additionally, the measurement points are few and sparsely distributed on the object surface.

2.3.3 Computed Tomography

Metrological Grade CT scanners are frequently used within AM metrology, due to their ability to perform dimensional and material quality control simultaneously [KBC+11]. This includes internal cavities and enclosed materials that are visually hidden or not reachable. Industrial CT scanners differ from their medical counterparts in terms of spatial resolution and accuracy, as well as they offer higher X-ray penetration power in order to capture dense materials such as metals [KBC+11]. With denser materials, or multiple of materials with abruptly varying densities, artifacts affecting the measurement accuracy emerge. Metrological CT show substantial promise within AM. However, less expensive and

artifact free optical methods have recently emerged and serve as the only industrial alternative to CT scanners [PDH13]. More information on this technology is provided in Section 2.4.1.

2.4 AM System Monitoring

As previously stated, there is an inherent lack of system monitoring for quality assurance in AM. This is in part due to the proprietary nature of the industry, where AM systems are black boxes that produce objects from CAD. For industries such as aerospace, automotive or the medical industry, where component failure may be life threatening, it is critical that quality assurance is up to similar standards as with conventional and established processes. As the case for AM becomes more applicable for these large industries, there is an increasing requirement for solutions. The need has been repeatedly highlighted in academic literature [PDH13, EHS+16].

Fortunately, AM manufacturers have begun to utilize in-situ process sensing to some extent. However, this has almost exclusively been applied to metal based AM processes for detection of porosity, melt pool monitoring and build height using optical systems such as high-speed CCD or CMOS cameras, photo detectors and coherent imaging systems [EHS+16]. In many cases, these sensors are used for in-line process correction of e.g. laser power, and not necessarily reported to the user.

Several challenges need to be overcome and much work is ahead if AM is to become a de-facto manufacturing method, requiring an enormous set of disciplines spanning many fields. The following sections will cover the relevant literature within the scope of this thesis. For a broader overview on process monitoring the reader is referred to [PDH13, TE14, MLD+15, EHS+16].

2.4.1 In-Line Geometric Metrology of 3D Print

Pedersen et al. [PHN10], presented the first in-line vision system and method for in-line 3D reconstruction of printed part geometries. A high resolution digital Single-Lens Reflex (SLR) camera, along with an electronic triggering interface, was used to autonomously capture 2D images of each printed layer of a powder based industrial AM system. After the print process, the part boundaries were determined for each slice and a voxel representation obtained. A visual comparison was performed between the measured geometry and the CAD rep-

resentation. The work was later expanded in [HP11a], where a quantitative comparison was made between the measured and nominal geometries. Results showed a maximum divergence of ±0.2 mm. In order to qualify the method itself, the printed test artifact was scanned using a 3Shape Q640 line-laser based optical 3D scanner. The maximum disagreement between the two methods turned out to be ±0.02 mm., underlining the high potential of the method and that with proper calibration, traceability is obtainable. The method was later adapted to an industrial DLP printer [APHN13] and an industrial SLM printer [PH14], therefore demonstrating the methods potential to work across several AM families. A more thorough description and background can be found in [PDH13]. Others have since then expanded on this method for use in SLM systems under the term 'Optical Tomography' [ZBL+15].

The limitation of the methods described above is that in some AM processes such as SLS and SLM, residual stress is inevitable, causing warping of the printed product not measureble by the in-line system. However, [PDH13], proposes that an accurate estimate of final geometry could be obtained using numerical warp analysis given the process boundary condition and measured geometry. To address for this, a high resolution structured light scanner has been used to map the topography of the powder bed in an in-line fashion [ZZFD16, LZZD15]. Additionally, the method has the potential to be used for surface characterization of the sintered part, validate powder spreading, and detect slight geometric deviations.

The work on in-line geometric acquisition has an added utility other than part metrology. The printed outcome can give an important description on the print process itself. In efforts to evalute perfomance of a Fused Deposition Modeling (FDM) printer [HNRP14], a calibration artifact was printed. This optomechanical artefact has previously been used as a tool to transfer tracability between traditional coordinate measuring machines (CMMs) and optical CMMs [HDC97, DCHM05, DCHM06]. The artifact plate was measured in an optical CMM and the measured features compared to nominal. From the error analysis it was possible to derive parameters such as geometric scaling errors and squareness of the 3D printer. Subsequently, this method was implemented on several AM platforms for performance comparison [DNRP14].

To conclude, it is stressed that all of the work presented above is concerned with post print verification and assessment of the printed part or the process itself.

2.4.2 Metrology of 3D Printed Color

Colorimetry is a mature field that has been successfully applied in the paper and textile printing industries as well as within digital media [WS82, GM98, SB02]. However, work on transferring the field and methodology to the new medium of 3D printing has been lacking [PWRH08, Sta10]. Here, an overview of the recent efforts will be given.

Parraman et al. [PWRH08] performed a colorimetric evaluation of a Zcorp Spectrum 510 powder color printer. Colored charts and cubes were printed, brushed, post-processed with a wax infiltration and finally measured with a spectrophotometer. Authors reported influence of surface orientation on color accuracy and the lack of color management systems available.

The work was promptly followed by [SLM+08], where colored test artifacts were used to investigate effects from different finishing methods; untreated, cyanoacrylate infiltration and epoxy-based infiltration. It was demonstrated that the finishing methods had an effect on the color to a varying degree, where cyanoacrylate resulted in the largest color gamut. A summary of both works is also found in [WHPS09]. A limitation of the measurement method is that only a single spectrophotometer measurement was used for each artifact and therefore lacking statistical significance, both in terms of color and instrument variability.

In [SLW10], a test artifact plate containing geometric features, was printed in various orientations on a Zcorp Z510 printer. The feature color was only in magenta, in order to evaluate only the performance of a single printhead. The plates were then analyzed in a Leica EZ4D stereomicroscope. The results agreed with previous findings on the effect of print orientation. More detailed information on the previously described work can be found in [Sta10].

Long term stability of color was investigated in [SLGS12]. In order to simulate long term exposure to external lighting sources such as artificial and sunlight, the authors proposed an accelerated setup where printed objects were exposed to a xenon-arc based weathering apparatus. The colorimetric effect was observed for different types of infiltrant. Results demonstrated a noticeable change in color based on several parameters. The work concluded that future investigations need to keep long term stability in mind as the technology progresses.

A pipeline for producing colored facial prosthetics printed in a powder based ink-jet system was proposed by [XZvNY14]. As an infiltrate, a clear medical grade silicon-polymer was used. The 3D data was obtained by a 3dMD camera system, and color profiled using a Macbeth ColorChecker DC chart (X-Rite). For printer profiling, a 3D model of the Macbeth chart was printed, yielding

240 measurement samples measured with a spectrophotometer. A third order polynomial regression model was used to describe the color transformation. The method was evaluated by printing a test plate of 14 skin-like colors, with an average $\Delta E^*_{ab} = 4.5$. With few samples used in the evaluation, as well as with the limited number of measurements in the printer characterization, it is hard to generalize on the performance of the color correction as a whole.

Arikan et al. [ABTU15] presented a color-managed 3D printing workflow for color based material jetting printers, that use highly translucent materials. They demonstrate that spectrophotometers are biased towards lower reflection, and propose an alternative vision system under controlled illumination. Their system is compared to a spectroradiometer, with deviations being within the inter-instrument variability of hand-held bidirectional spectrophotometers commonly used in graphic arts. They proposed the deviation could be reduced further by using a spectral imaging system. The authors further expanded their work on color printing with translucent materials [BAU15], using a layered halftoning approach, where different colored voxels are placed several layers under the surface in order to produce a photorealistic appearance.

2.5 The Digital Ecosystem

Given the fact that AM could potentially be a new de-facto manufacturing process in a digital manufacturing ecosystem, perhaps even replacing traditional processes, it is important to consider its place and function in such an environment. Particularly, in terms of how we operate and use these machines and how they interact with other technologies, both old and new. This is becoming increasingly more important due to increasing amounts of data available in the modern factory. Answering these questions is part of a greater effort known as *„Industry 4.0"* which originated as a high-tech strategy from the German government, concerning industry digitalization [KHHW13]. In the next secions, a brief overview is given on the recent advances in web and high performance mobile technology that may be used to improve upon traditional manufacturing. Specifically, augmented reality, the technology often referred to in the context of industry 4.0.

2.5.1 Augmented Reality

Augmented Reality (AR) has the ability to enhance the physical world by combining it with virtual elements in real-time. As such, useful and relevant in-

formation can be spatially augmented on demand. However, the information flow is not unidirectional, as the virtual object can present itself i.e. as a human input device. This could for example be a touch panel, where an operator can interact with the virtual world, even causing actions in the physical. As the technology matures, this boundary between physical and virtual will become less clear. Recent development in mobile embedded systems such as smartphones, tablets and head mounted devices (HMD) [Mic17, DAQ17] have yielded enough computing power to enable augmented reality applications at a low cost. For further information on the subject, the reader is referred to [ON13, FdSB16, BZ15, BFKR14, GSLZ14] and for historical reasons [Azu97]. The manufacturing applications that have been made possible are many, and a relevant subset of them will be discussed.

Applications

Repair and maintenance of complex machinery is a prime example of AR within production. In this case, instead of having to rely on bulk blueprints and text manuals, the relevant information is virtually made available to the user. Going beyond blueprints on paper, where step-by-step repair instructions and tasks are displayed in an animated fashion, assisted with audio cues and success indicators. This opens up applications such as remote technical support, where even untrained workers can perform maintenance or repairs under remote guidance [BK02]. The technology may also be used for worker training [WBE+13] and even for design purposes [NOCM12].

Process monitoring is another example where AR is beneficial. Due to the rapid increase in available data that is generated by the modern factory, AR can serve as an abstraction to that data, such that only contextually relevant information is presented to the user on demand. This can also be in the form of visualizing sensor data, such as from a thermal sensor. Here, a heat map can be overlaid on the part instead of displaying only numbers, thus reducing the cognitive overload. Furthermore, planned paths of robot co-workers or machine tools can be visualized via simulations, before committing to the process. Process monitoring can also be extended to process control, as this unique digital window enables users to visualize and modify planned and queued processes and process parameters, in order to quickly respond to external changes. The AM related application areas are explored further in [Contribution K].

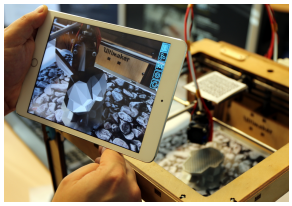

(a) Handheld, from [Contribution K]

(b) Head mounted.

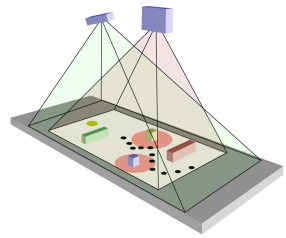

(c) Projective, from [Contribution I]

Figure 2.7: Examples of different augmented reality modalities.

Principles of AR

At the heart of most traditional augmented reality implementations is a high performing vision system, that for each frame identifies a predetermined set of markers that describe the context or identify the relevant user interface. The algorithm can typically be structured into three parts: i) marker detection, ii) marker tracking and iii) marker pose estimation. The pose estimation can be obtained by solving the perspective n-point problem based on 3D-2D point correspondences [GHTC03, QL99]. With the perspective transform obtained, it is possible to augment digital content in the same reference frame.

Markers that employ natural features, require the marker to be known by the system before hand. For these applications, feature descriptors that are scale and rotation invariant are necessary [ADP12, LA08, BETVG08, Low99]. Quick Response (QR) codes are an example of markers with stored information that can be used by the AR system. The code can for instance present itself as a web page holding a user interface. However, these types of implementations are more sensitive to variations in scale. Other notable markers include ArUco [GJMSMCMJ14], Vuforia's VuMark [Vuf16] and a new marker implemented by the author [HEM17]. Once the marker has been identified, a less processing intensive tracking takes place using methods such as optical flow [LK+81].

Software solutions and libraries have recently emerged that show great potential for use within industrial AR, these include the open source Open Hybrid [Ope17] and ARToolKit [ART17] and the commercial Vuforia [Vuf17]. From a hardware perspective the technology appears in various forms, as can be seen in Figure 2.7. Next, a brief overview will be given on common implementations.

Handheld implementations are perhaps the most recognizable. In this case, consumer mobile devices such as phones or tablets are used as a window into

AR content. Due to recent advances in embedded systems, these devices have become powerful processing computers, that now are capable of performing the necessary computation in real-time. The additional benefit is that the technology is low-cost and does not require any wearable elements. The AR interfaces are only presented on demand by the user. An industrial use case using this modality is the topic of [Contribution K].

Head Mounted devices have gained momentum for the past years, especially seen from an industrial perspective. The most notable two being the Microsoft Hololens [Mic17] and the smart helmet from DAQRI [DAQ17]. Both being similar in nature, they consists of a suite of sensors and cameras that observe the enviroment, whilst projecting stereoscopic AR content through a glass like display into the users eyes. An example of a head mounted virtual reality device is presented in [Contribution J], where gyroscopic flywheels are used to simulate external forces.

Projective augmented reality, unlike the two prior cases, does not require a vision system per se, although they are commonly used. In this case a projector is fixed over a workstation, or industrial machine and projects relevant information onto the scene. The benefit being, that no user hardware is required as in the two previous examples. However, the AR experience is localized to that particular area and therefore not as flexible. An example of this technology is found in [Contribution I].

Chapter 3

Contributions

The aim of this thesis work has been to apply computer vision to manufacturing and additive manufacturing in particular. The work serves as a step towards widerspread industry adoption of the technology as a de-facto manufacturing modality. As mentioned, this is essential, as the technology serves a pivotal role in all industry 4.0 efforts and has not received adequate attention. Furthermore, we take a step back and investigate the boundary between physical and digital objects, in order to facilitate a fluid integration of AM within industry.

As a result, the work falls into three main categories: The two first concern appearance and geometry of process and quality control in AM. The third category concerns machine interaction, where we allow ourselves to explore future interaction paradigms within additive manufacturing from an industrial perspective. In all three categories, we demonstrate how modern computer science can be applied in beneficial ways within AM.

For a complete list of the contributions discussed in this section, the reader is referred to page **ix** of the thesis.

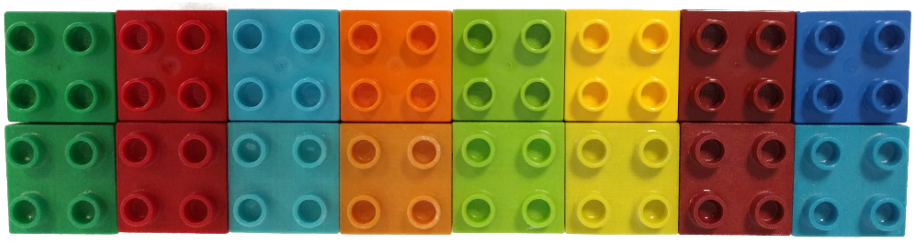

Figure 3.1: Example results from the color correction pipeline presented in [Contribution C, D]. (Top row) Original toy blocks. (Bottom row) 3D printed reproductions. Note: Orange, yellow and dark blue fall outside of the printers gamut.

3.1 Appearance and Color

In relation to appearance, the need for robust and rapid appearance measurements was presented in a positional paper [Contribution A]. In particular, AM was identified as a field where this is of significant importance in terms of quality assurance. At that time, the state of the art in color metrology of 3D printed parts was significantly under-represented in literature. As described in Section 2.4.2, previous work had identified the importance of this type of research, as well as investigated how different factors such as post processing affected color. In efforts to bring 3D color printing closer to the classical practices of the paper printing industry, three contributions have been made.

[Contribution B], presented a novel quantitative analysis on the positional accuracy of 3D printed color features. The work both presented and demonstrated a general method for spacial color verification, inspired by classical metrology. The method was demonstrated on a Zcorp Zprinter 650 color printer, where special test artifacts were printed that consisted of precisely located features in CMYK colors. The positions of these features were then measured using a DeMeet 220 optical CMM. The analysis demonstrated general error trends in the position of the color features, due to printer scaling error, non-orthogonality and printhead misalignment. The global spatial accuracy of the machine was found to be less than 350 µm. Using this characterization of the color placement, compensating corrections to the 3D model could be made resulting in a more precise print.

In the second contribution, [Contribution C], it was demonstrated and proposed for the first time, to the authors best knowledge, how it is possible to reliably measure and quantify color of 3D printed objects in a metrological context.

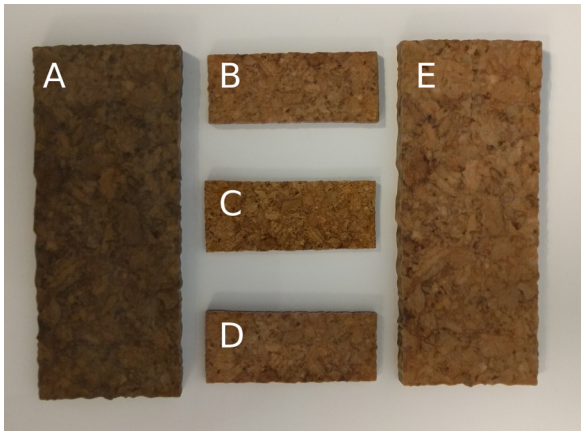

Figure 3.2: Qualitative comparison of the color correction pipeline from [Contribution D] showing 3D printed replicas with complex textures.
A: Printed cork without color correction.
B, D & E: Printed cork with color correction.
C: Original cork sample.

A series of colored plates, spanning the entire RGB gamut were printed and measured using VideometerLab, which is a multispectral imaging system. A statistical method for full gamut characterization of the printed plates was presented, and the forward color transformation was obtained using a 3D LUT. Using the forward model, it was demonstrated that it was possible to predict the colors of 3D printed parts. The prediction was quantitatively evaluated with a mean $\overline{\Delta E^*_{00}} = 1.5$ and standard deviation of $\sigma = 0.75$, thus barely noticable according to the JND definition. This was further improved upon in [Contribution D], where a precision full color characterisation and calibration pipeline was presented. Building on the previous method, the changes in gamut for dry and infiltrated prints was qualitatively and quantitatively compared. This confirmed prior studies [SLM+08], in which the color gamut is expanded by infiltration. However, more color variance is introduced due to the extra post-processing step. From the forward 3D LUT, an inverse table was constructed that relates printed outputs to their respective input colors. By doing so, the pipeline is capable of performing automatic color correction, providing print prediction capabilities, along with the possibility of specifying colors. In other words, input color requests are corrected such that the desired color is produced. From an industrial perspective this is of great importance, both for rapid prototyping and for quality control. The work was accompanied with an intuitive color design tool used for correction and visualization of parts prior to print. The pipeline was qualitatively evaluated by replicating an object with complex color textures,

see Figure 3.2. Additionally, saturated replications with colors falling outside of the printable gamut are demonstrated in Figure 3.1.

Finally, as part of collaborative research efforts within our group, a contribution using the underlying technology was made for capturing complex scenes for use in photo- and physically accurate rendering [SDO+17].

The listed contributions in general contribute to the further advance of color quality control within additive manufacturing by bringing it closer towards the methods used for decades in the paper printing industry. As stated, this is crucial as the technology converges to a print-to-consumer paradigm. Color AM must therefore receive the same amount of attention as geometry.

To summarize, the following contributions have been made:

1. The need for rapid appearance measurements within industry was presented.
2. A method for precisely characterizing positional accuracy in 3D color printing was developed.
3. A method for precisely characterizing the color transform of a 3D printer, enabling print prediction, was developed.
4. Development of a full color management pipeline for a 3D color printer. Thus, enabling print predictions and the specification of color, allowing for part duplication.
5. Bringing 3D printing towards the methods used for decades in the paper printing industry.

3.2 Geometry

In relation to geometry, we built upon the work performed on in-line monitoring of geometry in 3D print [PDH13], by developing a novel vision system and calibration method for binder jetting and powder bed fusion processes [Contribution E]. The work proposes using a contact image sensor, similar to the sensor of a consumer flat bed scanner, instead of a camera. This has several benefits, as the sensor can be mounted on the powder feed carriage, which provides the mechanical actuation required for the sensor to traverse over the build area. The implementation is significantly more compact than achievable by using a camera, which is restricted by its view geometry. An additional benefit is

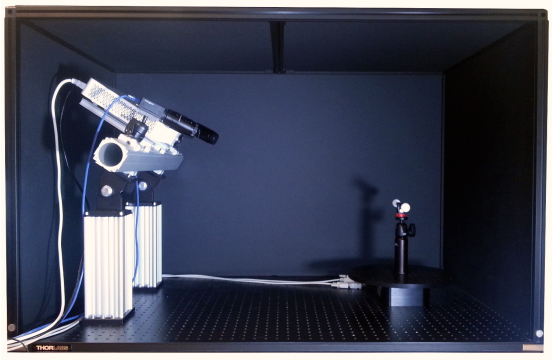

Figure 3.3: Structured light system developed during the PhD project. Consists of two high resolution industrial cameras, a Full-HD DLP projector and a precision rotary stage. From [Contribution F].

that the scanner can sample a large build area in high resolution. The scanner calibration method makes it possible for the sensor to be included in any AM system that includes a wiper or carriage feed. This is possible without any hardware modification to the printer itself, as the method determines the scanners position from observations of a printed geometrical reference. In the ideal case, this position is best obtained from the printer hardware, however, this is rarely possible. As sample rates and resolution increases in these sensors, it will open new possibilities of process monitoring in AM. If detecting individual powder grains becomes possible, it will allow for more precise geometry verification, and give insights into their size distribution and packing density. Additionally, defects from the powder consolidation process may be detected, all of which can be used for closed-loop control of the printer.

As an effort to verify post print geometry, we explored structured light 3D scanning, which is commonly used in free form geometric metrology. As part of a collaborative effort, we developed a high precision structured light system using commercial off the shelf components. In [Contribution F], we explore the accuracy and precision obtainable using standard components and methods. Furthermore, we explore what are the dictating factors in this regard. We demonstrate how the industrially accepted standard VDI/VDE 2634 (Part 2) may be used as a quantitative metric to compare different pattern strategies and changes in the calibration process. We quantitatively investigate answers to common questions within structured light. Questions such as: i) what calibration parameters should be included in the procedure, ii) what angular range of checkerboard observations is required in the calibration, iii) how many checkerboard observations are required and iv) which SL pattern strategy is the overall best performer. Finally, we demonstrate that our system performance is com-

parable to an industry leader within industrial metrology using SL. In relation to this, work was performed in the development of practical methods for such systems, namely, an image-based automatic alignment of point clouds from several viewpoints [MWE+17]. Currently, the structured light system serves as an educational- and research platform. As an example, it has been used for scanning archaeological specimen [TDG+16] and used in ongoing cultural heritage studies.

As discussed in Section 2.4.1, in-line geometry estimation has previously been used as a post print analytical tool. To improve upon this, we extended this to in-line process control of a top down vat photopolymerisation process. Here, in-situ observations directly influence and control the print process in a closed-loop fashion. By doing so, a new AM modality has been realized in a patentable, functional and novel 3D printing system [Contribution G, H]. The system improves significantly on the state of art in terms of print speed without compromising print quality, therefore, solving a major bottleneck faced by the industry. This system, built specifically for this purpose, is of the same kind as used for producing 90% of all custom fitted hearing aids, as well as hyperflexible "soft tooling" for injection moulding processes.

All commercially available 3D printers today manufacture components in a layer by layer fashion. Much of the process time relates to the motion in between layers, at which no active material solidification occurs. Our prototype takes another approach to the build process by continuously solidifying material, where the time consuming mechanical recoating mechanism has been factored out of the process, thus saving significant amount of time. However, doing this requires a special patentable control process which is the core of the invention. The print process is monitored in real-time using a computer vision system, which controls the consolidation process in a closed loop. This allows for self correcting behaviour of the printing process in relation to the speed and processing material. Reducing the time to print from days to hours and hours to minutes, will substantially reduce the time-to-market for printed products e.g custom fitted hearing aids. Additionally, reducing time and cost of R&D activities which will enable businesses to become more agile and faster to adapt to rapidly changing markets. As a result of this work, a patent has recently been filed [Contribution G, H], and therefore peer review publication has not been possible.

Finally, we collaborated on the development of an automated calibration method for a delta type printer [PEHN16], where the printer performs fast probing of a flat build platform in order to estimate and correct for mechanical deviations in its construction. The calibration procedure, taking less then 3 minutes, achieves vertical positioning repeatability of $\pm 3\,\mu m$. The rapid self-calibration allows for geometrical re-mapping prior to every print job. As a result, the printer maintains a calibrated state and compensates for drifts after extended use.

The presented contributions have built upon previous work within AM geometry [PDH13]. By combining competences from mechanical engineering and computer science, innovative AM methods and processes have been developed. This demonstrates the importance of embracing a cross-disciplinary approach within AM.

To summarize, the following contributions have been made:

1. Novel method for in-line metrology using a line-scanner sensor (contact image sensor) was presented.
2. Development of a high precision structured light 3D scanner, used as a research and educational tool.
3. Demonstration of how industrial standards may be used for parameter and algorithm evaluation in structured light. Thus, shedding light on common uncertainties regarding the calibration process in structured light scanning.
4. Image based alignment method in structure light scanning using multiple observations.
5. A novel invention of a continuous 3D print modality based on vat-polymerisation and closed-loop process control. Increasing print speed by a factor of 100 compared to state of the art.
6. An automated calibration method for a delta type printer was developed.

3.3 Human Machine Interaction

The third of the main categories, encapsulates work performed where the 3D ecosystem of AM is investigated as a whole. This mainly consists of interdisciplinary exploratory work on AMs place in the factory of the future, and how both old and new technologies might facilitate a successful and fluid integration in that context. The work concerns human machine interaction, where focus has been placed on augmented reality, a technology frequently referred to in the context of industry 4.0. Part of the work was performed in a research collaboration with the MIT Media lab, following an external research stay.

With rapidly increasing amounts of data produced by modern machine tools, AR can serve as a medium that provides operators with contextually relevant data, on demand. Thus, bridging a gap that may be created as content complexity increases. The scalability enabled by AR interfaces has the potential

to be an enabling technology for modular production platforms, rapid product development and hyper-flexible automation.

Three common modalities, applicable within industry, were initially investigated. First, tangible user interaction with projective AR was explored in [Contribution I]. A virtual scene was projected onto a table containing toy blocks, used for user interaction with the virtual scene. The position of the blocks in the scene were detected and recognized using a Microsoft Kinect distance camera. Secondly, an investigation into virtual reality was conducted. Here, a novel force feedback mechanism for head mounted devices using gyroscopic flywheels was presented [Contribution J]. The perceived torque caused by the gyroscopic effect could be used for head guiding purposes, or subtle nudging cues. By instantaneously stopping the flywheels, a strong torque is perceived, which could be used as an alert mechanism in an industrial environment. Finally, a robust and novel marker system for use within AR was presented in [HEM17]. The main benefit of the marker system is that humans can easily distinguish and decode the marker. Both the marker generator and decoding application for mobile devices are available online[1].

Having explored the potential technologies commonly associated with the digital manufacturing paradigm, the findings were combined and the work tied into the central topic of this thesis. That is, augmented reality with focus on its use within AM was explored [Contribution K]. An augmented reality interface was developed using a consumer mobile device, and consequently used to monitor and control a commercial 3D printer. The work demonstrated a novel interaction mechanism for simultaneous monitoring and controlling of a 3D printer. It is important to note that the presented augmented reality interfaces are not limited to AM. In fact, similar augmented interfaces can be implemented on any kind of manufacturing tools and machinery, including Computer Numerical Control (CNC) machine tools, water jet- and laser cutters and injection moulding machines.

The work demonstrates the importance of embracing augmented reality within manufacturing engineering. With AR, advanced manufacturing processes and process chains can be interfaced in a simple and intuitive manner.

To summarize, the following contributions have been made:

1. An intuitive and tangible projective augmented reality system was demonstrated.
2. Novel and untethered force generation mechanism in head mounted devices

[1] `http://hrqr.org`

for virtual or augmented reality was developed.

3. Development of a new augmented reality marker system that is decodable by humans.

4. Development of novel methods and interfaces for monitoring and controlling industrial machines using augmented reality and low cost hardware.

3.4 Other Work

The nature of the work discussed has been performed across multiple disciplines, which are not entirely reflected within the above mentioned contributions. These consist of applied systems engineering and the extensive laboratory hours required. Substantial amount of work constituted as reverse engineering of the industrial AM systems available at our institute. These, and other commercial systems, are proprietary black boxes. In order to improve on their performance and push them to the limits of their capability one must be resourceful. Disassembly and inventive modifications are therefore required. In some cases, the best option is to build new printers from scratch in a more research friendly framework, as has been done in [Contribution G, H].

Chapter 4

Conclusion

The work performed in this thesis has addressed several important challenges, all aiming towards a common goal. By applying computer vision within the field of additive manufacturing in an inter-disciplinary fashion, the aim has been to solve many of the challenges required for additive manufacturing to reach its full envisioned potential.

Quality control is a major milestone to overcome in this regard. To address this, focus has been placed on two main areas. First is color quality control of 3D printed components, where applied methods within color science were adapted to the new medium in novel ways. This facilitates capabilities to predict and control the produced color, followed by a quantitative analysis for quality assurance, both in terms of color and spatial accuracy.

Secondly, focus was placed on geometrical quality control, building on the previous work performed at the Technical University of Denmark. Innovative sensing solutions for additive manufacturing were presented, along with the development of a low cost and high precision 3D scanning platform. The work then led to the development of a novel and significantly faster 3D printer technology, addressing a major bottleneck within additive manufacturing. A patent application is ongoing.

As has been highlighted in the thesis, there are several aspects that influence

the successful adoption of AM in the industry. Specifically related to its integration within digital manufacturing. To address this, an exploratory study has been performed on future technologies that are commonly associated with the factory of the future. These studies condensed into a contribution where future interactions for additive manufacturing were presented using augmented reality. The work serves to exemplify a fluid integration of the technology within digital manufacturing.

To conclude, we will take the opportunity to revisit a previous topic within the thesis, regarding the fundamental research efforts required for AM to reach its full potential and widerspread adoption within industrial manufacturing. Huang et al. [HLMD15] specifically recommended six key areas in this regard. As before, they will be listed here. However, this time they will be annotated with the thesis contributions, in order to demonstrate their broad scope and relevance. The recommendations were:

- Materials: Development of process materials with known and specified properties.
- Design: Focus on design tools throughout the pipeline.
  [Contribution C, D]
- Modeling: Development of physically based mathematical process models.
- Sensing and Control: Development of sensors for quality and process control.
  [Contribution A, B, C, D, E, F, G, H]
- Process Innovation: Development of faster and improved AM processes.
  [Contribution G, H]
- Systems Integration: Cross-disciplinary integration from a systems perspective and its place in the cyber-physical factory.
  [Contribution I, J, K]

The above recommendations remain relevant to this day. Although some topics have received more attention than others, it is believed that innovation within sensing and control will contribute significantly to the other areas. In particular, it will increase understanding of the various AM processes, and will as a result serve as an empirical foundation for physically based process modelling and material development. Therefore, the emphasis should be to relay the work of this thesis into practice within industry. In order to facilitate adoption of these technical demonstrators, it is important that these solutions are standardized with established traceability. Therefore, continued development needs to maintain a metrological focus.

It is clear that the work performed in this thesis has contributed to relevant topics within additive manufacturing. In particular, the work has related to the aforementioned recommendations for successful adoption of AM within industry. In the end, it is believed that the work has improved state of the art, made possible due to a cross-disciplinary approach.

Contribution A

Quality Assurance Based on Descriptive and Parsimonious Appearance Models

Material Appearance Modeling Workshop (2015), pp. 1–4
Holly Rushmeier and Reinhard Klein (Editors)

Quality Assurance Based on Descriptive and Parsimonious Appearance Models

J. B. Nielsen, E. R. Eiriksson, R. L. Kristensen, J. Wilm, J. R. Frisvad, K. Conradsen, H. Aanæs

Technical University of Denmark

Abstract

In this positional paper, we discuss the potential benefits of using appearance models in additive manufacturing, metal casting, wind turbine blade production, and 3D content acquisition. Current state of the art in acquisition and rendering of appearance cannot easily be used for quality assurance in these areas. The common denominator is the need for descriptive and parsimonious appearance models. By 'parsimonious' we mean with few parameters *so that a model is useful both for fast acquisition, robust fitting, and fast rendering of appearance. The word 'descriptive' refers to the fact that a model should represent the main features of the acquired appearance data. The solution we propose is to reduce the degrees of freedom by greater use of multivariate statistics.*

Categories and Subject Descriptors (according to ACM CCS): I.4.1 [Image Processing and Computer Vision]: Digitization and Image Capture—Reflectance

1. Introduction

Much work has gone into formulating radiometric models of surface reflectance for believable photorealistic rendering of material appearance. This has led to a number of physically plausible models with intuitively meaningful parameters that are appropriate for direct manipulation [MHH*12]. In this positional paper, we discuss the use of appearance models in a different context, namely in quality assurance of physical and digital products. We argue that this area of application requires models with few parameters, or parsimonious models. Through our example use cases, we further argue that there is a significant need for such parsimonious models, and that effort should be put into their development.

The need for parsimonious radiometric models manifests itself when we need to estimate the radiometric properties of surfaces in practice, e.g. when doing industrial inspection to ensure that the products have the specified visual properties, or when we would like to acquire photorealistic models from images. In such cases, the number of measurements is limited, maybe 5 to 20 per surface patch. This should be seen in light of the number of measurements needed to reliably estimate a general bidirectional reflectance distribution function (BRDF). A BRDF is modeled by a 4D manifold and is typically measured using a spherical gantry (a gonioreflectometer). This means that a very large number of measurements is required, which in many cases is practically infeasible.

According to the philosophy associated with Occam's razor, the formulation of descriptive and parsimonious models will also force us to better model and understand the underlying radiometric phenomena. Thus, in the end, our models should hopefully lead to physically plausible models with few intuitively meaningful parameters as is needed for the more classical applications of appearance models. We believe that it is possible to make large advances in this direction, meaning that the task of formulating parsimonious models does not seem to be a frugal one.

2. Relating to existing models

Previous work has shown that the classical empirically and physically based computer graphics reflectance models cannot fit all measured reflectance data well [NDM05]. This has led to a quest for models that provide a better fit [BSH12, LKYU12]. The cost of a better fit is an increase in the number of model parameters, and the simplest model (the Phong model [Pho75]) already has two parameters per color band and one parameter to describe the material glossiness. As such, the simplest model requires at least seven measurements although ideally many more to robustly fit measured reflectance data. In applications of real-time reflectance acquisition, this quickly becomes infeasible.

The fitting of most parametric models is far from triv-

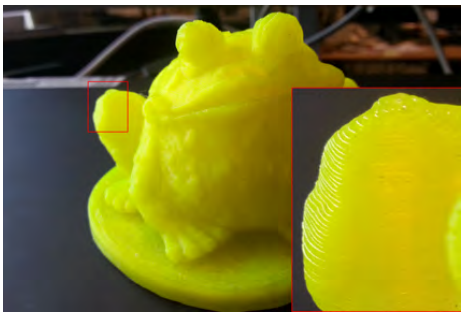

Figure 1: *Frog printed out of Polylactic acid (PLA) plastic using a Fused Deposition Modeling (FDM) printer.*

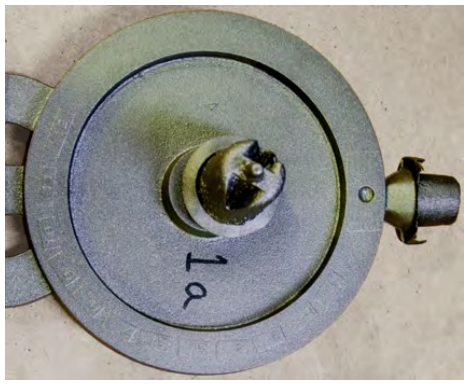

Figure 2: *Example of iron casting [VSRT15], where the mould has introduced a surface roughness affecting the visual appearance of the product. Image is courtesy of Nikolaj Kjelgaard Vedel-Smith.*

ial. Major challenges include determining what optimizers to use and what objective functions they should minimize. For the latter, various suggestions have been proposed including L_1 minimization [NFCA14] and log-transformation with cosine-weighting of observed data [NDM05]. To address the issues of non-linear model fitting, alternative approaches have been proposed where reflectance is modeled by linear combinations of basis functions. Suggestions to basis functions include spherical harmonics [WAT92], wavelets [SS95], and densely sampled reference reflectances [MPBM03]. The advantage here is that fitting models to observations becomes extremely easy as this corresponds to solving a linear system of equations. The challenge however, which is an unsolved problem, is identifying a *sparse* set of basis functions that model a wide variety of material appearances well. We need, as a community, to work on this.

3. Relevant Cases

To argue relevance, we now describe four cases where we have identified that the current radiometric models or acquisition methods simply do not suffice. The cases are (1) additive 3D printing, where the 3D microstructures caused by the printing process cannot be modeled well by standard reflectance models; (2) real-time monitoring of reflectance in metal production; (3) estimation of surface reflectance on massive objects (wind turbine blades); and (4) reflectance models to be used with 3D scanners to allow simultaneous acquisition of geometry and appearance. These are all problems that cannot be solved by conventional methods.

3.1. Additive Manufacturing

For the past decade, additive manufacturing (3D printing) has been an accepted production method. Today, it is possible to manufacture products in multiple materials ranging from soft polymers to metals [WC13]. A rapidly growing market of internet printing services is emerging (shapeways.com and i.materialise.com, for example) where users can upload their own 3D models for printing. Fast and realistic material rendering is of great interest to these types of services, allowing users to previsualize the printed outcome of their models prior to committing to purchase. However, accurately obtaining these radiometric models is a challenge. The layer-like nature of the printing process yields surface artifacts, the most prominent known as the 'staircase effect' which drastically alters material appearance for some materials. Visually, we observe this as a local anisotropy, often correlated with the surface curvature, see Figure 1. Thus the printing process itself must be considered when producing an accurate model of the printed appearance.

Radiometric model acquisition also has an application in the quality assurance aspect of additive manufacturing. So far, most effort has been placed on in-line geometric verification of parts [HNRP14, PH14] and color verification [EPA15]. These optical systems capture each and every layer during the print in order to verify its correctness. Combinations of such systems along with rapid radiometric acquisition could prove beneficial as slight deviations from the material optical properties could indicate failure due to e.g. overheating (color change) or structural collapses (surface normal orientation). In essence, we need to verify the quality of 3D prints, but practical constraints limit the number of measurements that it is possible to acquire.

3.2. Metal Casting

Metal casting is still an actively used production method. Casting allows for the creation of seamless and rigid structures in various materials. However, post machining of said

Figure 3: *Wind turbine blade right after molding.*

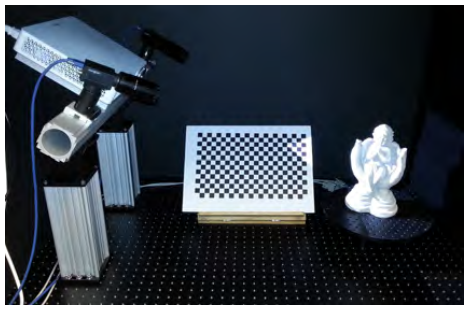

Figure 4: *Structured Light system scanning a statue.*

objects is in many cases required due to the rough surface texture resulting from the casting process, see Figure 2. Measurements of surface roughness parameters are useful for industry and academia in order to optimize the casting procedure as it is related to the overall cast quality. Obtaining surface roughness parameters from optical reflectance is thus of great interest and is an active field of research [NTH13]. As in the case of additive manufacturing, we see a scenario where practical constraints limit the feasible number of measurements, thus creating a demand for accurate parsimonious reflectance models that enable robust fitting.

3.3. Wind Turbine Blades

One of the most important steps in quality inspection of wind turbine blades is to find transverse folds in their longitudinal fiberglass mats. The longitudinal mats run all the way from the root of the blade to the tip and provide the blade with the bulk of its rigidity and strength. Multiple layers of longitudinal mats are needed to provide the necessary strength, and the load must be evenly distributed across the layers. If one layer has a fold, that layer will be tightened harder than the rest of the layers, thus carrying more load when the blade is being operated. Over time, this increased load will wear the fold-layer down to the point where it snaps and thereby compromises the entire structure of the blade. Usually, this sudden release of tension creates a force on the remaining layers so that these also snap. The result is a broken blade.

Before painting, wind turbine blades are translucent due to their composition of transparent epoxy resin and fiberglass (see Figure 3). A fold on a fiberglass mat will create a bulge beneath the surface which alters the optical properties of the material. Currently, specially trained quality engineers shine powerful light parallel to the surface and look for changes in the reflections. An accurate automated measure of surface BRDFs could increase the efficiency and accuracy of the quality assurance by transforming the fold inspection from a qualitative process into a quantitative process.

3.4. Creating 3D Content

Optical 3D scanners are actively used throughout various fields such as archaeology, biology, production, entertainment, medicine, and art. All aiming to capture high resolution 3D models in a relatively short amount of time. However, in order to produce realistic and applicable digitization of scanned objects, their radiometric properties must also be determined. Many commercial systems provide the ability to capture surface textures in order to provide more aesthetically pleasing models, but are often limited to assuming Lambertian behaviour or at most a simple parametric model, such as Phong [Pho75] or Ward [War92]. As indicated in Section 2, these models fail to fit the reflectance properties of many real-world materials. Trouble is that we cannot improve the fit by increasing the number of model parameters as we need to acquire reflectance properties at speeds comparable to the 3D scanning process. This underlines the need for descriptive and parsimonious appearance models.

An interesting property of structured light (SL) scanners is the fixed angle between observer (camera) and lightsource (SL projector). This is illustrated in Figure 4. Using only existing components of such a setup thus poses a constraint on the observable regions in the BRDF domain. Likewise, the geometry also dictates illumination and view directions relative to the surface normal. Hence, again we see a practical limitation on the available observations, which causes a demand for parsimonious models that enable robust fitting.

4. Discussion

From the above, it is evident that there are number of relevant cases where today's methods do not suffice. We believe that the problems in the mentioned cases can be solved, but that they require us to approach material appearance modeling from a new angle. Specifically, we believe that data analysis and multivariate statistics should be involved more than we see it today, and also that we should introduce stronger priors on the data. Such tools are necessary to considerably

reduce the degrees of freedom in the problems. A solution of this kind will greatly contribute to streamlining and automating the entire production pipeline, which is an essential part of agile product development.

Conclusively, we would like to reiterate that descriptive and parsimonious reflectance models seem indispensable if we are to use material appearance models in the context of quality assurance of printed, molded, and digitized products.

References

[BSH12] BAGHER M. M., SOLER C., HOLZSCHUCH N.: Accurate fitting of measured reflectances using a Shifted Gamma micro-facet distribution. *Computer Graphics Forum (Proceedings of EGSR 2012) 31*, 4 (June 2012), 1509–1518. 1

[EPA15] EIRIKSSON E., PEDERSEN D., AANAES H.: Predicting color output of additive manufactured parts. In *Proc. ASPE Spring Topical Meeting on Achieving Precision Tolerances in Additive Manufacturing (26-29 April 2015, Raleigh, North Carolina, USA)* (2015), pp. 95–99. 2

[HNRP14] HANSEN H., NIELSEN J., RASMUSSEN J., PEDERSEN D.: Performance verification of 3d printers. In *Proc. ASPE Spring Topical Meeting on Dimensional Accuracy and Surface Finish in Additive Manufacturing (13-16 April 2014, Berkeley, CA, USA) pp* (2014), pp. 104–107. 2

[LKYU12] LÖW J., KRONANDER J., YNNERMAN A., UNGER J.: BRDF models for accurate and efficient rendering of glossy surfaces. *ACM Transactions on Graphics 31*, 1 (January 2012), 9:1–9:14. 1

[MHH*12] MCAULEY S., HILL S., HOFFMAN N., GOTANDA Y., SMITS B., BURLEY B., MARTINEZ A.: Practical physically based shading in film and game production. In *ACM SIGGRAPH 2012 Courses* (2012), no. 10. 1

[MPBM03] MATUSIK W., PFISTER H., BRAND M., MCMILLAN L.: Efficient isotropic BRDF measurement. In *Rendering Techniques (Proceedings of EGSR 2003)* (June 2003), pp. 241–247. 2

[NDM05] NGAN A., DURAND F., MATUSIK W.: Experimental analysis of BRDF models. In *Rendering Techniques (Proceedings of EGSR 2005)* (2005), pp. 117–126. 1, 2

[NFCA14] NIELSEN J. B., FRISVAD J. R., CONRADSEN K., AANÆS H.: Addressing grazing angle reflections in phong models. In *SIGGRAPH Asia 2014 Posters* (2014), ACM, p. 43. 2

[NTH13] NWAOGU U. C., TIEDJE N. S., HANSEN H. N.: A non-contact 3d method to characterize the surface roughness of castings. *Journal of Materials Processing Technology 213*, 1 (2013), 59–68. 3

[PH14] PEDERSEN D., HANSEN H.: Comparability of the performance of in-line computer vision for geometrical verification of parts, produced by additive manufacturing. In *Proc. ASPE Spring Topical Meeting on Dimensional Accuracy and Surface Finish in Additive Manufacturing (13-16 April 2014, Berkeley, CA, USA) pp* (2014), pp. 179–183. 2

[Pho75] PHONG B. T.: Illumination for computer generated pictures. *Communications of the ACM 18*, 6 (1975), 311–317. 1, 3

[SS95] SCHRÖDER P., SWELDENS W.: Spherical wavelets: Efficiently representing functions on the sphere. In *Proceedings of the 22nd annual conference on Computer graphics and interactive techniques* (1995), ACM, pp. 161–172. 2

[VSRT15] VEDEL-SMITH N. K., RASMUSSEN J., TIEDJE N. S.: Thermal distortion of disc-shaped ductile iron castings in vertically parted moulds. *Journal of Materials Processing Technology* (2015), 262–271. 2

[War92] WARD G. J.: Measuring and modeling anisotropic reflection. In *SIGGRAPH 92* (1992), pp. 265–272. 3

[WAT92] WESTIN S. H., ARVO J. R., TORRANCE K. E.: Predicting reflectance functions from complex surfaces. *Computer Graphics (Proceedings of ACM SIGGRAPH 92) 26*, 2 (July 1992), 255–264. 2

[WC13] WOHLERS T., CAFFREY T.: Additive manufacturing and 3d printing state of the industry annual worldwide progress report. 2014. *Wohlers Associates* (2013). 2

Contribution B

Spatial Accuracy of Embedded Surface Coloring in Color 3D Printing

SPATIAL ACCURACY OF EMBEDDED SURFACE COLORING IN COLOR 3D PRINTING

David B. Pedersen[1], Hans N. Hansen[1], and Eyþór R. Eiríksson [2]
[1]Department of Mechanical Engineering
[2]Department of Applied Mathematics and Computer Science
Technical University of Denmark
Kgs Lyngby, Denmark

INTRODUCTION

Recent years, the industrial market for full-color AM is growing rapidly. In the AM industry, most of the major technology providers are developing new systems with improved color capabilities and with improved materials. In the last 12 months alone, 5 new technology platforms have been revealed capable of full-color printing in polymers[1]. Industrial service providers increasingly expand their product-range of full-color print services, and as of today, the industry for full-color parts has grown rapidly, into a million-dollar industry [2]. With a new market emerging at such pace, it is believed a necessity to consider a new surface-metrological issue. To what accuracy are colors embedded to the surface of geometries, with relation to where specified from input data? This paper investigate the accuracy of surface coloring, by adopting a well-known metrological approach from calibrating Coordinate Measurement Machines (CMM's) and Machine Tools, that already has been transferred to be applicable for AM machine tools, [3] in order to determine the spatial accuracy of embedded color features to artifacts printed on a zCorp 650 color 3D Printer. The spatial color verification artifact is a flat plate with a series of checkered fields on the surface.

METHOD

Following an approach developed by Hansen et al.[3] for geometrical verification of 3D printers in the horizontal plane, a series of four checkered plates was generated. Each artifact contains a series of checkered fields in one of the z650 printer's base colors, as illustrated in *figure 1*.
Upon printing the checkered artifacts, one for each base-color, these can subsequently be mapped by means of an optical CMM. A calibrated DeMeet 220 from Schut Geometrical Metrology was used to find the centre of each checkered field in order to determine the spatial position of these. The measured positions are compared to the ideal of the CAD body, and the differences are mapped. The mapping of the geometrical coloring accuracy in the horizontal plane is finally plotted, in order to describe the spatial color performance of each color channel of the zCorp printer.

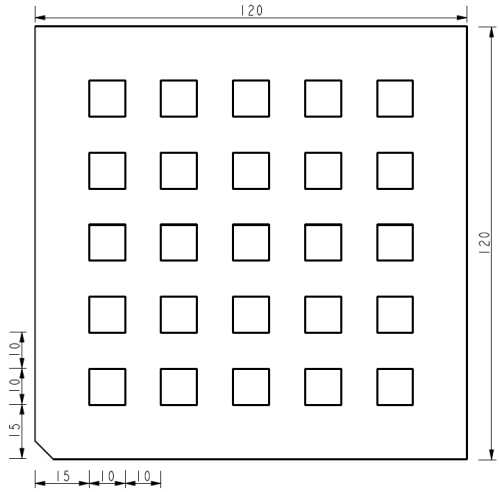

FIGURE 1. Color calibration artifacts. Each checkered field represent a field colored in one of the base colors of the 3D printer.

ARTIFACT GENERATION

A common method for embedding colors to 3D geometries is by texturing. If textures are applied to geometry, the spatial accuracy of the color representation is governed on-screen by the texture file format. Image textures on CAD bodies are often handled in image file formats employing lossy image compression that will introduce a pixilation effect known as compression artifacts.[4] As a result of this, the subsequent printing of the geometry will be carried out by multiple inkjet print heads, using more than one base-color. Furthermore the

capabilities of the engine in the software renderer used to display the geometry affect the accuracy of the rendered geometry, predominant when texture wrapping occur. Following this analogy, there is a risk that the accuracy of the color representation on the printed verification artifacts will be affected by the proprietary job generation software of the printer if a textural coloring of the calibration artifacts was used. To prevent this, it was decided to generate the checker board geometries by means of a tailored python script. This makes it possible to output the 3D geometries in the .OBJ with a per-face color definition, as seen in *figure 2*, to serve as the calibration artifacts. With this approach, it can be ensured that no issues related to texture interpretation and misalignment in the proprietary printer software can occur as each checkered field was generated as facet pairs, with a per-face base color defined. This eliminates the risk of error sources from the 3D body that may be transferred to the print job.

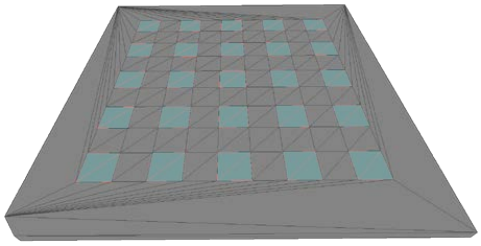

FIGURE 2. Per-face coloring of checkers. Each checker is comprised of a facet-pair in one of the CMYK base colors.

ARTIFACT MANUFACTURING

A series of four artifacts was 3D printed. Each artifact was manufactured on the z650 ink-jet based powderbed printer. z151 powder was used and the print was carried out at 0.89mm layer height with a specified 540x600 - XY DPI resolution, which corresponds to a theoretical horizontal resolution of 4.7µm. All four plates were manufactured in one print-job, and stacked in the vertical plane, so that the same kinematic characteristics in the horizontal plane was present during the manufacture of all four artifacts. *Figure 3* shows the four printed artifacts upon removal from the build-chamber of the 3D printer. No infiltration or other post-processing was carried out, in order to prevent the colors to bleed and deteriorate with respect to spatial accuracy. All artifacts have been manufactured in an orientation so that within the context of this paper, the X direction is in the direction of the print head carriage, whereas the Y direction is in the travel direction of the gantry of the printer.

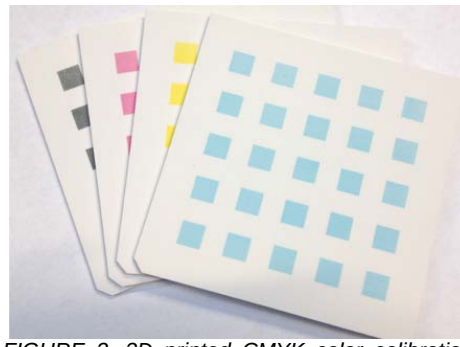

FIGURE 3. 3D printed CMYK color calibration artifacts

SPATIAL PLACEMENT

Each artifact in the CMYK color space, was measured, and for every checker, the spatial center position was determined. Measurements were carried out on a DeMeet 220 from Schut Geometrical Metrology, with x5 optics, maintained with a budgeted uncertainty of approx. ~16µm. The choice to define the spatial position of each checker by its center is in order to limit measurement uncertainties from the effect of ink bleeding out from the deposited area and into the surroundings. As seen in *figure 4* (right), it can be difficult to determine the exact outline of the checkers, whereas for yellow color (left), it can be hard to distinguish the color pigment from the background. Yet, the center of each checker is unaffected with respect to where along the boundary gradient, that the measurement is taken, if kept constant.

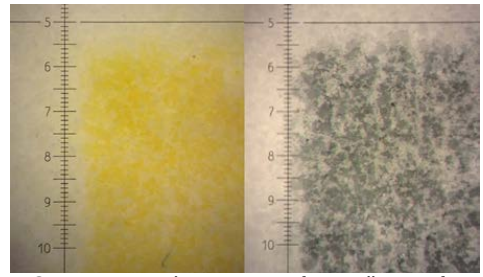

FIGURE 4. Microscopy of gradients from checker to background, K and Y color channel.

With the DeMeet 220, an NC programme was defined to allow for the construction of four lines following the sides of each checker. The line intersections define the corners of the checker, and is exported to a data file. From the four corners, two new lines are constructed. Since these four lines will not be perfect diagonals, their intersection is calculated from equations (1) and (2), for the intersection of two lines, and following the diagram in *figure 5.*

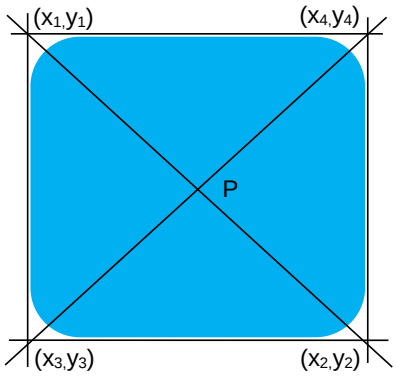

FIGURE 5. Diagram showing the center point definition (P) of a checker.

$$Px = \frac{(x_1y_2 - y_1x_2)(x_3 - x_4) - (x_1 - x_2)(x_3y_4 - y_3x_4)}{(x_1 - x_2)(y_3 - y_4) - (y_1 - y_2)(x_3 - x_4)} \quad (1)$$

$$Py = \frac{(x_1y_2 - y_1x_2)(y_3 - y_4) - (y_1 - y_2)(x_3y_4 - y_3x_4)}{(x_1 - x_2)(y_3 - y_4) - (y_1 - y_2)(x_3 - x_4)} \quad (2)$$

Finally the spatial position of every checker and thus the spatial color representation capabilities can be mapped in one plot, showing how well the z650 printer perform on the CMY and K color channel.

RESULTS

Figure 6 show the complete mapping of geometrical position errors within the four color-fields in the CMYK-space, magnified by a factor of 50, with a common origin in the lower left corner of the space. For each color channel, a grid show the position errors of each square centre, relative to the ideal position, which is shown as slashed gridlines. This makes it possible, in a single graph, to study the behavior of the z650 in the color- and the spatial domain.

An evident general trend, is that for all color channels, the scaling in both the X and Y directions of the machine are too short, resulting in an under-shoot. The error is seemingly linear, and of a magnitude of approx. 100µm in the X-direction (print head travel direction) and approx. 150µm in the Y direction (gantry travel direction). Thus, it will be extremely simple to compensate for this error contribution, if manual machine calibration will be allowed by the machine manufacturer.

Second, it can be seen that the grid lines for all color channels are skewed to the left. This is an indication of the machine axes not being orthogonal. The contribution from this error is largest in the point farthest from the common origin, with a spatial error component of app. 100µm The maximum combined position error cross the 80x80mm artifact error was found to be approx. 350µm.

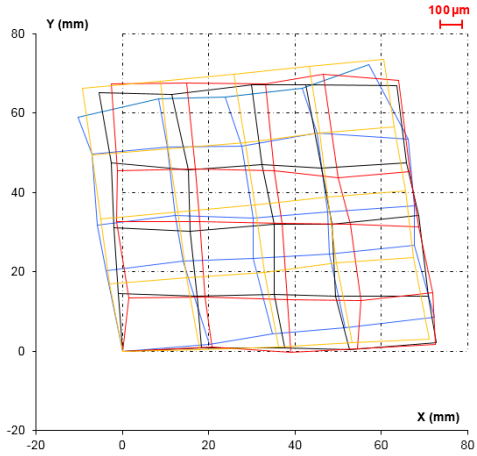

FIGURE 6. Center position of checkers compared to the ideal per color channel. Spatial position errors magnified 50 times.

The error mapping plot does also reveal errors inherent to the individual base colors, and thus the alignment of the print-heads within the tool-head of the printer. Since each color channel has been plotted with a normalized common origin, each color plot should theoretically be identical. When this is not the case, it can be

ruled down to one of two causes. First, it can be measurement errors from the measurements of the artifacts, which in this case has been carried out on accredited equipment. Second, and more plausible given the magnitude of the variance within the color-space is that it can be related to the printer having trouble with compensating for print head misalignment in software. The z650 printer has an automated print head alignment routine The routine is constituted by first, the print of a multi-colored grid spanning over the entire build plane of the machine. Subsequently a photo-sensor detects the grid, and computes a compensation matrix, that is superimposed over the machine movement, to ensure correct color deposition for all color channels. When each color channel of the verification plot in figure 6 share common origin, then it is then evident that variance between the different color channels could be directly linked to performance of the color calibration of the printer itself. Any variance within the CMY & K color can originate from this built-in routine for compensation of print head misalignment. Indications are therefore that the print heads in the z650 is aligned to ±100 µm over the area of the verification artifact.

CONCLUSIONS

Aimed to bring attention to the spatial color accuracy of Additive Machine Tools with full-color capabilities, a study was carried out to determine the spatial coloring accuracy of a zCorp 650 color capable 3D printer in the horizontal plane. The global spatial accuracy of the machine was found to be no more than 350 µm within the extent of the calibration artifact. The main error components was identified to be general axis scaling errors and skewness of the axes, affecting all color channels. A lower, yet significant error component relates to the individual color channels of the printer, and can be seen as the variance of the CMY & K grids in figure 6. Since all color channels share a common gantry and carriage, the variance between the grids from the different colored artifacts was expected to only reflect the measurement uncertainty of the CMM used for the mapping of the verification artifacts. The variance was however found to be approx. ±100 µm, well beyond the measurement uncertainty, and a suspected source of this variance has been proposed, relating to the built-in print head alignment routine of the printer. It is too early to conclude if this indeed is the direct contributor, yet a sub-standard print head alignment strategy will be a valid explanation to the cause behind the variance seen.

FUTURE WORK

It is believed that in order to achieve better spatial coloring accuracy of ink-jet based full-color AM technologies, further attention to the importance of machine calibration and verification this must be raised, and routines for correcting and optimizing color deposition must be improved. A variance between color channels of the manufactured verification artifacts indicated that better spatial coloring accuracy can be achieved by implementing a better print head alignment strategy than the one used in the machine subjected to this study. It is suggested to expand on the analysis to span over the entire horizontal build-envelope, and to expand the study to multiple artifacts for each color channel in order perform statistical hypothesis testing. Finally, this study aimed to propose a general method for spatial color verification within full color Additive Manufacturing. Vertical spatial color verification has not been carried out yet, but will yield more evidence of the capabilities of the method proposed.

REFERENCES

[1] Davide S., *Something3D Announces the Chameleon Full Color Desktop 3D Printer.* 3D Printing Industry Ltd., February 6, 2015

[2] Hooves Inc., *Company Information Register*, Accessed feb 2015. Key figures taken from Shapeways Inc, Twinkind GmbH et al.

[3] H.N. Hansen et al., *Performance Verification of 3D Printers,* ASPE Spring Topical Meeting 2014, Berkeley, California

[4] Mei-Yin Shen, C.-C.Jay Kuo, *Review of Postprocessing Techniques for Compression Artifact Removal,* Journal of Visual Communication and Image Representation, Volume 9, Issue 1, March 1998, Pages 2–14

Contribution C

Predicting Color Output of Additive Manufactured Parts

PREDICTING COLOR OUTPUT OF ADDITIVE MANUFACTURED PARTS

Eythor R. Eiriksson[1], David B. Pedersen[2] and Henrik Aanaes[1]
[1]Department of Applied Mathematics and Computer Science
[2]Department of Mechanical Engineering
Technical University of Denmark
Kgs. Lyngby, Denmark

ABSTRACT
In this paper we address the colorimetric performance of a multicolor additive manufacturing process. A method on how to measure and characterize color performance of said process is presented. Furthermore, a method on predicting the color output is demonstrated, allowing for previsualization of parts prior to print. Results show that color prediction can be achieved with an average color difference error of $\overline{\Delta E^*_{00}} = 1.5$ and std.dev $\sigma = 0.75$, with similar order of magnitude as the literature defined threshold for „Just Noticeable Difference" (JND).

INTRODUCTION
Additive manufacturing has been an accepted means of production for the past decade and is a rapidly growing market. Today, additive manufacturing technologies are offering multi-color printed parts in an assortment of different materials[1]. Availability of print per order parts, where customers can supply their own high resolution color textures and geometries, has become a reality[1][2][3][4]. Therefore, geometry and color quality assurance is required. So far, research focus has been placed on geometrical verification, giving promising results, whereas less effort has been placed on color verification[2][3]. Here we address the colorimetric performance aspect.

When converting 3D color models to the physical domain, through additive manufacturing, the enormous range of color available during modeling is not reproducible by the printer. The complete range of producible colors is known as the printers *gamut*. Any input colors outside the printable gamut will simply be constrained to a gamut boundary color, as illustrated in Figure 2. This is a known problem in the paper printing industry and is normally solved through printer profiling. Printer manufacturers sometimes offer these printer profiles which describe the printers color production capabilities according to a standard defined by the International Color Consortium (ICC).

In order to fully profile a printers color gamut, one would ideally define the input 3D model in terms of the printers native color space (*CMYK*). Unfortunately this is not possible, as color 3D mesh representations are derived from the *RGB* space. This is to be expected, as these data formats are mostly intended for use in *RGB* based devices such as a computer monitor. It is clear that the growing market of color 3D printing calls for a new or updated mesh format. To the authors best knowledge, no color 3D printing manufacturer offers color profiles or color management features. That being said and due to most printers proprietary nature, any color correction needs to be made at the 3D modeling level.

MATERIALS AND METHOD
In order to characterize the gamut of a ZCorp ZPrinter 650, a patched color plate was printed as seen in Figure 1.

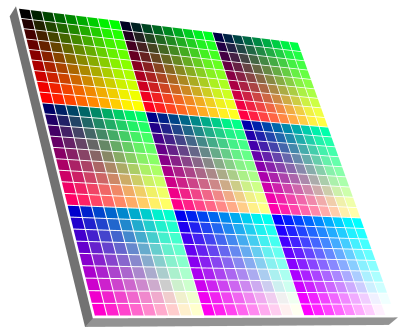

FIGURE 1. 3D model of the color calibration plate, providing 729 unique color patches.

[1]shapeways.com
[2]twinkind.com
[3]i.materialize.com
[4]figureprints.com

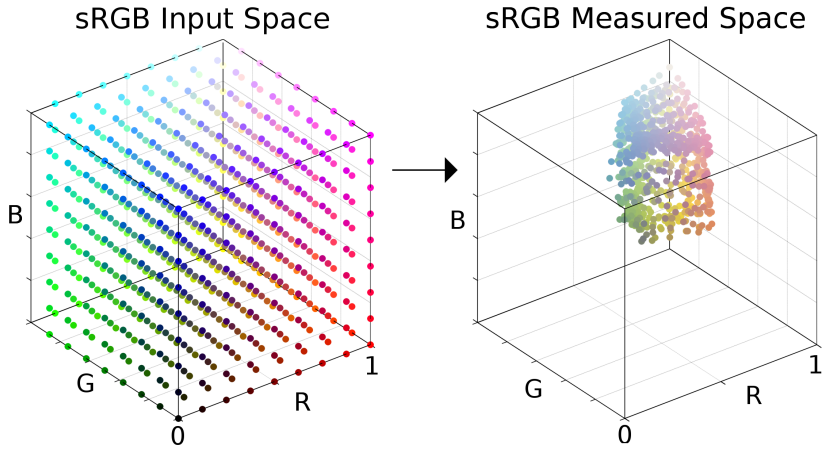

FIGURE 2. Comparison of input sRGB values to the actual measured values after print. The printers color generation limitations are apparent. Any colors outside of this printer gamut are not printable.

3D Model Generation

The color plate was generated in the Wavefront `.OBJ` format where each square in the plate was defined with a unique face color. This method was selected over applying a color image texture onto a blank plate. Thus, eliminating all uncertainties of texture handling and mapping in the printer software. The 729 unique color patches were sampled evenly from the entire three dimensional *sRGB* space, as visualized by Figure 2. This $9 \times 9 \times 9$ sample was selected due to physical size constraints set by the color measurement system used. The final plate dimensions are therefore $64.25 \times 64.25 \times 3$ mm with individual patch size of 2.15×2.15 mm.

Print Procedure

In order to capture the variability between prints, a set of 15 plates were printed in a stacked configuration, centered in the build volume. Layer thickness was set to 89 µm, bleed compensation enabled and the ZP150A powder was used. Special care was taken in thoroughly removing residual powder as to minimize color variations between prints whose effect can be seen in Figure 3. As it is known, infiltrating substances have significant effect on color vibrancy, and therefore the prints were not infiltrated in order to minimize additional variability. Modeling of this effect, dependent on infiltration type is a subject for future work.

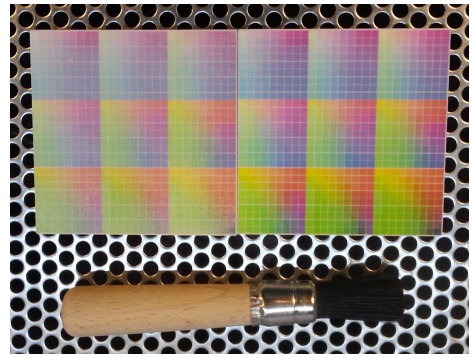

FIGURE 3. Two color plates, before brushing (left) and after brushing (right).

Measurement

Each color patch was measured using the multispectral imaging system *VideometerLab2*.[5] The VideometerLab2 allows for rapid color capture of an entire plate, contrary to other point sample based color measurement devices such as a colorimeter. Measurements were made in the device independent *CIELAB* color space under the D50 illuminant. Example output from the instrument can be seen in Figure 4. An automated color patch extraction algorithm was implemented

[5] www.videometer.com

and for each colored patch an average color value was computed, ideally simulating the perceptual integration as some color values are printed in dithered like patterns.

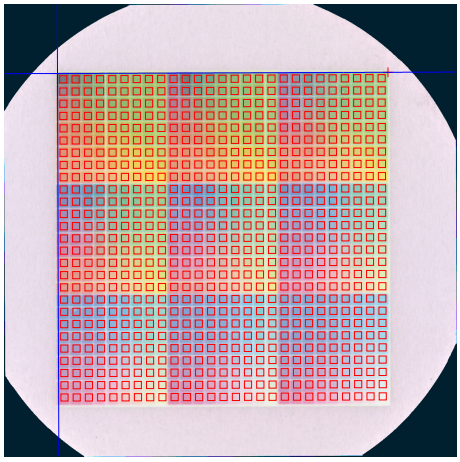

FIGURE 4. Automated patch extraction algorithm collects patches and computes their average color value.

RESULTS

An average plate was computed from all of the 15 measured plates. The color difference metric ΔE^*_{00} from the average color was computed for each color in the *CIELAB* space[4]. The color difference distribution from the mean for each plate is shown in Figure 5.

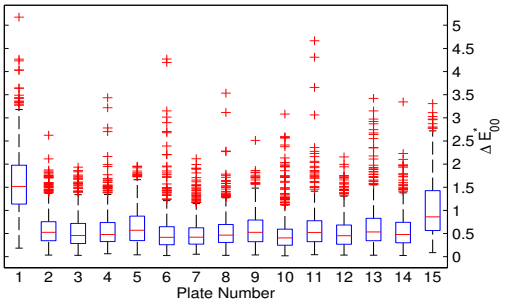

FIGURE 5. Boxplots illustrating color difference ΔE^*_{00} from the group mean. Median value is shown as a line in each box; Box edges are the 25th and 75th percentiles; Whiskers extend to the most extreme data points not considered outliers; Outliers are plotted individually.

It is apparent from the figure that the first and last plates in the stack differ significantly and are therefore omitted from the model. Further study is needed in order to evaluate whether this is a reoccurring trend. Figure 2 shows the transformation from the input *sRGB* values and the measured values. It is clear that the printer is not capable of printing a large majority of the input colors. Figure 6 clearly shows the printers inability to produce darker colors and the average color error is $\overline{\Delta E^*_{00}} = 21.4$, std.dev $\sigma = 4.15$. Several studies have tried to estimate the Just Noticeable color Difference threshold (JND) of the ΔE^*_{00} metric, however many are in disagreement. Documented JND threshold values range from 1 to 5.9[5]. The average systematic error was estimated by repeatedly measuring the same plate several times and an identical analysis performed. The measured systematic error difference was $\overline{\Delta E^*_{00}} = 0.11$ and std.dev $\sigma = 0.07$, orders of magnitude lower than the variations between prints.

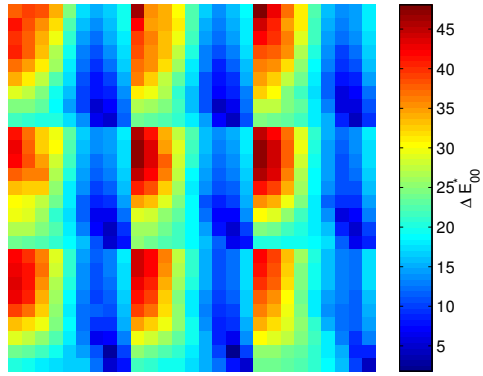

FIGURE 6. Color difference between the ideal plate and an average of the measured plates.

From the average color plate measurements, a 3D Look-Up Table (3D LUT) was constructed relating the input *sRGB* space to the measured *CIELAB* space. The input LUT is essentially a 3D lattice structure where each lattice corner contains *CIELAB* measurement data. From there, any intermediate points within a single lattice cube can be estimated using trilinear interpolation. This 3D LUT model can thus be used to predict resulting color measurements of a printed object given an input color. 3D LUTs are commonly used for this color conversion purpose and can be efficiently implemented on modern hardware.

MODEL EVALUATION

A week after the initial prints were made, a color plate as seen in Figure 7 was generated with random color values. A print prediction was performed using the 3D LUT model and the plate was printed using identical procedures as before. Post print, the plate was measured and compared to the predicted output. The color difference from the prediction obtained from the 3D LUT model and the measured plate is illustrated in Figure 8. The computed error mean was $\overline{\Delta E^*_{00}} = 1.5$ with std.dev $\sigma = 0.75$.

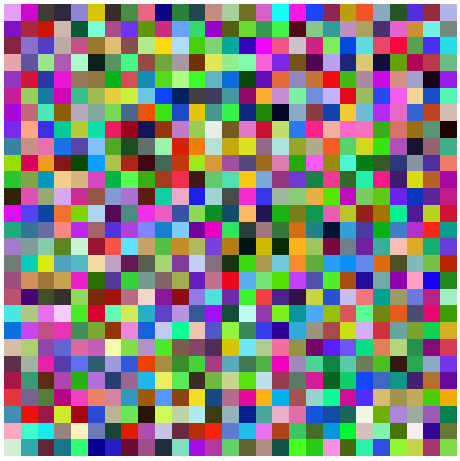

FIGURE 7. Plate with randomly generated colors, used for model verification.

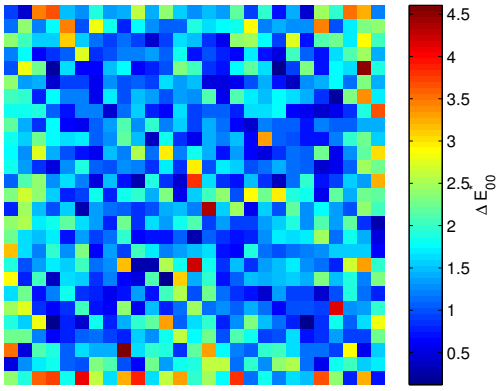

FIGURE 8. Color difference between prediction and actual measurements of the random plate.

DISCUSSION AND SUMMARY

The method described in this paper has been applied on an inkjet based 3D printer. Its variability and color limitations were visualized. When looking at the group statistics of the plates we observe the bottom and top plates to be statistically different from the rest. For the plate located in the bottom, we have two hypotheses. Firstly, the powder in the build chamber might not be compact enough in the bottom prior to print, thus yielding different surface textures. Secondly, the print head might not have reached a steady state of operation so early in the print. For the top plate, we believe it might be a factor of powder compression and drying as only a few extra layers of powder are deposited over the last plate. The remaining plates were measured using a multi-spectral imaging system with determined average systematic color measurement error of $\overline{\Delta E^*_{00}} = 0.11$ and std.dev $\sigma = 0.07$. Upon comparing the input data to an average of the measured data it was apparent that a large part of the input colors was not printed to specification. In fact, the average color error was $\overline{\Delta E^*_{00}} = 21.4$, std.dev $\sigma = 4.15$ and maximum color error greater than 45. Significantly exceeding the literature defined noticeable color difference threshold which ranges from 1-5.9. The largest error contribution was from the darker colors, particularly in the absence of red and green. These error regions are expected to somewhat heal by infiltration, where darker regions are known to benefit greatly. However, this might come at the price of the more lighter colors, as white will appear more grayish. A 3D Look-Up Table was constructed relating the input color values to the empirically measured color values. This allowed for a simple and efficient way to perform a color prediction given an input color value. If an input color value was not present in the table, trilinear interpolation was performed from the known values, yielding a color estimate. To evaluate the prediction model, a new color plate was generated consisting of randomly generated color patches. It was printed on the same printer and finally compared to the generated prediction model. The model captured the color conversion well with reasonable accuracy and an average color difference error of $\overline{\Delta E^*_{00}} = 1.5$ with std.dev $\sigma = 0.75$. This result lies within the noticeable color difference threshold range, making this method a promising candidate for color correction. Some error contribution is due to interpolation of color values, to which extent is unknown. The effect could be minimized by an even greater

sampling of the input color space. An important aspect of this study lies in the fact that the model and model verification was performed at a weeks interval, whilst the printer underwent normal use. It is therefore, interesting to see the stability of the print process and that the model holds, making this a candidate for longer term production runs utilizing the current setup.

FUTURE WORK

Reverse modeling methods will be attempted, relating the *CIELAB* output space to the *sRGB* input space. Color correction could thus be applied to the 3D modeled part prior to print. Furthermore, a further statistical analysis on the error components will be conducted.

ACKNOWLEDGEMENT

The work of this paper was supported and made possible by the Manufacturing Academy of Denmark (MADE).[6]

REFERENCES

[1] Wohlers T, Caffrey T. Additive manufacturing and 3D printing state of the industry annual worldwide progress report. 2014. Wohlers Associates. 2013;.

[2] Hansen HN, Nielsen JS, Rasmussen J, Pedersen DB. Performance Verification of 3D Printers. In: Proc. ASPE Spring Topical Meeting on Dimensional Accuracy and Surface Finish in Additive Manufacturing (13-16 April 2014, Berkeley, CA, USA) pp; 2014. p. 104–107.

[3] Pedersen DB, Hansen HN. Comparability of the performance of in-line computer vision for geometrical verification of parts, produced by additive manufacturing. In: Proc. ASPE Spring Topical Meeting on Dimensional Accuracy and Surface Finish in Additive Manufacturing (13-16 April 2014, Berkeley, CA, USA) pp; 2014. p. 179–183.

[4] Sharma G, Wu W, Dalal EN. The CIEDE2000 color-difference formula: Implementation notes, supplementary test data, and mathematical observations. Color Research & Application. 2005;30(1):21–30.

[5] Larraín R, Schaefer D, Reed J. Use of digital images to estimate CIE color coordinates of beef. Food Research International. 2008;41(4):380–385.

[6] www.made.dk

Contribution D

Designing for Color in Additive Manufacturing

DESIGNING FOR COLOR IN ADDITIVE MANUFACTURING

Eythor R. Eiriksson[1], Andrea Luongo[1], Jeppe R. Frisvad[1], David B. Pedersen[2] and Henrik Aanaes[1]
[1]Department of Applied Mathematics and Computer Science
[2]Department of Mechanical Engineering
Technical University of Denmark
Kgs. Lyngby, Denmark

ABSTRACT
In this paper we present a color design pipeline for 3D printed or additively manufactured parts. We demonstrate how to characterize and calibrate a commercial printer and how to obtain its forward and backward color transformation models. We present results from our assistive color design tool, allowing for colorimetric accurate prints and visualization of the printed outcome, prior to print. Lastly, we demonstrate our pipeline by accurately reproducing a real physical object.

INTRODUCTION
Due to physical constraints in the 3D color print process, it is impossible to print parts in all colors that we are presented with in the digital domain. The rich saturated colors are simply not available with current printer technology. Failure to acknowledge this limitation results in both disappointment and dull prints. The paper printing industry has been dealing with these problems for decades, still we have yet to see any of the solutions made available for the 3D domain. As of today, no formats supported by the additive manufacturing (AM) printer industry offer CMYK (Cyan, Magenta, Yellow, Black) color inputs, despite it being the native color space of most color printers [1]. Instead, RGB (Red, Green, Blue) is used, as the 3D formats were initially intended for display in RGB based devices, such as computer monitors and televisions.

The transformation from additive RGB colors to subtractive CMYK is handled within the printers hardware. Due to its proprietary nature and lack of color management features, any color related efforts must be made on the 3D model level. A designer is thus designing colored parts in the blind as no relationship exists between the color presented in the computer monitor and the final printed output. Previous efforts focusing on color in additive manufacturing has addressed color placement [2], appearance [3] and attempted to shed light on this problem by modeling the color conversion, thus allowing for color print prediction [4].

In this paper, we take inspiration from the paper printing industry and apply known methods on the new medium. We present a full end-to-end color design pipeline which allows for color specification. The ability to accurately specify colors and appearance of 3D printed objects has applications ranging from rapid product design, printing prosthetics or dentures seamlessly matching their hosts, and for physical replication of objects.

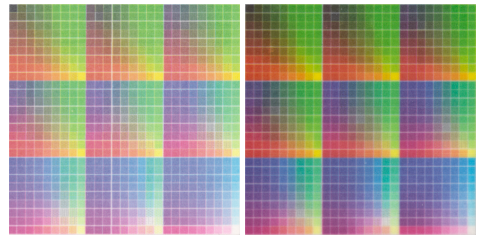

(a) Dry *(b) Infiltrated*

FIGURE 1. Printed color calibration artefacts used in this study.

CALIBRATION
In order to print user specified colors, it is important to understand the color capabilities of the printer. This is obtained by characterizing and modeling the printer's output colors in relation to its input. In this section, we present a calibration method which produces forward and backward color models of the print process. Using the forward model, it becomes possible to previsualize the resulting printed color given any input color. Furthermore, if one wishes to print a specific color, the backward model will return the input color required for producing the desired printed color or the closest available color. The calibration procedure is described in the following steps:

Step 1: Calibration Plates
A 3D color plate was generated which has colors sampled uniformly from the RGB color space. A total of 9 samples were made per dimension, resulting in 729 unique colors. We chose this value due to size restrictions of our color measurement system. Ideally, the more samples used in this process the more accurate the characterization and calibration.

Step 2: Print
Two color calibration plates were printed on a Zcorp Zprinter 650 color printer. The plates were thoroughly brushed in order to remove any residual surface powder. One plate was infiltrated with cyanoacrylate whereas the other was kept dry without any infiltration.

Step 3: Measure
Both plates were measured using the multispectral imaging system VideometerLAB 4[1]. Both CIELab D50 and sRGB D65 measurements were obtained for each color patch using an automated algorithm. Figure 2 illustrates the measured range of printable colors possible. It is clear the color gamut is significantly enhanced after infiltration, however at a slight cost of the lighter colors such as white.

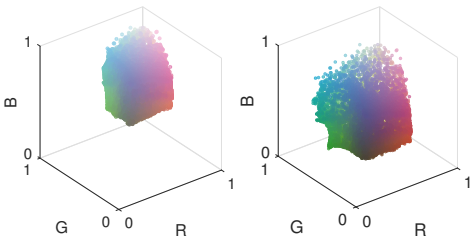

(a) Dry *(b) Infiltrated*

FIGURE 2. Visualization of the printable color range. (Gamut)

Step 4: Forward and backward model
From the empirical measurements relating input colors to measured colors we construct a 3D look up table (3D LUT) of $9 \times 9 \times 9$ elements. The table is then linearly interpolated up to $256 \times 256 \times 256$, thus covering the 8 bit RGB representation. Using the forward lookup table, it is possible to predict measured colors for all input colors. For the backward model a reverse 3D LUT was made of dimensions $256 \times 256 \times 256$ mapping measured colors to its input. For all colors outside of the printable gamut, the nearest neighbor color value was used. This resulted in an 8 bit 3D LUT which returns a color measurement for all possible inputs. By precomputing the LUTs, it becomes possible to efficiently use them as 3D textures commonly used by the computer graphics community.

Step 5: Verification
In order to verify the forward model, a new color plate was printed consisting of random colors. The plate was measured and the color difference metric ΔE^*_{00} between the model and the measurements was computed for each color in the *CIELAB* space [5]. The results for the dry and infiltrated model can be seen in Figure 3. For the dry plate we obtain an mean prediction error of $\overline{\Delta E^*_{00}} = 1.3$ and std.dev $\sigma = 0.9$. For the infiltrated plate we obtain $\overline{\Delta E^*_{00}} = 1.5$ and std.dev $\sigma = 1.2$. The increase in standard deviation is as expected since additional variability is introduced in the infiltration process. From Figure 3, it is clear that majority of points lie within the documented just noticeable difference (JND) range from 1 to 5.9 [6, 7]. The prediction model is thus considered satisfactory.

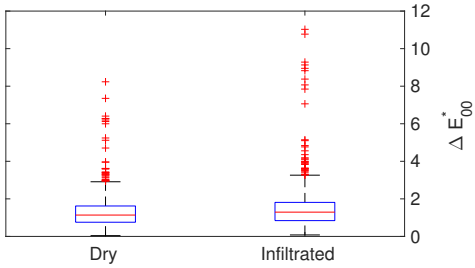

FIGURE 3. Boxplots illustrating color difference ΔE^*_{00} between the measurements and the prediction model. Median value is shown as a line in each box; Box edges are the 25th and 75th percentiles; Whiskers extend to the most extreme data points that are not considered outliers; Outliers are plotted individually.

COLOR DESIGN TOOL
After the printer characterization, we used the calibration data to develop a design tool which enables us to pre-visualize parts before print and to perform color correction if needed. The tool has been developed using the Unity-Game Engine[2].

[1] videometer.com

[2] unity3d.com

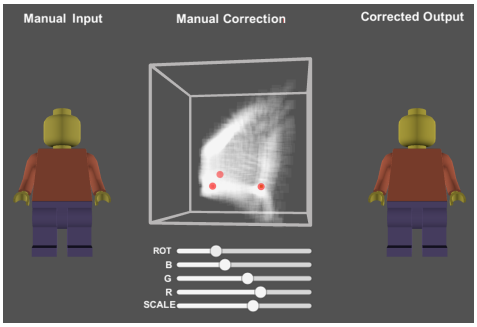

(a) Manual Mode

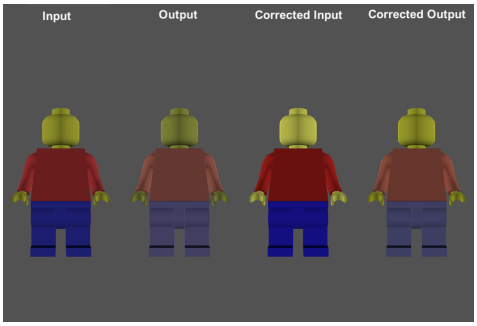

(b) Automatic Mode

FIGURE 4. Screenshots from our design tool. Showing manual and automatic modes of operation.

Figure 4 shows screenshots captured during operation. The pre-visualization feature makes use of the forward 3D LUT in order to visualize the resulting print of a 3D color model. The reverse 3D LUT is used to perform color compensation on the 3D model in order to account for the change in color due to the print process. Figure 5 shows a toy example for a 3D model of an elephant using the infiltrated 3D LUTs. It is clear that the print prediction of the model (Figure 5b) looks different from the original model (Figure 5a), while after applying the appropriate color compensations the print prediction of the model (Figure 5d) is closer to the original model even though there are still some differences in the colors of the eyes and of the tusks of the elephant.

A good color correction can be done only if the colors of the 3D model lie inside the printable color range. Our design tool provides a feature for visualizing which colors of a 3D model are outside the gamut and therefore are not possible to

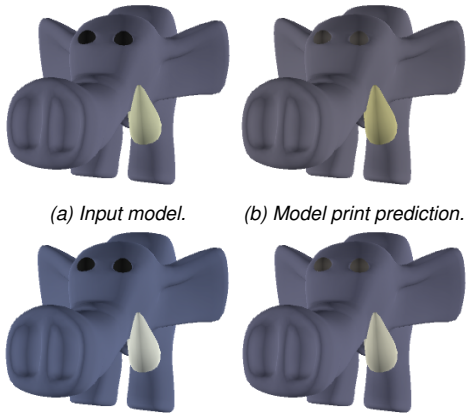

(a) Input model. *(b) Model print prediction.*

(c) Color corrected model. *(d) Corrected model: Print prediction.*

FIGURE 5. Design tool results (Infiltrated LUTs).

correct by using the measured 3D LUTs. Figure 6 shows the elephant model using the infiltrated 3D LUTs where the colors of the eyes and tusks do not lie inside the printable gamut shown in Figure 2b. As result, they are highlighted with a reddish color. For each color that is not printable, the reverse 3D LUT provides the nearest printable color, and while in some cases, e.g. elephant's tusks, this approximation might give acceptable results in other cases, e.g. elephant's eyes, the corrected color is far away from the original color. In terms of colorimetric accuracy, this might not be acceptable. However, if the goal is to produce visually pleasing results, the tool allows the user to maintain the relative relationship of colors.

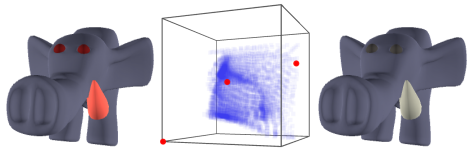

(a) Input model. Out of gamut colors highlighted in red. *(b) Gamut and input color visualization.* *(c) Print prediction.*

FIGURE 6. Design tool output using infiltrated LUTs. Model colors are marked as red dots, whereas the printable region is depicted in blue. On the model, the out-of-gamut colors are highlighted in red, alerting the user that these colors will not be printed correctly.

In order to correct the colors outside of the gamut, our tool gives the possibility to manually change the colors of the model until they all lie inside the printable color range. Then, by performing an automatic compensation based on the forward and reverse LUTs, we can visualize the print prediction of the manually-corrected 3D model. An example of this feature can be seen in Figure 6, where we see a 3D input model with the highlighted out-of-gamut colors, and the resulting print prediction of the corrected 3D model. Additionally the RGB color space is visualized dynamically where the printable gamut (blue region) and the colors included in the original 3D model (red dots) are shown. This gives the user a dynamic visual feedback of how many colors of the input model are lying outside of the gamut and therefore not printable.

The manual color correction is performed by scaling and translating the red dots representing the colors of the input model until they fit inside the region covered by the gamut. This is done interactively using sliders. The colors that are manually placed inside the gamut become printable and the reverse and forward LUTs show dynamically the color correction print prediction of the model as close as possible to the manually corrected input model. A designer thus has full control over the colors in a 'What you see is what you get' (WYSIWYG) fashion, greatly simplifying the design process.

EXAMPLE: PART REPLICATION.

To further evaluate our model and design tool, we measured a sample of cork in order to create a 3D printed replica. Figure 7 shows results from our design tool which given an input 3D color model (Figure 7a), visualizes its resulting print (Figure 7b). The tool then produced a corrected version (Figure 7c) where the infiltrated reverse 3D LUT was used to compensate for the change in color during the print process. For user verification the corrected print prediction is shown in Figure 7d.

The corrected color model shown in Figure 7c was printed on a Zprinter 650, allowed to dry, thoroughly brushed and then finally infiltrated with cyanoacrylate. In parallel, the cork was printed with and without color compensation in various sizes. The final printed output can be seen in Figure 8 where the cork replica with color compensation closely resembles the actual object, whereas the cork without compensation is observably darker.

(a) Original sample as measured. *(b) Original sample: Print prediction.* *(c) Color corrected Sample.* *(d) Corrected sample: Print prediction.*

FIGURE 7. Results from our color design tool. Demonstrating pre-visualization of parts prior to print. c) shows the color corrected sample as would be used as input to a print process. d) shows the end result, which accurately matches the original sample a).

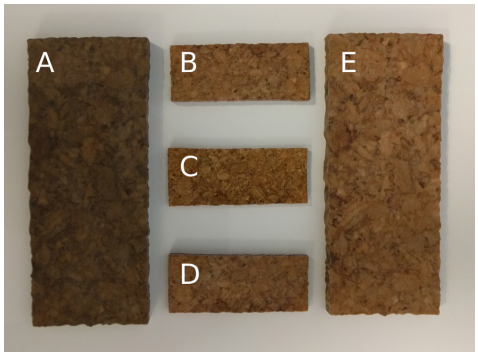

FIGURE 8. Final printed results.
A: Enlarged printed cork without color correction.
B & D: Printed cork with color correction.
C: Original cork sample.
E: Enlarged printed cork with color correction.

DISCUSSION

The process described in this paper has been implemented on an industrial color 3D printer. We demonstrated a successful calibration procedure and a method to verify its validity. The results show that accurate color predictions and calibration can be obtained with color difference error averaging comfortably under the JND metric threshold. We presented preliminary results from our

color design tool that can pre-visualize parts before print as well as apply automatic color compensation based on the calibration models. Furthermore, it offers manual means of correcting for color whilst providing visual feedback to the user in the form of a dynamic print prediction and 3D gamut plot. Lastly, we show an example where we produce a 3D replica of a real physical object. Our results show that with color compensation and careful modeling of the print process it is possible to print accurate color replicas closely matching the original object's appearance. With the help of our pipeline, it is thus possible to specify printed colors accurately. This enables the printing of colored prosthetics or dentures seamlessly matching their hosts as well as delivering true and accurate prints of designs during product development.

The design tool will be made publicly available in the near future.

ACKNOWLEDGEMENT
The work of this paper was supported and made possible by the Manufacturing Academy of Denmark (MADE).[3]

REFERENCES

[1] Wohlers T, Caffery T. Wohlers Report 2015: Additive Manufacturing and 3D Printing State of the Industry: Annual Worldwide Progress Report. Fort Collins: Wholers Associates, Inc; 2015.

[2] Pedersen DB, Hansen HN, Eiríksson ER. Spatial Accuracy of Embedded Surface Coloring in Color 3D Printing. In: ASPE 2015 Spring Topical Meeting;. p. 147–150.

[3] Brunton A, Arikan CA, Urban P. Pushing the Limits of 3D Color Printing: Error Diffusion with Translucent Materials. ACM Transactions on Graphics (TOG). 2015;35(1):4.

[4] Eiríksson ER, Pedersen DB, Aanæs H. Predicting Color Output of Additive Manufactured Parts. In: ASPE 2015 Spring Topical Meeting; 2015. p. 95–99.

[5] Sharma G, Wu W, Dalal EN. The CIEDE2000 color-difference formula: Implementation notes, supplementary test data, and mathematical observations. Color Research & Application. 2005;30(1):21–30.

[6] Hardeberg J. Acquisition and reproduction of color images: colorimetric and multispectral approaches. Universal-Publishers; 2001.

[7] Larraín R, Schaefer D, Reed J. Use of digital images to estimate CIE color coordinates of beef. Food Research International. 2008;41(4):380–385.

[3] www.made.dk

Contribution E

In-Situ Monitoring in Additive Manufacturing Using Contact Image Sensors

IN-SITU MONITORING IN ADDITIVE MANUFACTURING USING CONTACT IMAGE SENSORS

David B. Pedersen[1], Eythor R. Eiriksson[2], Henrik Aanaes[2] and Hans N. Hansen[1]
[1]Department of Mechanical Engineering
[2]Department of Applied Mathematics and Computer Science
Technical University of Denmark
Kgs. Lyngby, Denmark

INTRODUCTION

With the growing acceptance of Additive Manufacturing (AM) as a family of hyper-flexible additive machine tools, it has been an on-going objective of the Technical University of Denmark to implement flexible computer vision based geometrical verification systems for AM machine tools, allowing for automated in-situ 3D metrology[1-4]. These systems allow for automated in-situ 3D metrology. Prior art value this type of automated geometrical verification as an enabling technology that will allow for efficient verification of highly complex components manufactured by the principles of mass-customisation [4]. Earlier implementations of in-situ monitoring systems by the authors have been achieved through CCD camera technology, and allowed for complete geometrical reconstruction of manufactured parts down to 20µm in accuracy [4].

This paper presents a new and novel method for acquisition of image data in powder-bed based AM machine tools based upon contact image sensors, that has the potential to push resolution and level of integration to new heights. Contact image sensors (or line scan image sensors) are the type of sensor devices commonly found in flatbed scanners. Recent developments have resulted in the readily availability of flatbed scanners with single digit micron resolution [5-6]. The sensor of a state-of-the-art flatbed scanner has an optical resolution of up to 9600 dpi (2.65 µm) [6]. As a result of this, flatbed scanner image sensor technology has recently been used as an enabler for establishing new and effective means for geometrical verification, here amongst the application for three-dimensional analysis of roughness parameters of milled surface by the scanning of samples [7].

With inspiration from these new advances, it is proposed by the authors that by letting a contact image sensor traverse the build chamber with the re-coating unit of a powder-bed based AM machine tool, an elegant image acquisition system can be integrated into the machine tool. This new and novel method will allow for future integration by machine manufacturers to provide for an unobstructed computer vision system that automatically will scan the surface of the powder bed during the recoating procedure. Single powder grains will from the high resolution of the optical sensor be identifiable on scans, and will not only allow for geometry verification of manufactured components, but allow for ultra-precise per-layer measurements of powder grain size distribution, packing density over the build chamber and defects from the powder consolidation process, all of which can be used for closed-loop control of the machine tool. This paper serves to propose the method, and proof the method by the introduction of a fully functional prototype system, which in its first instalment will be employed for geometry reconstruction from line scan data.

In spirit of the obvious benefits from a manufacturer-integration of the system, focus has been on the realization of a prototype system, that by implementation will not increase the mechanical system complexity and does not affect the manufacturing rate of the AM machine tool onto which the system has been retrofitted. Unlike previous CCD based implementations, lens distortion and ambient light variations are not present in this new system. Image data can be used to verify the manufactured geometry, as done by the authors through Prior Art, and has the potential to generate much higher quality data than what can be achieved through CCD imaging.

METHOD

The prototype system of the proposed contact image sensor based in-situ verification system has been constructed at the Additive Manufacturing research group at the Technical University of Denmark. The system that can be seen in figure. 1 has been retrofitted on a zCorp

310 plus. The zCorp z310 is an older powder-bed system from zCorporation (now 3D Systems) that excel in its simplicity and was thus deemed an obvious candidate for the implementation of the system. The contact image sensor is a 297 mm wide image sensor from a Mustek A3 scanner with an optical resolution of 2400dpi (11µm) and with software Interpolated resolution of 9600 dpi (2.6µm). The scanner has been set up, so that the sensor will scan the build-chamber as an integrated part of the powder recoating sequence.
The current implementation does not possess an optical scan resolution where individual powder grains can be identified in acquired image data, as can be achieved, since the contact image sensor module had to be sourced with ease-of-integration in mind. Single grain identification is possible through oversampling and interpolation, but has not yet been pursued during the initial proofing of the prototype system.

Proofing and testing the system was done to prove the geometrical reconstruction capabilities of the system, based upon Prior Art [2-4] and carried out by manufacturing a hole plate artefact. From this artefact the robustness of the prototype system is subsequently assessed.

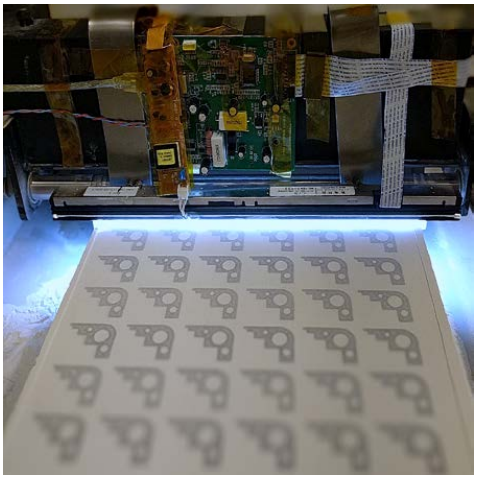

FIGURE 1. Contact Image Sensor based acquisition system on a zCorp z310 plus during a production run.

For each image acquired from the contact image sensor, a sequence of image processing is carried out. Since the contact image sensor is retrofitted to the z310, the raw image from the contact image sensor will be distorted since it is hitching along with the stock powder recoating unit, and is dependent on the predefined motion pattern for spreading a new layer of powder over the build chamber. Acceleration of the recoating unit deceases sampling density and will compress the scanned image whereas deceleration of the recoating unit increases sampling density and will stretch the scanned image. The effect can be seen in figure 2. The direction of travel of the gantry, and thus the scan direction is from left to right, where on the right hand side, the image has been stretched from the increasing sampling density during deceleration of the gantry system.

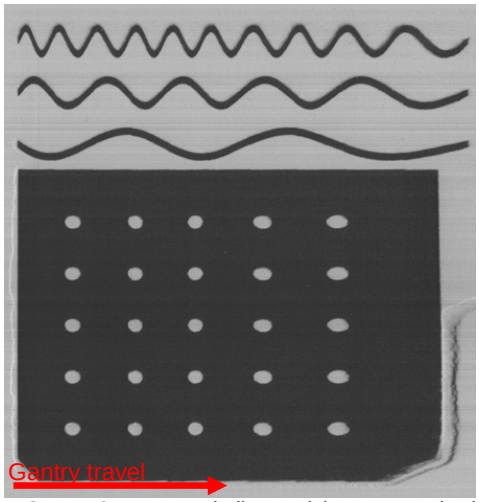

FIGURE 2. Raw and distorted image acquired from the contact image sensor. Top: Sine wave for image correction purposes Bottom: Calibration plate printed to validate the process.

The primary obstacle that was faced from treating image data was to derive the position of the gantry and recoating unit during scanning in order to take the stretching of the image into account. The position cannot be extrapolated from the machine software real-time, and it was optioned not to tap into the machine rotary encoder system. To solve this, it was chosen to use a sinusoidal position reference so that the position of the gantry of the z310 could be accounted for at all times. On a production setup

featuring the proposed in-situ scanning system, this reference is preferably comprised of a stand-alone calibrated waveform imprinted on a straight glass scale.

Spite this, it was decided to manufacture a geometry shaped as a sine wave directly with the z310 as part of the build-job, to be used as a positional encoder. This method relies on the geometrical accuracy of the z310, to validate itself, and can therefore be regarded as being flawed in its implementation. This is done by intent, to distinctly show the robustness of the system. By letting the z310 manufacture its own calibration standard along with each manufactured layer, error constituents from the vision system can be isolated. If a subsequent analysis of a reconstructed geometry shows that any measure deviates from nominal value, this is a direct indication of the variance of acquisition of image data from the contact image sensor system, and thus the reproducibility of the imaging system.

IMAGE PROCESSING & ALGORITHMS

Image processing is comprised of two major steps. The initial is to clean up and apply correction to each image frame captured during a build job. The second step is to reconstruct geometry from each captured image frame, by identifying the holes in the hole plate so that a reconstruction of the manufactured artefact can be obtained. The latter is carried out according to Prior-Art published by the authors [1-4]. Clean up and correction is carried out as follows for each image frame.

Bias removal

In order to remove intensity inhomogeneity from the raw image, a sample of the bias field is taken from the image background. From this a gain calibration matrix is generated from the bias field sample. An element-wise division of the image matrix with the gain calibration matrix is subsequently done to remove the bias field from the image.

Sine extraction

The sine wave is extracted by an element-wise thresholding in order to binarise the waveform matrix. The waveform is gathered from a mean of the thresholded waveform matrix as seen in figure 3. The waveform is finally normalized to amplitude of 1.

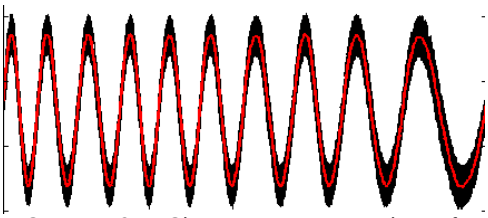

FIGURE 3. Sine wave extraction for extrapolation of contact image sensor position.

Phase extraction and unwrapping

From the sine wave, the phase is extracted using Hilbert transform. The phase angle is calculated from the Hilbert transform, and then unwrapped. The procedure can be seen in figure 4.

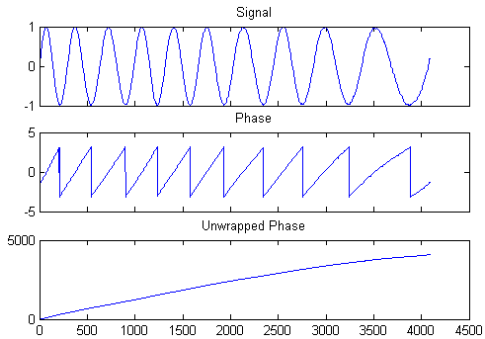

FIGURE 4. Phase extraction and unwrapping of the sine waveform.

Finally the image correction can be applied according to the unwrapped phase in the direction of gantry travel, and data gaps can be interpolated in the image matrix. This is followed by a scaling to match sensor resolution along the gantry to the length of the unwapped phase vector over the gantry travel distance.

Circle Hough Transform

Finally, in order to validate the quality of the processed image, a circle Hough Transform feature extraction is applied in order to detect the circles on the hole plate artefact. It is a specialization of Hough Transform. The result can be seen in figure 5.

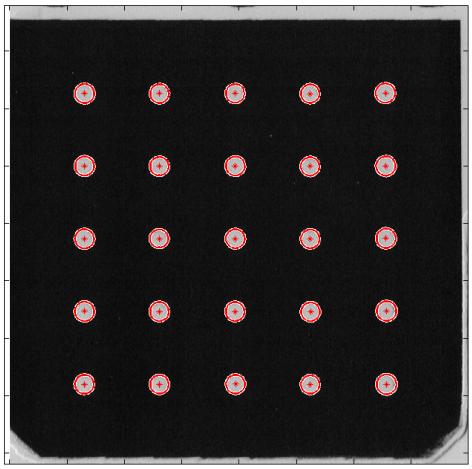

FIGURE 5. Holes detected by the Circle Hough Transform method.

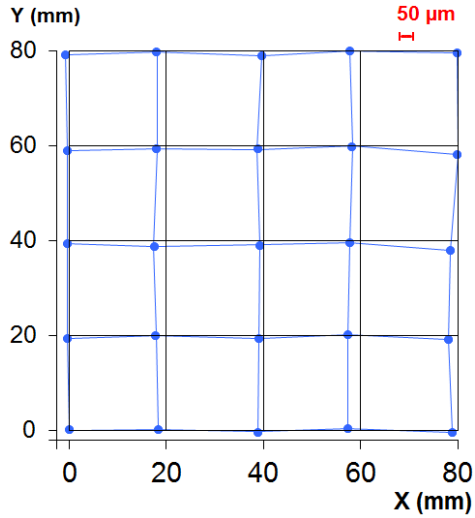

FIGURE 6. Hole positions (blue) as measured by the contact image scanner system referenced to nominal values(grid lines) at 10 X error magnification.

VALIDATION & RESULTS

Since the prototype system manufactures its own sinusoidal reference standard, all measurements are expected to conform to nominal values. Momentarily assuming the absence of measurement uncertainty from the contact image scanning system, and a complete stable AM process, every measured point will theoretically match nominal values of the manufactured artefact. Any divergence from this ideal, is therefore an expression of the decreased robustness to the ideal image acquisition system.

Validation of the method has been carried out from manufacturing the geometrical features previously depicted in figure 2. A series of 6 images was randomly chosen for validation of the method, yielding comparable results. Thus the analysis was continued focusing on one randomly selected image.

For the selected image, upon processing, each hole location detected has been correlated with the corresponding nominal value (shown as a grid) in figure 6. The plot has been magnified by a factor of 10 to clearly visualize errors that would otherwise not be perceived, and a scale bar is present in the upper right hand corner of the plot.

It can be seen that no data point in the plot is further from nominal than 50µm, and as such the image acquisition system as a whole conform within said range. More noticeably is it that the horizontal error component is larger for all data points, which indicate that better performance can be yielded if the assumptions relating to the quality of the sinusoidal reference and stability of the process not hold true, and an external calibrated sinusoidal reference is used.

CONCLUSIONS & FUTURE WORK

A method and a fully functional prototype system for Contact Image Sensor based in-situ verification of powder-bed based AM machine tools has been demonstrated. The motivation behind this work is manifold. A robust in-situ process monitoring and geometrical validation system is highly advantageous, especially if aiming to meet the visions of increasing enrolment of manufacturing equipment, tailored for mass customization. Furthermore the technology will offer the potential to monitor and control powder bed based AM processes from parameters such as the powder grain size distribution and the corresponding packing within the build chamber. Finally the system is very easily integrated into powder-bed based

systems due to the seamless integration potential with the recoating subsystem, which already traverse the build for each recoating sequence.

The system in its first implementation has shown promising results in its capabilities for acquiring image data in-situ while the machine tool is building objects, layer-by-layer. The system was shown to be in accordance with reference measurements within 50µm. A fixed calibrated sine wave ruler will in future retrofitted implementations easily be attached along the build-chamber in order to provide calibrated positional feedback. It is expected that from the current state of development within the contact- and line image sensor technology, and through ASICS/FPGA hardware, it is a matter of implementation to unleash the capability of providing ultra-high resolution scans of the powder bed surface with single digit micron precision, and real-time mapping of the powder, and thus has the potential to be one of the most capable sensor technologies for the powder-bed AM machine tool of tomorrow.

REFERENCES

[1] H.N Hansen J.S Nielsen, D.B.Pedersen, In-line monitoring and reverse 3D model reconstruction in additive manufacturing, IWMF, Daejeon, Korea, 2010

[2] H.N Hansen, D.B. Pedersen, Absolute 3D geometry reconstruction of complex additive manufactured parts using layered mesh generation, Preceedings – AEPR, Association Francaise de Prototypage Rapide, France 2010

[3] U.V Andersen, H.N Hansen, J.S. Nielsen, D.B.Pedersen, In-process 3D Geometry Reconstruction of Objects Produced by Direct Light Projection, International Journal of Manufacturing Technologies, September 2013, Volume 68, Issue 1-4, pp 565-573

[4] D.B. Pedersen, H.N Hansen, Comparability of the performance of in-line computer vision for geometrical verification of parts, produced by Additive Manufacturing, Proceedings - ASPE 2014 Spring Topical Meeting: Dimensional Accuracy and Surface Finish in Additive Manufacturing, 2014

[5] Epson Perfection V370 Photo - Flatbed scanner Specifications Sheet, Manufacturer Part# : B11B207221

[6] Canon CanoScan 9000F Mark II Flatbed Scanner Specification Sheet, Manufacturer Part#: 6218B009

[7] C.S. Goh,M.M. Ratnam, Assessment of Areal Three-Dimensional) Roughness Parameters of Milled Surface Using Charge-Coupled Device Flatbed Scanner and Image Processing – Experimental Techniques 2015, Society for Experimental Mechanics, doi: 10.1111/ext.12168

Contribution F

Precision and Accuracy Parameters in Structured Light 3-D Scanning

PRECISION AND ACCURACY PARAMETERS IN STRUCTURED LIGHT 3-D SCANNING

Eyþór R. Eiríksson[a], Jakob Wilm[a], David B. Pedersen[b] and Henrik Aanæs[a]

[a] Department of Applied Mathematics and Computer Science
[b] Department of Mechanical Engineering
Technical University of Denmark
{eruei,jakw,aanes}@dtu.dk, dbpe@mek.dtu.dk

KEY WORDS: Structured Light, 3d Scanning, Accuracy Assessment, VDI 2634 (2)

ABSTRACT:

Structured light systems are popular in part because they can be constructed from off-the-shelf low cost components. In this paper we quantitatively show how common design parameters affect precision and accuracy in such systems, supplying a much needed guide for practitioners. Our quantitative measure is the established VDI/VDE 2634 (Part 2) guideline using precision made calibration artifacts. Experiments are performed on our own structured light setup, consisting of two cameras and a projector. We place our focus on the influence of calibration design parameters, the calibration procedure and encoding strategy and present our findings. Finally, we compare our setup to a state of the art metrology grade commercial scanner. Our results show that comparable, and in some cases better, results can be obtained using the parameter settings determined in this study.

1. INTRODUCTION

Structured Light (SL) systems enable robust high quality capture of 3D geometry, and are actively used throughout several fields. These systems can be constructed using commercial off the shelf (COTS) hardware, making them accessible and affordable. The obtainable accuracy and precision of such systems vary considerably, and are mainly functions of several design parameters. The influence of these parameters has not been studied extensively in the literature. Previously, no combined study has systematically investigated the effect of common parameter choices on the final result and quantified them using an established standard.

To address the lack of work in this regard, we investigate how common design choices influence precision and accuracy. Our analysis is based on our own active stereo-vision setup consisting of two industrial cameras and a consumer projector. We empirically show our parameter selection such that maximum performance is obtained, and quantify using the VDI/VDI 2634 (Part 2) guideline. Finally, we compare our results to a commercial metrology grade scanner (GOM ATOS III Triple Scan) as a benchmark against state of the art, with decent results. Throughout this study we seek to employ widely available and accepted methods & models used in such systems to obtain easily reproducible results.

The contribution of this paper lies in the attempt to quantitatively answer the following questions

- What calibration parameters should be included in the calibration procedure?
- What angular range of observations is required in the calibration procedure?
- How many observations are required for calibration?
- Which SL encoding strategy is the overall best performer?

We believe this to be valuable information for practitioners wanting to build their own system, *e.g.* as part of research projects or industrial implementations.

This paper is structured as follows. Section 2. covers related work. Section 3. gives an overview of our experimental setup. Section 4., 5. and 6. covers our investigations on calibration parameters, calibration observations and encoding strategies respectively. In section 7. we compare our system to a commercial system and finally, we conclude in section 8..

2. RELATED WORK

Much work has been devoted to the field of SL systems *e.g.* (24, 7, 6, 11, 30). These contributions have mostly dealt with the methodological development of such systems whereas less focus has been placed on quantitative accuracy and precision analysis. One of the most important factors with respect to accuracy is system calibration. While recent focus has been placed on projector-camera calibration (32, 18, 17), we here consider an active stereo vision setup (14, 31, 33), without projector calibration. Precision is considered to be mostly dependent on the encoding strategy. A vast selection of methods have been proposed, see (26, 10, 8) for recent surveys. While many of these methods aim to reduce the number of patterns, the amount of outliers and computational complexity, less focus has been placed on precision. Here, we compare selected encoding strategies from a precision and accuracy perspective.

Characterising SL systems in terms of accuracy is a challenging and ongoing problem, which despite its relevance has only seen few published guidelines and standards. The only currently published standard is the German VDI/VDE 2634 Part 2 guideline (1, 13), *Optical 3-D measuring systems – Optical systems based on area scanning*. This guideline aims to capture the complex nature of such a system, using a number of length and shape measurements throughout the scanning volume. Researchers have already accepted this guideline for evaluation of 3D scanning systems (4, 20, 3, 2). We here argue that the guideline is lacking to some extent. Firstly, it fails to capture frequency response characteristics of SL systems using the proposed low frequency artifacts. Lastly, the artifacts are optically ideal for SL scanning. Therefore, results only indicate 'best case' results, given that particular material. The standard is however well suited for relative measures *e.g.* for acceptance testing and benchmarking purposes.

This contribution has been peer-reviewed.
doi:10.5194/isprsarchives-XL-5-W8-7-2016

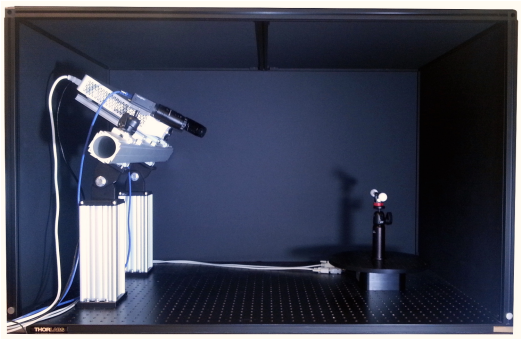

Figure 1: Our structured light system setup with two high-resolution industrial cameras, a Full HD LED projector and a rotation stage mounted on a rigid aluminum mount. Specifications are given in Table 1.

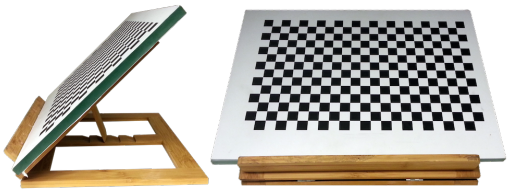

Figure 2: The calibration plate used in this study sitting on a rigid wooden support frame. Manufactured from $(400 \times 280 \times 12\ \mathrm{mm}$ unhardened float-glass. A high resolution printed checkerboard is glued on the flat surface.

Limited work has been conducted on SL parameter investigations and their effect on overall performance (19). However, to the authors knowledge, no quantitative evaluation has been performed on how the different SL parameters directly influence the final results as defined by the VDI/VDE guideline.

3. EXPERIMENTAL SETUP

Our structured light setup, as seen in Figure 1, consists of two industrial cameras (Point Grey Research GS3-U3-91S6C-C) and a high resolution DLP projector (LG PF80G) mounted on a rigid aluminum beam structure. Technical specifications are given in Table 1. In addition, a high precision turntable is used in order to provide automatic rotation of a calibration checkerboard. The apparatus and scan objects can be fully enclosed during capture, in order to prevent ambient light contamination.

Parameter	Specification
Cameras CCD	Sony ICX814 1”
Cameras Resolution	3376×2704 px
Camera Lens Focal Length	16 mm
Camera Lens Aperture	5.6
Camera Exposure	66.66 ms
Projector Resolution	1920×1080 px
Camera Baseline	450 mm
Camera Object Distance	~ 750 mm
Stereo Field of View (FOV)	$(300 \times 300 \times 230)$ mm

Table 1: Technical specifications of our structured light setup.

Figure 2 shows the calibration plate and Figure 3 shows the VDI/VDE 2634(2) measurement artifacts used during this study. The artifacts consist of a flat white painted aluminum plate and two ceramic spheres separated by a known distance. Both artifacts have been measured according to procedure T3-01 of ISM3D using a coordinate measurement machine (CMM), and traceability has been established through the virtual CMM method. Specifications for nominal values and attached uncertainties are listed in Table 2 and 3.

Figure 3: Calibration artifacts according to the VDI/VDE 2634(2) standard. Top: painted and lapped aluminum flat. Bottom: alumina-circonium ceramic spheres on a carbon-fiber rod. Nominal values are given in table 2 and 3.

Following the VDI/VDE 2634 (2), we use four quality parameters:

- Probing error form, P_F, which describes the radial range of residuals from a least squares fit sphere with up to 0.3% of the worst points rejected.
- Probing error shape, P_S, measuring the signed deviation between the least squares fit diameter and the nominal. Again, up to 0.3% of the worst points are rejected.
- Sphere distance error, SD, denoting the signed difference between the estimated and nominal distance between the spheres. Up to 0.3% of the worst points are rejected.
- Flatness, F, which is the range of residuals from the measured points to a least squares fitted plane, with up to 0.3% of the worst points rejected.

P_F and P_S are measured using one of the spheres at 10 positions within the system’s FOV. SD is measured with the ball-bar at 7 positions, while F is determined using the flat in 6 positions. These positions are illustrated in Figure 4.

Parameter	Value
Center distance	198.9612 mm
Distance uncertainty	0.001 mm
Diameter ball 1	24.9989 mm
Diameter ball 2	24.9969 mm
Min. dev. from sphere 1	-0.0013 mm
Max. dev. from sphere 1	$+0.0006$ mm
Min. dev. from sphere 2	-0.0011 mm
Max. dev. from sphere 2	$+0.0020$ mm
Deviation uncertainty	0.0018 mm

Table 2: Specification of the dumbbell used for our experiments.

Parameter	Value
Minimum deviation from plane	-0.0030 mm
Maximum deviation from plane	$+0.0012$ mm
Deviation uncertainty	0.0018 mm

Table 3: Specification of the flat plane used for our experiments.

This contribution has been peer-reviewed.
doi:10.5194/isprsarchives-XL-5-W8-7-2016

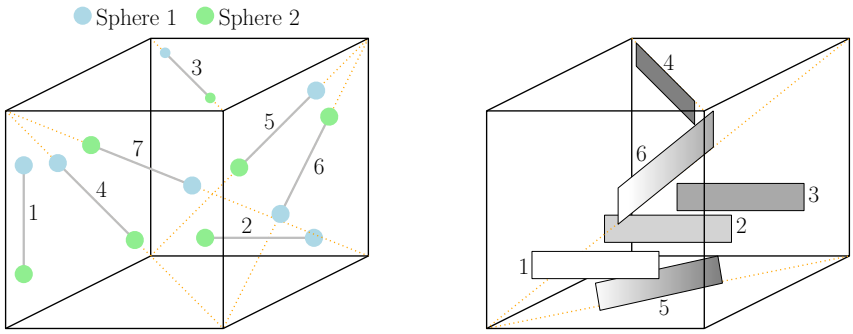

Figure 4: Measurement positions used throughout the paper. The outer frame represents the FOV, as seen from the cameras (Position 1 being closest). Left: ball-bar positions used for sphere distance SD. Right: positions of the flat used for the flatness error metric, F.

4. CALIBRATION PARAMETERS

The industry standard models that are essential for calibration of an SL system contain several parameters. Which of these parameters to include in the calibration process is unclear. To solve for the calibration parameters we employ the commonly used method proposed by Zhang (33). We use the 4 parameter pinhole model with the addition of up to five lens distortion parameters. Hence, the camera is modeled as

$$\begin{bmatrix} f_x & 0 & c_x \\ 0 & f_y & c_y \\ 0 & 0 & 1 \end{bmatrix} \tag{1}$$

The use of a non-unit aspect ratio (*i.e.*, $f_x \neq f_y$), makes it possible to model non-square pixels and/or capture compound non-uniformity in the lens. Likewise estimation of the principle point, (c_x, c_y), makes it possible to describe cameras in which the principle ray does not strike the image sensor in it's exact center. With quality components such as ours, we would expect these parameters to be unnecessary. At the same time, the inclusion of these parameters increases the risk of false estimation, numerical instability and non-convergence. In fact, it was shown, that principle point estimation is especially prone to misinterpretation, and that the parameter can often be neglected in cameras of medium to long focal length (25).

Radial lens distortion is modeled according to

$$x' = x(1 + k_1 r^2 + k_2 r^4 + k_3 r^6) \tag{2}$$
$$y' = y(1 + k_1 r^2 + k_2 r^4 + k_3 r^6) \quad , \tag{3}$$

where (k_1,k_2,k_3) are the three distortion coefficients. Tangential distortion is modeled

$$x' = x + (2p_1 xy + p_2(r^2 + 2x^2)) \tag{4}$$
$$y' = y + (2p_1(r^2 + 2y^2) + 2p_2 xy) \tag{5}$$

where (p_1, p_2) are the tangential distortion parameters. This five parameter "Brown-Conrady" model is widely accepted (5).

The stereo relationship between cameras is described using three rotations and three translations. Due to weak inter-dependencies, the calibration can be performed individually per camera, followed by stereo calibration. Still, the risk of over-fitting and converging to local minima remains, and therefore higher order distortion parameters are used only when considered relevant. To investigate these factors, we calibrate using 8 different configurations of parameters and evaluate by means of VDI/VDE quality parameters. Each calibration is performed using 81 observations of the calibration board, evenly sampled in the range from -40 to 40 degrees relative to baseline.

Figure 5 shows performance results for the different calibration parameter configurations. The baseline setting generally yields sub-millimeter results. The free aspect ratio ($f_x \neq f_y$) and principal point estimation degrade the performance from "baseline". These results show that in a typical setup, omitting the principle point estimation makes calibration significantly more stable. It can be seen that by enabling the first two distortion coefficients, significant improvement is obtained. This is especially noticeable in the sphere distance metric, SD, being a measure of accuracy. No significant improvement is obtained with additional distortion parameters.

Conclusion Given our setup, only the k_1 and k_2 distortion coefficients are required for accurate calibration. The inclusion of both aspect ratio and principle point estimation makes the calibration procedure unstable, and considerably better results are obtained without them. With their removal, we see consistently low results of P_F, SD and F, while the estimation of sphere sizes (P_S) is biased to positive values. This indicates that one should carefully consider which camera model is used.

5. CALIBRATION OBSERVATIONS

An important question in calibration is in which poses the calibration board needs to be observed. Viewing the calibration board at very shallow angles means higher uncertainty in point localization. In addition, the effect of non-planarity becomes larger. However, it is necessary to observe some degree of foreshortening for focal length estimation (33).

In this section we attempt to obtain the optimal angular range of observations relative to the baseline. We tested 8 different ranges starting from -5° to 5° relative to baseline and ending in -40° to 40°. For each range, we sample evenly 11 images of the calibration board. For the rotations performed, most foreshortening will be observed around the rotation axis, thus constraining the focal length parameter f_x well. With a fixed aspect ratio, this in turn constraints f_y also.

The results from the experiment can be seen in Figure 6. It is seen that increased foreshortening affects the sphere distance parameter (SD) positively indicating better calibration. In general, the results are quite comparable for all ranges. Comparing to Figure 5 it is also apparent that using 11 observations and 81 observations ranging from -40 to 40 yields similar results.

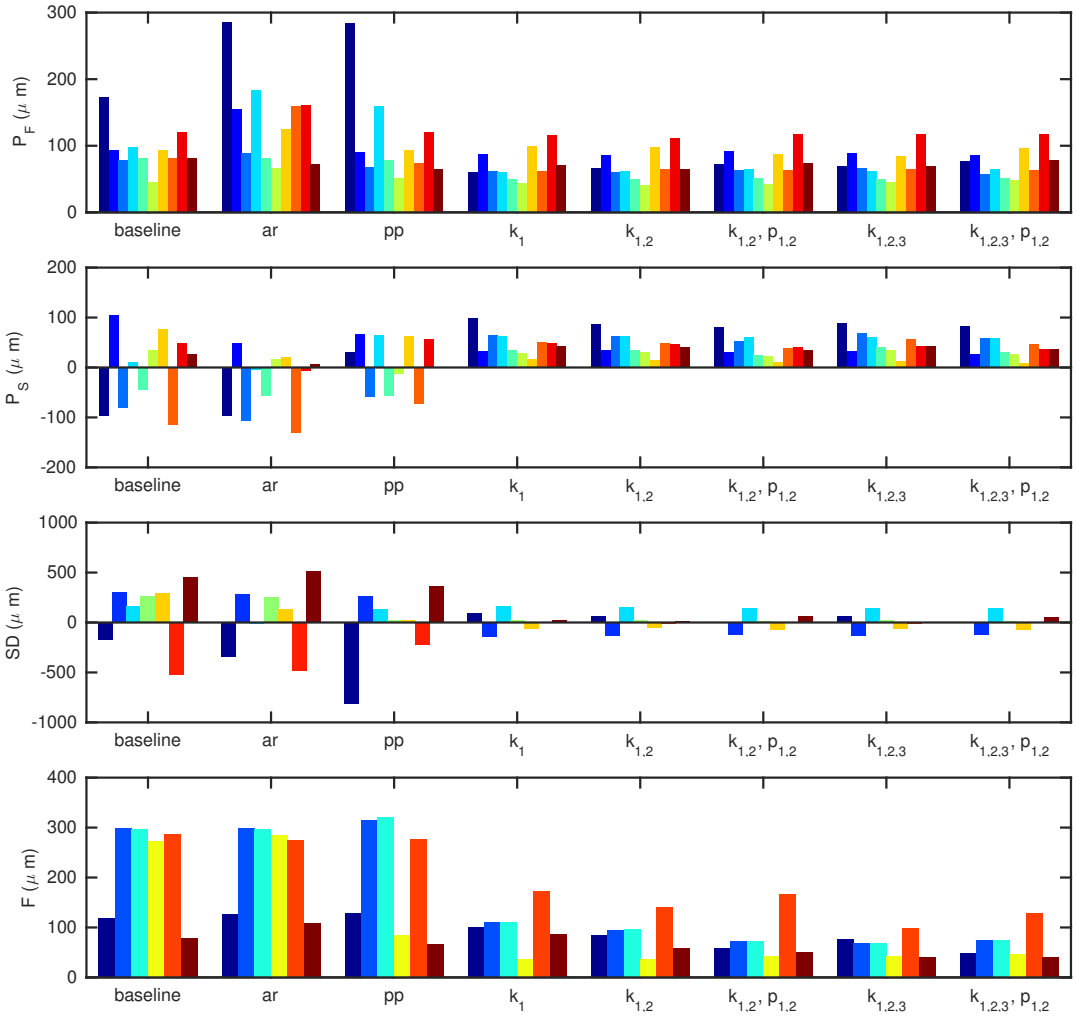

Figure 5: Results obtained with different camera and lens models. Colors represent different positions of the dumbbell or flat artifact according to Fig. 4 (Position 1 being the leftmost bar). Baseline denotes the pinhole model with fixed aspect ratio, fixed principle point and without distortion parameters. ”ar” adds aspect aspect ratio, ”pp” principle point determination. The other groups show results when different combinations of lens parameters are used. From this we see significant improvements when lens distortion parameters are added. The inclusion of both aspect ratio and principle point estimation makes the calibration procedure unstable, and considerably better results are obtained without them.

Conclusion In terms of accuracy, it is slightly beneficial to use a large angular range during calibration. However, even a smaller amount of foreshortening is sufficient to accurately estimate parameters. We opt for the 80° range. Furthermore, the difference between 11 and 81 observations is negligible, thus for the sake of practicality we proceed by using the former.

6. ENCODING STRATEGIES

The encoding strategy of a structured light system determines how correspondences are found, and can be expected to be a major factor in system precision. We identify three main categories of algorithms which are relevant in this setting:

- Fourier methods, prominently phase shifting (PS) methods (28).
- Binary boundary based methods (23), *e.g*. Binary and Gray coding.
- Line shifting (12), which is the same principle underlying triangulation based laser line scanners, with multiple lines sweeping the scene simultaneously.

Phase Shift (PS) based methods encode the scene by means of a series of shifted sinusoidal patterns. The phase is then recovered and matched between cameras (16). The advantage is that the scene can be densely encoded using at least 3 patterns, and more can be naturally added to increase precision. For correct encoding, the projector-camera system should have a close to linear intensity-response. The frequency of sinusoids can also be altered, with higher frequencies yielding higher precision at the cost of phase ambiguities, which then have to be "unwrapped" using additional patterns. Our PS implementation performs 32 steps at the highest frequency sinusoidal pattern (period $19.2\,\mathrm{px}$), and unwraps the resulting phase using two sets of lower frequency patterns (34). The total number of projected patterns is 64.

Binary boundary based methods, such as the Gray Code method, encode scene points directly by means of binary codes, which are decoded and matched in the cameras. These methods are flexible in the number of patterns, and allow for the natural addition of redundant information, which can then be used to reject outliers. Feature points locations can be estimated with sub-pixel accuracy. Our Gray code implementation encodes uniquely every other column in projector space, and employs patterns and their inverse for added robustness. Boundaries are detected at the intersection of the pattern and its inverse with subpixel accuracy. The total number of patterns is 20.

Line shifting can be performed with a single laser line as the projection source, however with a digital projector, many lines can be projected in parallel. Correspondence points are found at the peak of the stripes. Several methods exist for subpixel peak detection (29). For Gühring's Line Shifting method, we employ Gray codes to partition the encoded space into 256 unique regions. For each of these regions, a single projector line then walks across it in 8 steps, resulting in a total of 28 patterns. The peak of each single line is determined as the first derivative zero crossing using a Gaussian derivative filter of size $5\,\mathrm{px}$.

These classes of encoding strategies have fundamentally different error characteristics. The binary and line shifting methods may be very robust against point outliers, but PS patterns are often less affected by projector and camera blur due to their low-frequency nature.

Parameter	PS	Gray	Line Shift
Number of patterns	64	20	28
Off-focus robustness	Excellent	Good	Moderate
Precision	Excellent	Good	Good
Accuracy	Excellent	Excellent	Excellent
Nr. of points (sphere)	$\sim 20\,\mathrm{k}$	$\sim 7\,\mathrm{k}$	$\sim 10\,\mathrm{k}$
Nr. of points (flat)	$\sim 450\,\mathrm{k}$	$\sim 150\,\mathrm{k}$	$\sim 250\,\mathrm{k}$

Table 4: Interpretation of the algorithm performance.

The SL system is calibrated with the previously determined angular range of 80 degrees and 11 positions. Furthermore, we use the $k_{1,2}$ parameter selection, as previously identified. A comparison of the VDI/VDE quality parameter results for these three encoding strategies is seen in Figure 7. A summary of the results may be seen in Table 4.

The precision of the different strategies can be indirectly estimated from the spherical form parameter P_F. This is because the calibration spheres cover only a small part of the scanning volume, whereas the flat plane occupies a substantial part. Flat plane measurements will thus be more affected by the quality of calibration and lens distortion correction. Both of which directly affect precision and accuracy.

From the results we confirm that the PS method is more tolerant to depth of field limitations, where positions close and far away show no signs of degradation. The PS method also shows superior precision characteristics in the P_F parameter. For the P_S parameter, there is a clear bias present in both the PS and Gray code method, whereas Line Shift appears bias free. Figure 8 illustrates sphere fitting results for the three methods. Here it is seen, that PS and Gray have systematic positive residuals towards the lateral edge in horizontal (encoding) direction. This in turn leads to slight overestimation of sphere diameters.

Conclusion In the quality parameters P_F (Spherical form) and F (Flatness), the PS encoding strategy provides the best results in all artifact positions. The sphere diameter is biased positively in the PS and Gray methods, while it appears unbiased with Line Shift. Overall it appears that the PS method is the best performing method.

7. COMPARISON TO METROLOGY SCANNER

Finally, we have compared our system to a high-end commercial scanner (GOM ATOS III Triple Scan), which has a FOV of $240 \times 320 \times 240\,\mathrm{mm}$, similar to the FOV of our system (see Table 1).

In this experiment we used the PS algorithm, and calibrated as in the preceding experiment. Again, quality measures defined by the VDI/VDE 2634(2) were measured. Results are seen in Figure 9. The results show that our system is more precise and in terms of P_F and exhibits lower variance. However, a bias is present in the P_S whereas the commercial system appears free of such. It is apparent from the sphere spacing term (SD) that the commercial system indicates better accuracy.

Interestingly, the GOM scanner shows significant improvements in the flatness form error metric, F, compared to the sphere form, P_F, where one would expect similar performance (as seen in our system). Reasons for this will only be cause for speculation as the scanning procedure and reconstruction is proprietary, that being said, some form of smoothing favoring planar surfaces might be at work.

Conclusion Our system generally performs better in the precision characteristic, P_F, while the the metrology scanner obtains

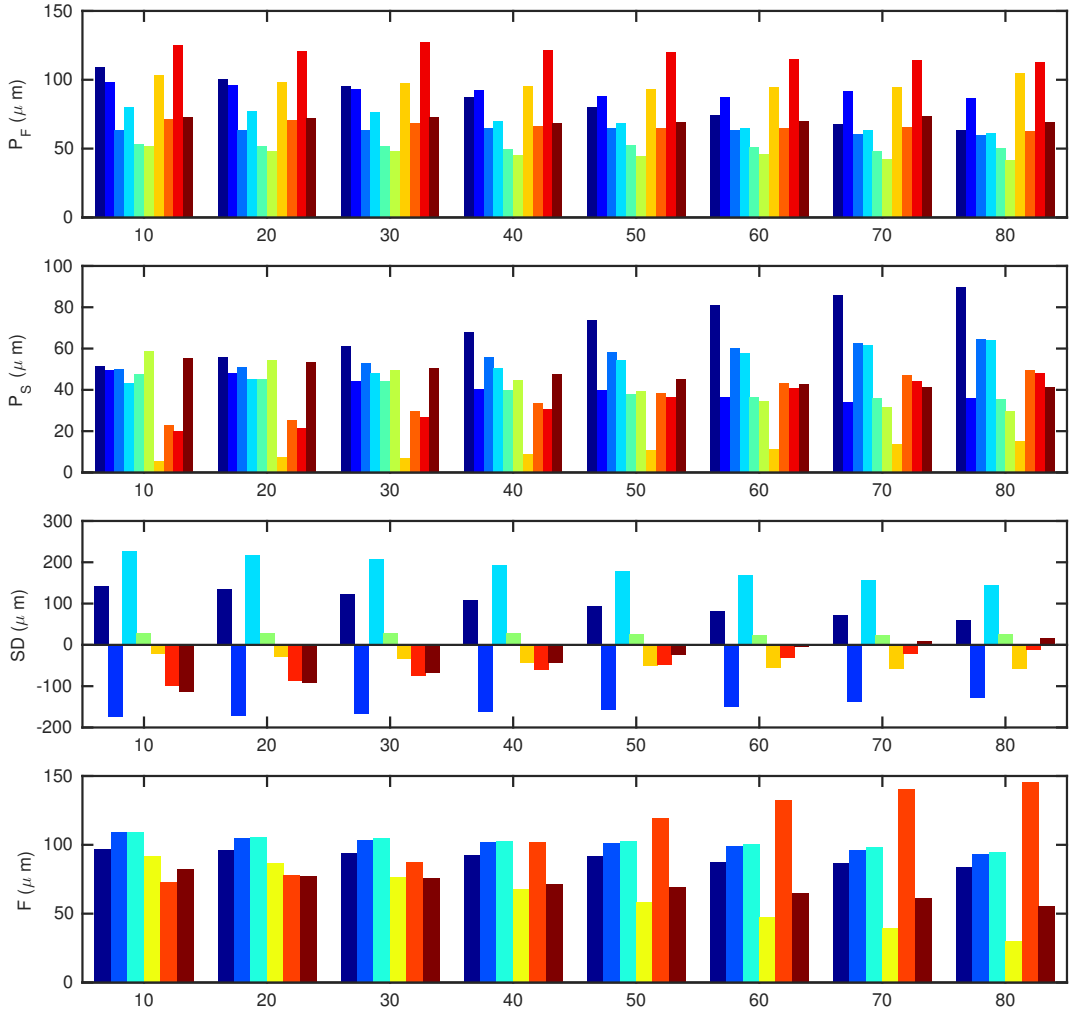

Figure 6: Results obtained with different angular ranges of the calibration plate relative to the camera baseline. Colors represent different positions of the artifacts according to Fig. 4 (Position 1 being the leftmost bar). We see that in terms of accuracy, it is slightly beneficial to use a large angular range during calibration. However, even a smaller amount of foreshortening is sufficient to accurately estimate parameters.

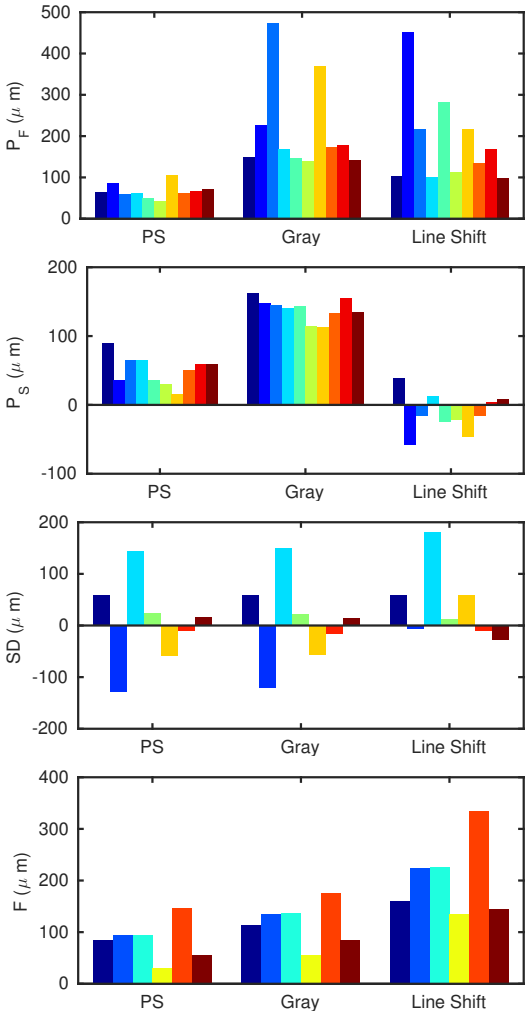

Figure 7: Results obtained with different encoding strategies. Colors represent different positions of the ball-bar or flat artifact according to Fig. 4 (Position 1 being the leftmost bar). Based on this we conclude the PS method to be the overall best performer, yielding significantly higher precision.

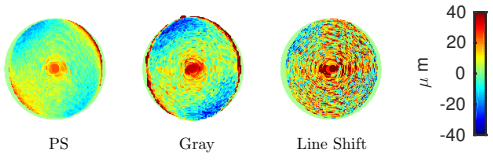

Figure 8: Fitted spheres in position 1 for our three algorithms. In PS and Gray, a bias is observed toward the edges in the horizontal (pattern encoding/epipolar line) direction, while Line Shift does not suffer from this bias. This results in an over estimation of the diameter, P_S, as seen in Figure 7.

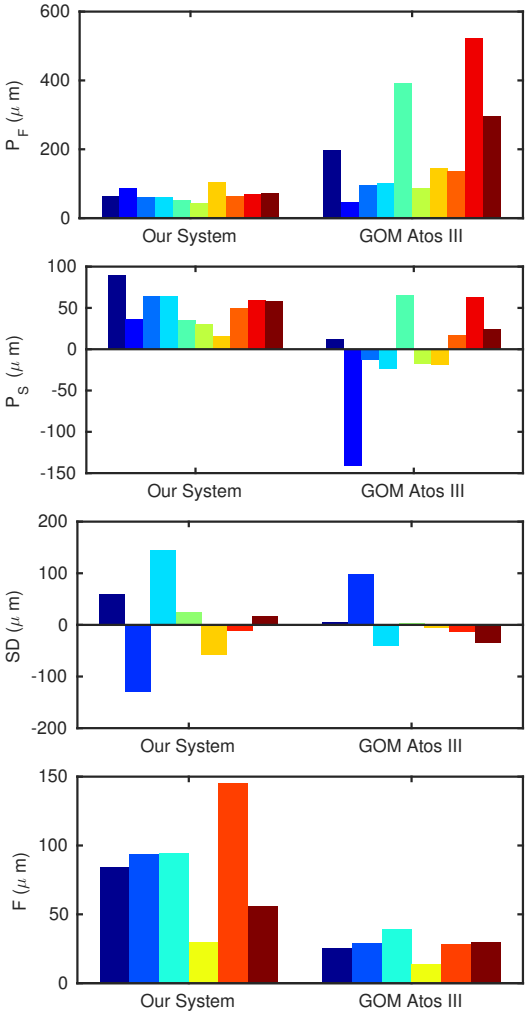

Figure 9: Results obtained with our system compared to results from a commercial metrology grade structured light scanner (GOM Atos III). Colors represent different positions of the dumbbell or flat artifact according to Fig. 4 (Position 1 being the leftmost bar).

unbiased sphere diameter results and achieves higher accuracy. Since accuracy is a deterministic noise component, this indicates that a custom calibration method could be advantageous.

8. DISCUSSION AND CONCLUSION

In conclusion, in this paper we have shown through quantitative analysis how the most common parameters within structured light systems affect the overall performance. Our quantitative measure is the accepted VDI/VDE 2634(2) guideline which nicely captures critical parameters in terms of precision and accuracy. We perform a series of experiments on our experimental setup using precision made calibration artifacts. We start by investigating calibration parameters as defined by the most commonly used models and follow by determining the angular foreshortening and the amount of observations required to yield the best results. We proceed by comparing three commonly used algorithms against each other in order to determine the best method. Finally, we compare our setup to a metrology grade commercial scanner, using the previously determined parameters. Our results show that comparable and in some cases better results can be obtained using standard methods and models if care is taken in the parameters choice. We expect these findings to be of help to practitioners wanting to build their own SL systems.

Even though the VDI guideline indirectly captures some of the error sources, such as depth of field, calibration performance and acquisition noise, it is lacking to some extent. The calibration shapes suggested consists of low frequency features, thus a Gaussian filtering operation on the measured point cloud will yield better results for some of the parameters. Although it is stated that all filtering operations must be noted; In many cases these filtering operations are required or inherent in the triangulation algorithms at a pre point cloud level. The use of such filtering will affect the frequency response of the system, where low-pass operations will limit the systems capability of resolving high frequency features. In order to better analyze a systems performance, a frequency analysis must be conducted, indicating if any such smoothing is taking place. Such a frequency response characterization calls for an additional calibration artifact in the form of a high frequency feature. In addition, results from the VDI/VDE only provide quantitative evaluation of the artifacts used. Thus the results cannot be transferred to other less optically ideal materials.

REFERENCES

The Association of German Engineers. VDI-Standard: VDI/VDE 2634 Optical 3-D measuring systems - Optical systems based on area scanning. *Beuth Verlag*, 2012.

J.-A. Beraldin, F. Blais, S. El-Hakim, L. Cournoyer, and M. Picard. Traceable 3d imaging metrology: Evaluation of 3d digitizing techniques in a dedicated metrology laboratory. *Proc. 8th Conf. on Optical 3-D Measurement Techniques*, 2007.

J.-A. Beraldin and M. Gaiani. Evaluating the performance of close-range 3d active vision systems for industrial design applications. *Proc. SPIE 5665, Videometrics VIII*, 2005.

J. Boehm. Accuracy investigation for structured-light based consumer 3d sensors. *Photogrammetrie, Fernerkundung, Geoinformation*, 2014(2):117–127, 2014.

D. C. Brown. Decentering distortion of lenses. *Photometric Engineering*, 32(3):444–462, 1966.

S. Chen, Y. F. Li, and J. Zhang. Vision processing for realtime 3-d data acquisition based on coded structured light. *IEEE Trans. Image Processing*, 17(2):167–176, 2008.

R. B. Fisher, A. Ashbrook, C. Robertson, and N. Werghi. A low-cost range finder using a visually located, structured light source. *Proc. Int. Conf. on 3-D Digital Imaging and Modeling 1999*, 24–33, 1999.

J. Geng. Structured-light 3d surface imaging: a tutorial. *Advances in Optics and Photonics*, 3(2):128–160, 2011.

A. Georgopoulos, C. Ioannidis, and A. Valanis. Assessing the performance of a structured light scanner. *Int. Archives of Photogrammetry, Remote Sensing and Spatial Information Sciences*, 38, 2010.

S. S. Gorthi and P. Rastogi. Fringe projection techniques: whither we are? *Optics and lasers in engineering*, 48(2009-001):133–140, 2010.

J. Gühring. Dense 3d surface acquisition by structured light using off-the-shelf components. *SPIE Photonics West 2001*, 220–231, 2000.

J. Gühring. Dense 3D surface acquisition by structured light using off-the-shelf components. *SPIE Photonics West 2001*, 220–231, 2000.

G. Guidi. Metrological characterization of 3d imaging devices. *SPIE Optical Metrology 2013*, 2013.

J. Heikkila and O. Silvén. A four-step camera calibration procedure with implicit image correction. *Proc. CVPR*, 1106–1112, 1997.

L. Iuliano, P. Minetola, and A. Salmi. Proposal of an innovative benchmark for comparison of the performance of contactless digitizers. *Measurement Science and Technology*, 21(10):105102, 2010.

P. Kühmstedt, C. Munckelt, M. Heinze, C. Bräuer-Burchardt, and G. Notni. 3d shape measurement with phase correlation based fringe projection. *SPIE Optical Metrology*, 66160B–66160B, 2007.

R. Legarda-Sa, T. Bothe, W. P. Ju, et al. Accurate procedure for the calibration of a structured light system. *Optical Engineering*, 43(2):464–471, 2004.

Z. Li, Y. Shi, C. Wang, and Y. Wang. Accurate calibration method for a structured light system. *Optical Engineering*, 47(5):053604–053604, 2008.

W. Lohry, Y. Xu, and S. Zhang, Optimal checkerboard selection for structured light system calibration. *SPIE Optics + Photonics*, 743202–743202, 2009.

T. Luhmann. 3d imaging: how to achieve highest accuracy. *SPIE Optical Metrology*, 808502–808502, 2011.

D. MacKinnon, B. Carrier, J.-A. Beraldin, and L. Cournoyer. Gd&t-based characterization of short-range non-contact 3d imaging systems. *Int. Journal of Computer Vision*, 102(1-3):56–72, 2013.

B. Møller, I. Balslev, and N. Krüger. An automatic evaluation procedure for 3d scanners in robotics applications. *IEEE Sensors Journal*, 13(2):870–878, 2013.

J. Posdamer and M. Altschuler. Surface measurement by space-encoded projected beam systems. *Computer Graphics and Image Processing*, 18(1):1–17 1982.

C. Rocchini, P. Cignoni, C. Montani, P. Pingi, and R. Scopigno. A low cost 3d scanner based on structured light. *Computer Graphics Forum*, 20:299–308, 2001.

A. Ruiz, P. E. López-de Teruel, and G. García-Mateos. A note on principal point estimability. *Proc. Pattern Recognition*, 2:304–307, 2002.

J. Salvi, J. Pages, and J. Batlle. Pattern codification strategies in structured light systems. *Pattern Recognition*, 37(4):827–849, 2004.

G. Sansoni, M. Carocci, and R. Rodella. Three-dimensional vision based on a combination of gray-code and phase-shift light projection: analysis and compensation of the systematic errors. *Applied Optics*, 38(31):6565–6573, 1999.

V. Srinivasan, H.-C. Liu, and M. Halioua. Automated phase-measuring profilometry: a phase mapping approach. *Applied Optics*, 24(2):185–188, 1985.

E. Trucco, R. B. Fisher, A. W. Fitzgibbon, and D. Naidu. Calibration, data consistency and model acquisition with laser stripers. *Int. Journal of Computer Integrated Manufacturing*, 11(4):293–310, 1998.

M.-J. Tsai and C.-C. Hung. Development of a high-precision surface metrology system using structured light projection. *Measurement*, 38(3):236–247, 2005.

R. Y. Tsai. A versatile camera calibration technique for high-accuracy 3d machine vision metrology using off-the-shelf tv cameras and lenses. *IEEE Journal of Robotics and Automation*, 3(4):323–344, 1987.

S. Zhang and P. S. Huang. Novel method for structured light system calibration. *Optical Engineering*, 45(8):083601–083601, 2006.

Z. Zhang. A flexible new technique for camera calibration. *IEEE Trans. PAMI*, 22(11):1330–1334, 2000.

R. Zumbrunn. Automated fast shape determination of diffuse reflecting objects at close range, by means of structured light and digital phase measurement. In *ISPRS Intercommission Conference on Fast Processing of Photogrametric Data*, 363–379, 1987.

Contribution G

Technical Note: Additive Manufacturing Apparatus

Technical Note: Additive Manufacturing Apparatus

Eyþór Rúnar Eiríksson[1] David Bue Pedersen[2]
Henrik Aanæs[1]

[1] DTU Compute, [2] DTU Mekanik
eruei@dtu.dk

1 Contributions

The following contributions have been made with this invention.

1. A liquid resin 3d printer capable of printing continuously and fast without traditional layer artifacts.
2. Surface topography measurements of liquids. Using methods such as but not limited to; shape from shading, photometric stereo, structured light, depth from defocus, deflectometry, reflectometry and interferometry.
3. (Possibly) Surface topography estimation using physical models.
4. Closed loop process control in a 3d printer using an optical sensor.
5. Method for realtime dynamic 3d model slicing using any 2.5D surface
6. Anti-aliasing of the projected mask for smoother prints.
7. Scalable for large print beds if multiple systems are used side by side and partially overlapping.
8. Scalable for faster prints using a more powerfull illumination source.

With the following benefits

1. Continuous print is faster than state-of-art.
2. Higher quality prints and surface finish. (no layers).
3. Possibility for quality assurance (using same camera hardware).
4. Any resin can be used.
5. Scalable design.
6. Low mechanical complexity. Only one moving element. Durable design.

2 Introduction

This invention is a novel approach over a conventional by-layer 3D printing method used for fabricating three dimensional objects through photo-polymerization. The technology functions by selectively exposing a light sensitive liquid polymer that will cure and set as a solid upon exposure. Traditionally a three dimensional model or object is dissected or sliced into thin horizontal two dimensional layers, which represent the projection mask for the object. Traditionally each layer is then built by the following procedure in order to create the physical object:

1. One layer is exposed onto liquid resin for a prolonged duration until that layer is fully cured.
2. The printed object is submerged into the liquid by one layer-height.
3. The surface of the photo polymer liquid is traversed with a scraper for recoating and minimization of surface tension effects.
4. The process repeats itself until all layers have been built.

Employing this conventional method yields manufacturing rates that can be measured in micrometers per minute, mostly due to the time consuming recoating process. Additionally due to the discrete and finite thickness of the slicing an undesirable artifact known as 'the staircase' artifact appears.

This invention proposes a continuous print method which makes away with the conventional by-layer method. Allowing for prints with excellent surface finishes and without discretization artifacts such as the staircase effect. In this method, only the first few layers are performed in a by-layer manner as used on traditional photopolymer 3D printers. This is done to ensure that a rigid mechanical adhesion to the build-platform has been obtained. Thereafter, a transition is made to dynamic closed-loop feedback control of the process. In this mode, the build plate is moved at a continuous downward feed while a projection or solidification radiation source, which projects a 2D solidification mask, is dynamically controlled. This results in a layerless print.

The faster the build platform travels, the faster the inflow of new resin over the projection mask, only limited by the flow mechanics of the photo polymer. The same effect can be obtained by reducing the light intensity of the light source. The advantage of modulating the light source is that the flow mechanics of the photo polymer can be controlled locally whereas a modulation of the downward feed affects the flow mechanics globally over the surface of the print. If the light source is modulated, the advantage is that the process can occur at the highest possible flow rate and thus solidification rate. A balance of both parameters (high feed and high baseline light intensity, with modulation) will yield high solidification rates with localized control. Figure 1 shows the light and resin interaction, and Figure 2 the control scenarios using an optical system.

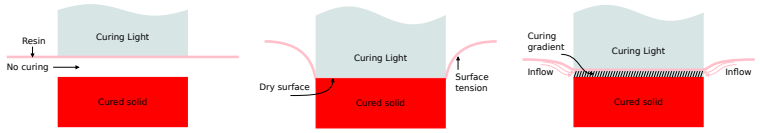

Figure 1: Curing light (Ultra-violet) is projected onto a liquid photo-polymer resin, which causes polymerization or curing of the resin into a solid 3D part. Left: Curing or polymerization rate is too slow, resulting in a flat surface and no cured part. Middle: Curing or polymerization is too fast, resulting in a dry surface that inhibits inflow of wet resin. Surface tension artifacts are observed. If overexposure continues, only a thin shell between the dry surface and liquid resin will be cured. Right: Optimal curing rate where surface wetness is maintained allowing new resin to flow over the solid object. Light intensity and build platform downward velocity are properly balanced.

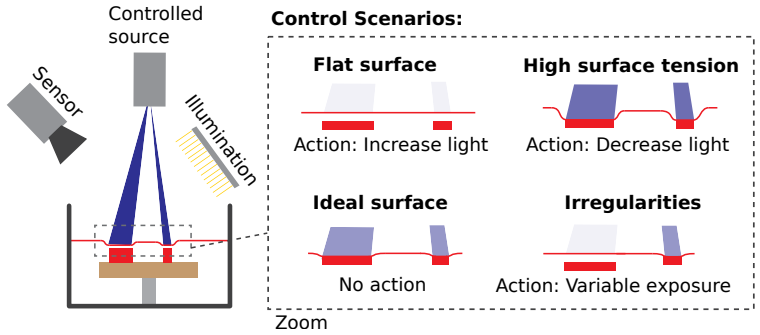

Figure 2: Proposed invention uses an optical vision system, to observe and measure the surface deviations caused by the polymerization and downward feed of the print platform. The projector light intensity is adjusted based on the measurements in a closed-loop control. When too little light is used to cure the object, the liquid resin is measurably flat and thus the controller would proceed to increase the light intensity. When too much light is used, high surface deformation is observe due to surface tension effects. Then the controller proceeds to decrease the light intensity. When the closed loop controller is in a steady state of operation, the liquid surface is only slightly curved as desired, as a optimal balance between light intensity and downward velocity has been obtained. Finally, this intensity modulation can be done on a pixel basis in order to find the optimal curing intensity for any local features over the print area.

For this to be achievable the surface topography or local curvature of the resin needs to be known. Additionally, due to the slight observable curvature that is a result of the print process, a vertical uncertainty is produced as the projection is not taking place on a perfectly flat resin. Figure 3 illustrates a solution to this effect.

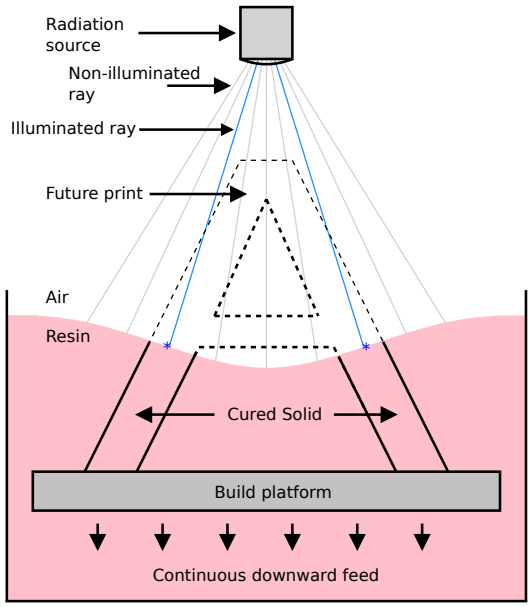

Figure 3: Any deformation of the resin surface will affect the print quality. However, if the surface topography is known it is possible to only solidify the resin in the locations where solidification should occur. If the intersection point of the projected pixel ray and the surface lies within the 3D model geometry, then that given pixel is illuminated. If that intersection lies outside of the 3d geometry, the pixel is turned off. Due to this effect, horizontal slicing or preprocessing of slices is not possible. Thus a dynamic slicing algorithm is required that works on a ray by ray basis given any resin topography. Such a solution compensates for any height differences in the resin.

3 Surface Estimation

Surface estimation can be obtained using methods such as, but not limited to; shape form shading, photometric stereo, structured light, depth from defocus, deflectometry, reflectometry and interferometry.

3.1 Using specular reflections

The geometry between the illumination source and optical sensor is such that the sources specular reflection in the resin is observed by the sensor. When the liquid resin is undisturbed, its entire surface is mirroring the illumination source to the cameras narrow field of view. Any surface deformations due to the photo-polymerization process or other effects will redirect the light outside the optical sensors field of view as well as distorting the reflection. Thus a measure of the surface deformation is possible which appears as a non-illuminated region in the resin seen from the optical sensors perspective. The magnitude of the **area** of the region is then related to the deformation of the surface. Using closed loop feedback control the radiation source (light source) intensity can be used as a process control variable that converges to maintain a minimal yet constant measured area and thus constant curvature of the resin. This specular light interaction is illustrated in Figure 4 and actual example of measurements using the optical vision system can be seen in figure 5.

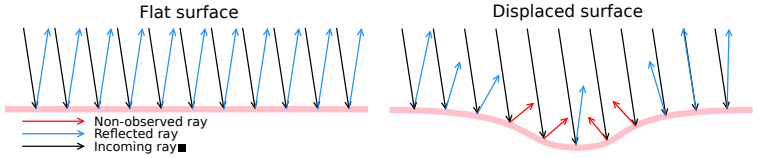

Figure 4: **Specular reflections for measurement of curvature:** Given an incoming light ray, its specular reflection will have the same angle of incidence relative to the resin surface normal. For a horizontal and level surface, it is possible to position a camera and light source in such a way that the specular reflections reach the camera sensor. Any deviation of the surface will affect its surface normal and thus change the direction of the specular ray. If the deviation is enough, the redirected ray will not reach the camera sensor and thus that region will appear darker.

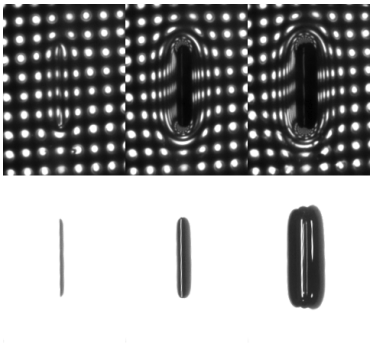

Figure 5: Example print of a wall test structure. (0.5 x 10 mm). Top row: Specular reflections, on a black resin, measured with a patterned light source. Bottom row: Specular reflections using a diffused light source. UV light intensity is increased from left to right. A thresholding operation is performed on the bottom row, and the number of pixels or area of the blob is used as an error signal that needs to be regulated to a fixed desired value.

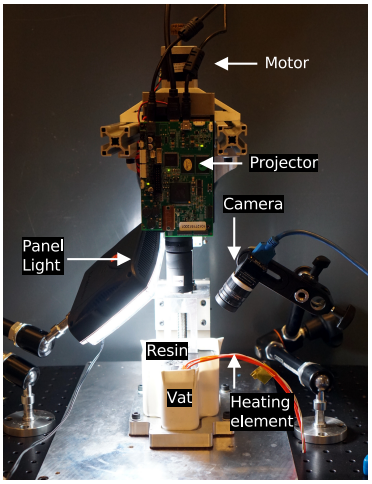

Figure 6: Implemented embodiement using specular reflections of a flat LED panel light.

Additional method of achieving this effect is with a collimated light source and beam splitter. See figure 7 and 8.

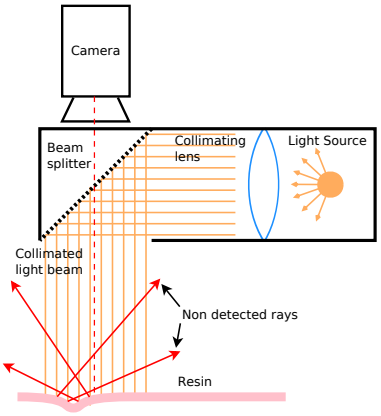

Figure 7: Beamsplitter

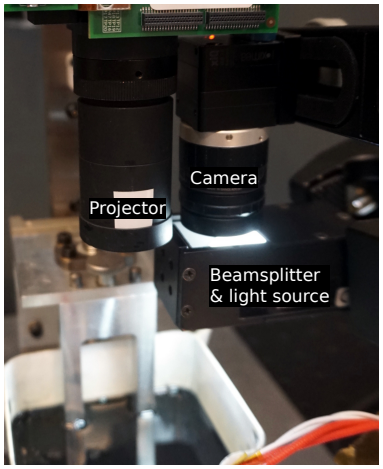

Figure 8: Implemented embodiement using specular reflections using a beam-splitter illumination source.

3.2 Using triangulation

By utilizing a 2nd color channel in the projector, it is possible to project structured light patterns onto the surface in parallel to the UV curing mask. A camera records these patterns and based on the intrinsic and extrinsic parameters of this optical setup, it is possible to perform triangulation on a pixel basis. Thus a 2.5D surface of the liquid can be measured.

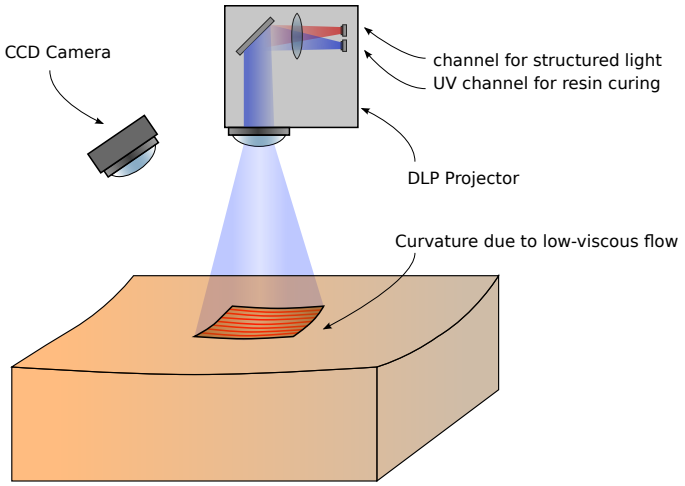

Figure 9: Example setup when using a structured light implementation for real-time liquid surface measurements.

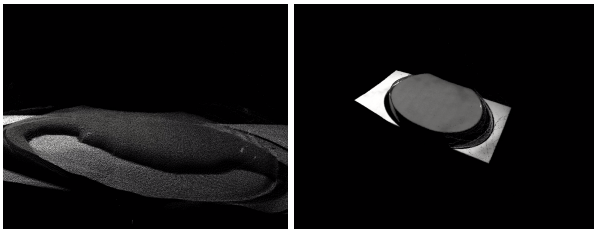

Figure 10: Example 3D topographics scans of flowing liquid resin in a circular container using a real time structured light implementation.

4 Dynamic Slicing Algorithm

We need to control what should be printed at any given resin height (relative to the build plate) due to height differences in the resin as previously described. In particular, we need to compute the intersections between the resin height and the intended geometry at any given time during the print process. In traditional printers, this is typically precomputed, in a process called slicing. In this case, the resin is flat during the print. Therefore, all layers of the intended geometry can be precomputed and used as print masks for the projector.

In our approach, the resin topography is not perfectly level, although it is known. This prevents us from pre-computing the print masks. As such, a part of our invention is that we need to dynamically compute the print mask in real time. This can be solved using novel methodology from computer graphics.

In our method we pre-compute at which heights all pixel rays emitted from the projector intersect the surface of the print geometry. That is, at which discrete heights a given pixel ray should change from ON to OFF or anything in between. This is a technique known in computer graphics as a layered depth map (LDM).

During real time operation, a topographic measurement is performed. This measurement gives us a distance Z for every projected pixel ray origin to the liquid surface. As the print platforms position is precisely known, it is possible to derive at which height in the 3D model the liquid currently intersects. The algorithm then proceeds to look up the precomputed data structure for ray-to-model intersections. The result from the look up will determine whether the projector pixel is turned ON or OFF.

Representing the heights at which intersection height a pixel should be turned ON or OFF allows for a memory efficient way of representing this data, with a resolution only limited by the machine precision (typically 32 or 64 bit). Additionally, the look-up can be performed fast which enables high framerate (>60fps) computation on a consumer CPU.

Figure 11 shows an example using a simulated surface.

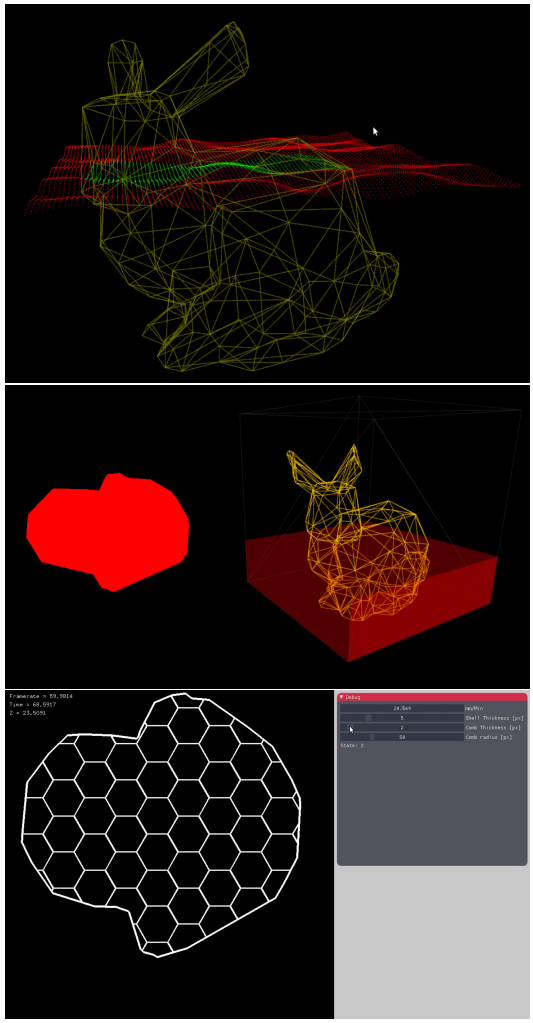

Figure 11: Examples from our dynamic slicing engine, at 60 fps using 1 million points running on a Lenovo W540 laptop. Top: Each individual green surface point are considered to be inside the print geometry and would consequently be projected by the UV projector. Red points are outside the geometry and therefore not illuminated. Middle: Example of planar slicing. Bottom: Example of real-time infill generation using honey-comb patterns.

5 Closed Loop Control

Figure 12 shows a closed loop controller used in the current embodiement. (Specular reflection measurements). A known wall feature (0.5 x 10 mm), as seen in figure 5, is constantly projected at a predetermined location, in parallel to the 3D object being printed. This feature is used for probing the resin characteristics and light is adjusted accordingly to obtain the desired characteristics. An image of the feature is captured as previously described and the observed area is calculated. The area is then used as a point of regulation for the closed loop controller. A set point of the measured area is set such that the desired print characteristics are obtained. The difference between the measured area and the desired area constitutes as an error signal which is used as an input to the controller. We use a classic PID (Proportional, Integral and Derivative) linear controller. However, we do not exclude other control topologies, both linear and non-linear. The magnitude of the error signal, its previous values and its derivative are in combination used to set the projectors light intensity, or current in the projection source. This in return changes the feature probes resin deformation and thus affects the measurable area. After the controller reaches a steady state, the error between the measured and set area is zero and the controller will proceed maintain that operation despite external influences. e.g due to changes in platform downward velocity, resin flow characteristics and other external effects.

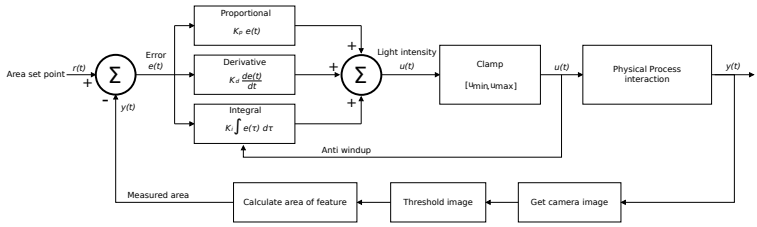

Figure 12: Closed loop feedback control using a classical PID controller and an optical vision system.

6 Software Flow Diagram

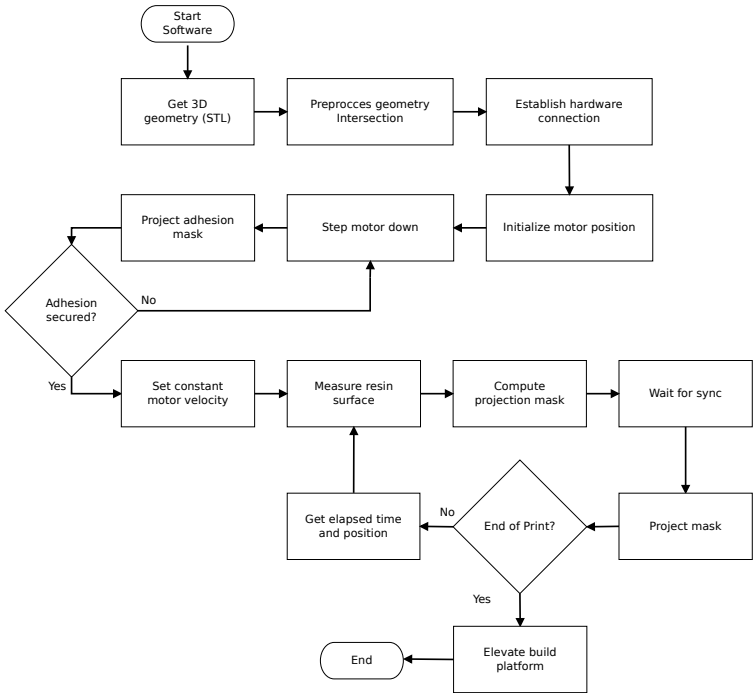

Figure 13: Flow diagram of the software

6.1 Hardware Components

The invention consists of the following hardware items

- Rigid mechanical structure
- Radiation source. Such as an ultra-violet Digital Light Processing (DLP) projector
- Linear motion stage, for precision build platform positioning.
- Build platform.
- Electrical motor and controller. Such as a servo or stepper motor incl. driver capable of obtaining precise and constant velocities.
- Illumination source, such as a flat panel light or collimated light source for resin surface estimation.
- Resin vat container.
- Optical sensor, such as a CCD or CMOS camera.
- Central Processing Unit. For computation and process control of hardware elements.

7 Example Print

Figure 14: Example continous print of a low polygon bunny.

Contribution H

Additive Manufacturing Apparatus

Additive manufacturing apparatus

Field of the invention

The present invention relates to additive manufacturing.

Background of the invention

In conventional vat photopolymerization additive manufacturing apparatuses (also known for instance as stereolithography, photo-solidification, and resin printing), a three-dimensional model of a product to be manufactured is "sliced" into thin horizontal two-dimensional model layers. A light source, such as a laser or a projector, is used to selectively solidify liquid photopolymer in accordance with the shape of these two-dimensional model layers during manufacturing to obtain a product having a shape corresponding to the model. In some additive manufacturing methods, the following procedure is used to create the physical product:

1. The liquid resin is exposed to radiation having a pattern corresponding to a two-dimensional layer of the three-dimensional object for a duration until that layer is fully cured (solidified).
2. The partially completed product is submerged into the liquid by the height of one layer.
3. The surface of the photo polymer liquid is traversed with a scraper for recoating and minimization of surface tension effects.
4. The steps above are repeated until all object layers have been realized, resulting in the product being completed.

Employing this conventional method yields manufacturing rates that can be measured in micrometers per minute. This is partly due to the time-consuming recoating process that involves resupplying resin and obtaining a flat surface. Additionally, due to the discrete and finite thickness of the slicing, an undesirable artifact known as the staircase artifact appears on the product.

Summary of the invention

Embodiments of the present invention can mitigate the situation described above.

A first aspect of the invention provides an additive manufacturing apparatus for building a product by additive manufacturing. The additive manufacturing apparatus comprises:

- a vat for holding a radiation-curable fluid to be selectively cured to form the product,
- a build platform for holding the product, the build platform comprising a platform stage for changing a position of the build platform relative to a surface of the radiation-curable fluid during building of the product, the platform stage being controlled by a platform stage control signal,
- a curing radiation source configured to receive a curing radiation source control signal and to emit a corresponding two-dimensional curing radiation pattern in a direction towards the surface of the radiation-curable fluid, whereby a corresponding part of the radiation-curable fluid is cured,
- a radiation sensor configured to produce a sensor signal representing radiation reflected by and/or emitted from the surface of the radiation-curable fluid,
- a control system configured to:
  i) provide a dynamic characterization of a shape of the surface of the fluid based on the sensor signal during building of the product,
  ii) retrieve a geometry information representing a planned geometry of the product to be built,
  iii) determine a curing radiation pattern and curing radiation intensity to be emitted by the curing radiation source in order to cure the radiation-curable fluid in accordance with the planned geometry, the determining being based at least on the geometry information and the dynamic characterization of the shape of the surface,

iv) provide a curing radiation source control signal to the curing radiation source corresponding to the determined curing radiation pattern, and

v) provide the platform stage control signal to the platform stage to cause a motion of the build platform during building.

In conventional additive manufacturing apparatuses, the geometry information is essentially the next "layer" to be built. These layers are known in advance because these apparatuses ensure that the surface of the radiation-curable fluid is flat. However, the present invention can provide high-quality products even when the surface is non-flat. The geometry information used in the present information represents at least a part of the product to be built, just as in known apparatuses. However, the curing radiation pattern and curing radiation intensity are adapted so that radiation-curable fluid is cured in accordance with the planned geometry even when the surface is non-flat. This is enabled by essentially determining an intersection between the planned geometry and the actual potentially non-flat shape of the surface of the radiation-curable fluid. Accordingly, in case the surface of the radiation-curable fluid is non-flat, embodiments of the invention actually build products in a correspondingly non-flat fashion. At each moment, it cures those parts of the surface that need curing in order to obtain the planned product. The invention, in a sense, may be thought of as using a "dynamic slicing algorithm" rather than the normal slicing into flat layers described above. The latter method can be used when the surface of the radiation-curable fluid is flat. However, because the shape of the surface of the radiation-curable fluid may be non-flat in the present invention, a corresponding non-flat slicing can determine which parts of the potentially non-flat surface should be solidified next.

In other words, the control system is configured to provide a curing radiation pattern that selectively cures a part of the radiation-curable fluid surface in

case said part coincides with a part of the planned geometry of the product.

The shape used for providing the dynamic characterization may be the shape of just a part of the surface. It needs not, and typically is not, the shape of the entire surface of the radiation-curable fluid.

The radiation-curable fluid is typically a resin.

In some embodiments, the curing radiation source is a projector, such as a DLP (Digital Light Processing) projector, an LED (Light-Emitting Diode) projector or an LCD (Liquid-Crystal Display) projector. The projector may for instance be a perspective projector or an orthographic projector.

In some embodiments, the curing radiation source is one-dimensional, such as a laser. By moving the laser rapidly, an effectively two-dimensional pattern can be provided.

In some embodiments, the control system is configured to enable the platform stage to move continuously while the curing radiation source is curing radiation-curable fluid. The motion can be with a constant speed or with a variable speed. Contrary to current additive manufacturing apparatuses, embodiments of the present invention allow for continuous motion of the platform. Platform speed can be used as a second control parameter. In this way, both platform speed and curing radiation pattern and intensity can be adjusted to provide the required curing. The precise method for doing this depends on the type of radiation-curable fluid used, its temperature, the frequency spectrum of the curing radiation source, and other factors.

In some embodiments, the characterization of the shape of the surface includes determining a topography of at least a part of the surface of the fluid. Topography is for instance a height of the radiation-curable fluid surface across the vat.

In some embodiments, the topography is determined by recording a plurality of two-dimensional images of reflected and/or emitted radiation from the surface of the radiation-curable fluid and determining surface height variations in the surface based on:

- intensity variations in one or more of the two-dimensional images, and/or
- temporal intensity variations in the two-dimensional images.

Intensity variations across an image can themselves represent a variation in surface height. Temporal changes in the same area from one image to the next can also provide useful information.

In some embodiments, the additive manufacturing apparatus comprises a separate illumination source for providing radiation to be reflected by the surface of the radiation-curable fluid for the dynamic characterization of the shape of the surface. The curing radiation may itself be used for determining the shape of the surface, but a separate source provides extra flexibility.

The radiation sensor may instead, or additionally, be capable of sensing infrared radiation generated by a reaction process, such as an exothermal process, occurring as the radiation-curable fluid is being cured.

In some embodiments that comprise an illumination source in addition to the curing radiation source, the radiation sensor may comprise an optical filter configured to filter out radiation from the curing radiation source. This may provide a higher signal-to-noise ratio in the sensing of radiation originating from the illumination source, leading to a more precise characterization of the surface.

In some embodiments, the optical filter only passes radiation from the illumination source.

In some embodiments, the illumination source is configured to emit one or more two-dimensional illumination patterns comprising a set of one or more pattern features, and the control system is configured to determine a topography of the surface of the radiation-curable fluid at least based on how the one or more pattern features are reflected onto the sensor by the surface of the radiation-curable fluid.

In some embodiments, the characterization of the shape of the surface includes monitoring radiation reflected and/or emitted from a part of the surface, and wherein a motion of the build platform and/or the two-dimensional curing radiation pattern and/or the curing radiation intensity are adjusted in response to changes in the radiation reflected and/or emitted radiation said part of the surface.

In some embodiments, a motion of the build platform and/or the two-dimensional curing radiation pattern and/or the curing radiation intensity are adjusted to ensure that a local flow of radiation-curable fluid onto cured radiation-curable fluid is sufficient for building a further part of the product in accordance with the planned geometry. If insufficient radiation-curable fluid is available at the surface, it will not be possible to cure further parts of the product in accordance with the planned geometry in such places. The term "sufficient" will, in light of the present disclosure, be clear to the person skilled in the art as being a functional term describing that enough radiation-curable liquid is available for proceding with building the planned product, but not in excessive amounts, as this could prevent curing in accordance with the planned geometry.

In some embodiments, there is a second curing radiation source in addition to the already included ("first") curing radiation source described above. The second curing radiation source is configured to receive a second curing radiation source control signal and to emit a corresponding second two-dimensional curing radiation pattern in a direction towards the surface of the radiation-curable fluid. In some embodiments, the second curing radiation

source emits the second two-dimensional curing radiation pattern in an at least partly non-overlapping fashion relative to the two-dimensional curing radiation pattern emitted by the first curing radiation source. Thereby, there is a non-overlapping surface part of the surface that receives curing radiation from the second curing radiation source, but not from the first curing radiation source. This allows easier building of larger products. In some embodiments, there is a second radiation sensor configured to produce a sensor signal representing radiation reflected by and/or emitted from the non-overlapping surface part of the surface.

A second aspect of the invention provides a method for building a product by additive manufacturing in an additive manufacturing apparatus in accordance with an embodiment of the first aspect of the invention. The method comprises:

- producing, using the radiation sensor, a sensor signal representing radiation reflected by and/or emitted from the surface of the radiation-curable fluid,
- providing a dynamic characterization of a shape of the surface of the fluid based on the sensor signal,
- retrieving a geometry information representing a planned geometry of the product being built,
- determining a curing radiation pattern and curing radiation intensity to be emitted by the curing radiation source in order to cure the radiation-curable fluid in accordance with the planned geometry, the determining being based at least on the geometry information and the dynamic characterization of the shape of the surface, and then providing a corresponding curing radiation source control signal to the curing radiation source, and
- providing the platform stage control signal to the platform stage to cause a motion of the build platform.

The considerations provided in connection with the first aspect of the invention apply similarly to the second aspect. For instance, the curing radiation pattern

and/or intensity are adapted responsive to the sensor signal to cause curing of those parts of the radiation-curable fluid surface that coincide with a corresponding part of the planned geometry of the product. If a part of the surface does not coincide with the planned geometry, no radiation is provided to that part, or at least not enough for that part of the surface to cure.

A third aspect of the invention provides digital computing hardware configured to act as the control system in an additive manufacturing apparatus in accordance with an embodiment of the first aspect of the invention.

It is possible to use a control system with certain analog elements. For instance, an illumination source and a photodiode may be placed in such a way that a certain amount of radiation from the illumination source enters the photodiode when the surface is curved and a different amount, for instance less, enters when the surface is flat, or vice versa. The current signal from the photodiode is subtracted from a set point. The difference is an error signal that can be fed into a feedback controller that produces a control signal that controls an intensity of the curing radiation source. This is mostly useful for products having a quite simple planned geometry.

A fourth aspect of the invention provides a computer-readable medium comprising instructions which, when executed on suitable computing hardware in an additive manufacturing apparatus in accordance with the first aspect of the invention, enables the additive manufacturing apparatus to perform steps i) to v).

Brief description of the drawings

Figures 1a, 1b and 1c illustrate resin curing at different curing radiation intensities.

Figure 2 illustrates an additive manufacturing apparatus in accordance with an embodiment of the present invention.

Figure 3 illustrates a working principle underlying the present invention.

Figure 4a schematically illustrates ray reflections from a flat resin surface.

Figure 4b schematically illustrates ray reflections from a distorted, non-flat resin surface.

Figure 5 illustrates thresholded binary images of diffused light reflected from the resin surface under various curing radiation intensities.

Figure 6 illustrates images of patterned light reflected from the resin surface under various curing radiation intensities.

Figure 7 illustrates the use of patterned light for obtaining information about the shape of the resin surface.

Figure 8 is a flow chart that illustrates an additive manufacturing process in accordance with an embodiment of the present invention.

Figure 9 illustrates the use two curing radiation sources, two illumination sources and two radiation sensors.

Detailed description of selected embodiments

Figs. 1a-1c illustrate differences in the build result obtained for three different curing rates resulting from different curing radiation intensities. In Fig. 1a, the curing rate is too low for building a continuous product geometry in the illustrated region. The platform on which the product is being built moves too fast, and as a result, the curing light is not sufficient for producing solidified material.

Fig. 1b illustrates a situation where the curing rate in the region is so high that fluid resin is not able to re-cover the solidified parts via an inflow of resin. This is due to resin being cured as it enters the radiation area, and in some cases it

is due to surface tension caused by the fluid-solid interface. The result, illustrated in Fig. 1b, is that either effect creates large surface height variations. These eventually make it impossible for resin to re-cover the necessary parts, and it makes for an uncontrollable process. The resulting products are not likely to match the product as intended.

Fig. 1c illustrates a desirable curing rate where surface wetness is maintained, allowing new resin to flow over the solidified parts. Curing radiation intensity and build platform downward motion speed are properly balanced. The product is built quickly, some parts even continuously, i.e. without regular stoppage of the platform, and in accordance with the desired product shape. A "curing gradient" may provide a gradual solidification, whereby overexposure is avoided.

Fig. 2 illustrates a schematic illustration of a conventional additive manufacturing apparatus 200. The additive manufacturing apparatus comprises a vat 201, a build platform 203 movable using a motorized stage 204, and a controllable electromagnetic radiation source 205 emitting radiation 213 that cures surface parts of the radiation-curable fluid in the vat to form solidified parts 212 that make up the product. In this example, the controllable radiation source is a projector having an ultra-violet LED (light emitting diode) light engine.

However, the additive manufacturing apparatus in Fig. 2 comprises three important additional elements:

1. An optional illumination source 211 for providing radiation 214 specifically for use in the dynamic characterization of the surface of the radiation-curable fluid.
2. A radiation sensor 207 for measuring radiation from the surface.
3. A control system 209 for receiving a sensor signal from the sensor 207 and in response determining a control signals for the curing radiation source 205 and the platform 203 that ensure that the product is built correctly, continuously and quickly.

Changes in the surface shape during building is of particular interest in the present invention when solidification is taking place and the platform is moving. In the prior art, the surface of the resin should be flat, as this is the only way to make sure the curing radiation provided by the curing radiation source has the intended curing effect. Accordingly, there is no need for an active monitoring of the surface, since the means for obtaining a level surface are considered sufficient and acceptable. Therefore, the required radiation patterns can be precomputed for all layers based on the knowledge that the resin surface is (virtually) flat.

The optical vision system comprising the illumination source and the radiation sensor feed information to the control system. The projector curing radiation intensity and projected pattern are adjusted based on the input from the optical vision system in a closed loop. When too little curing radiation cures the surface, the fluid resin is measurably flat and thus the control system would proceed to increase the curing radiation intensity. When too much curing radiation is used, high surface deformation is observed due to, among other things, surface tension. In that case, the control system proceeds to reduce the curing radiation intensity. When the control system is in an optimal steady state of operation, the fluid surface is curved, but only slightly (as in Fig 1c), and there is a balance between radiation intensity and downward motion of the platform. When using a projector as a curing radiation source, as in the present example, the radiation intensity changes can be performed on a pixel-by-pixel basis in order to find the optimal curing radiation intensity for the features that make up the final product.

The detail on the right-hand side of Fig. 2 illustrates the steps that are taken in the various build scenarios.

Fig. 3 illustrates partly a principle behind the solution provided by the inventors. (Note that Fig. 3 is merely for illustrating the principle; it is not an embodiment of the present invention.) Contrary to existing methods, the present invention works even if the fluid surface is not planar during the build

process. In previous solutions, any deformation of the resin surface would affect the print quality adversely, as discussed above. The inventors realized that if the surface topography is known, it is possible to only solidify resin in the locations where solidification should occur, even with a curved resin surface. If the intersection of a projected pixel ray and the resin surface lies within the 3D model geometry of the product (the planned geometry), then that pixel is illuminated. If there is no intersection between the surface and the 3D geometry of the product, that pixel is turned off, or its intensity at least reduced to a sufficiently low level to avoid solidification.

In particular, Fig. 3 illustrates a building process where a product part 301 below the resin surface has been solidified. A Part 303 (shown "above" the resin surface) has not yet been manufactured, but should be in order to form the illustrated "A"-shaped product. The resin surface is not planar, so under normal circumstances, a product of very low quality would result from such a build process.

To ensure that a local flow of radiation-curable fluid onto cured radiation-curable fluid is sufficient for building a further part of the product in accordance with the planned geometry, for instance as illustrated in Fig. 3, a motion of the build platform and/or the two-dimensional curing radiation pattern and/or the curing radiation intensity must be dynamically adjusted. For instance, if a large area is cured, more time is required to allow radiation-curable fluid to cover the cured area. A slowdown of the motion of the platform may be required in that case. As another example, if the curvature of part of the surface increases, this might indicate that the curing radiation intensity is too high. A reduction of the curing radiation intensity may be required. The control system is configured to ensure that the parameters described above are adapted properly.

In Fig. 3, arrow 305 illustrates a ray that ends at the resin surface in a point at which resin should be solidified, since the planned geometry intersects the surface of the resin; in other words, this point is contained within the product

part 303 to be manufactured. Accordingly, the projector 205 should provide curing radiation at that point to ensure that this part of the product is ultimately built. The projector 205 in Fig. 3 is a perspective projector. An orthographic projector could also be used. This has the advantage that at high surface curvatures where the perspective projector might be shadowed by curving resin (due to surface tension), the orthographic projector can mitigate this problem.

Ray 307 illustrates a radiation path along which there should not be any radiation. The ray traces to a part of the resin surface at which there is no intersection between the resin surface and the product to be built. Therefore, the projector should not provide curing radiation to that part.

In a sense, the invention employs what may be thought of as an adaptive curing radiation pattern determination, adapting the curing radiation source pattern or intensity to compensate for height differences in the resin surface. As described above, the adaptation of the curing radiation pattern is performed on a ray-by-ray basis, dynamically adjusting the projected pattern in such a way that when the radiation reaches the (potentially curved) resin surface, the radiation cures the desired fluid resin in accordance with the planned geometry, even if the resin surface is not planar.

In some embodiments, the control system simply measures the intensity reflected from a prototype geometry added next to the actual product to be manufactured. This could for instance be a bar or rod (which are structures that have a constant cross sectional area during the build). The overall intensity of the projected image is changed in response to changes in the size or total intensity reflected from this prototype geometry.

To adapt the curing radiation pattern, it is necessary to estimate the shape of the surface. Surface estimation can be obtained using methods such as, but not limited to: shape from shading, photometric stereo, structured light, depth from defocus, deflectometry, and interferometry.

In the present embodiment, the arrangement of the illumination source 211 relative to the vat and the radiation sensor 207 shown in Fig. 2 is such that the illumination source's specular reflection in the resin can reach the sensor 207, which is necessary for the feedback control. When the fluid resin is undisturbed, as shown in Fig. 4a, the surface is mirroring a part of the radiation from the illumination source 211 onto the radiation sensor 207. Surface deformations, for instance due to the solidification process or other effects, will cause a redirection of part of the radiation from the illumination source such that it does not enter the sensor 207, and will also cause the reflected image of the illumination source to be distorted compared to that emitted by the illumination source. Thus, one measure of the surface deformation involves determining seemingly non-illuminated region in the resin, at least as recorded by the sensor. This is illustrated in Fig. 4b. The circled arrows have directions that are not directed into the sensor. In the schematic, only a single ray reaches the sensor from the deformed region. Accordingly, this region will generally appear relatively dark compared to its surroundings. The size of the dark area is related to the deformation of the surface. Using the sensor signal as feedback, one way of maintaining a high quality, high speed, continuous build process includes adjusting the radiation image intensity and/or the platform speed in such a way that the dark area is present, but relatively small, and of a substantially constant size. The presence of the dark area means that there is an unevenness in the surface. Its relatively small size is acceptable. The constant size during building is a sign that the balance between solidification and inflow of fluid resin is optimal or near optimal.

In Fig. 5 and Fig. 6, a rectangular bar, described above, having cross-sectional dimensions 0.5 x 10 mm is printed as an addition to the actual product. Fig. 5 illustrates specular reflection when a diffused light source is used as illumination source. Fig. 6 illustrates the specular reflection of a patterned illumination source from the surface.

In Figs. 5 and 6, curing radiation intensity increases from left to right. An increase in radiation intensity leads to a higher curvature over a larger area, which Fig. 5 and Fig. 6 also clearly show. Note that an intensity thresholding operation is performed on Fig 5, resulting in a binary image representation separating flat regions from curved regions. Pixels are given a value of '0' if they fall below the threshold intensity value. These pixels are then classified as representing curved geometry. Pixels above the threshold intensity value are given a value of '1'. These pixels are then classified as representing flat geometry. The number of pixels with the value '0', that is, the pixels representing curved parts, are counted and represent the area of the curved part. This number can be used as an error signal relative to a fixed desired area.

Fig. 6 is the result of using a two-dimensional pattern to characterize the surface. Fig. 6 illustrates a pattern comprising lit LEDs arranged in a rectangular grid. This is merely for illustration purposes only, as it makes it easy to get a sense of the shape of the surface. The pattern is recorded by a two-dimensional sensor. Because the emitted pattern is known, it is possible to calculate the shape of the surface in great detail. Sinusoidal fringe patterns, as commonly used in three-dimensional scanning, provide significantly better resolution in this context compared to the simple example in Fig. 6 (but would not be easily recognized in a figure). Based on the principle shown in Fig. 3, the projector image is adjusted to take the determined shape into account.

Fig. 7 illustrates schematically the use of an illumination source 711 that provides one or more two-dimensional patterns 760 on the surface 770 of the radiation-curable fluid. Element 709 provides curing radiation. In this example, the projector 705 that provides curing radiation during the manufacturing of the product also comprises the illumination source 711, but whether the illumination source is built into the curing radiation source or not is optional. A radiation sensor 707 monitors the area (or a part of the area) of the surface illuminated by the illumination source 711.

Fig. 6 illustrated the use of a single two-dimensional pattern for dynamic characterization of the shape of the surface of the radiation-curable fluid during building. Fig. 7 schematically illustrates a series of patterns (above reference number 711) that might be used for performing a dynamic three-dimensional characterization of the surface of the radiation-curable fluid during building. As is well known from the field of three-dimensional scanning, use of such patterns can provide a high-resolution three-dimensional characterization. In the context of the present invention, this can translate into a more precise dynamic adjustment of the projected curing radiation pattern during the building of a product. This is in turn translated into products that are even more true to the planned geometry.

Fig. 8 illustrates a method 800 in accordance with an embodiment of invention for building a product using additive manufacturing. To build the product, geometry information of the planned product is retrieved in step 801. As described previously, the surface of the resin might not be, and preferably is not, completely flat during the build process when embodiments of the present invention are used. The method therefore includes determining the shape of the surface of the resin in step 803. Based on the geometry information and the determined shape of the surface of the resin, the method determines, in step 805, a projector image and intensity required to solidify material that should be solidified in order for the planned product to be realized. The determined image is then projected onto the resin surface, in step 807. During the building, the platform is moved, as illustrated by step 809. The build platform is advantageously and preferably moved continuously in the process, perhaps with variable speed with only occasional stops, if required. However, the adaptation of images in step 805 typically allows the build platform 203 to be moved continuously. In prior art methods, the surface must be level before a new layer can be manufactured, and to provide a level surface, the build platform is moved into the correct position, and then the surface is flattened. If the platform is moved continuously in the prior art methods, the resin surface would not be flat due to, among other things,

surface tension in the resin, and the planned product would not materialize in a high quality.

In step 811, it is determined whether the product is completed. If yes, the build process ends in step 813. If not, the method retrieves new geometry information representing further parts of the product to be built by returning to step 801.

Fig. 9 illustrates schematically the use of two curing radiation sources 909a and 909b providing at least partly non-overlapping curing radiation patterns on the surface 970 of the radiation-curable fluid. This allows for parallel production, for instance to manufacture larger products. The additive manufacturing apparatus in Fig. 9 further comprises two illumination sources 911a and 911b associated with each of the curing radiation sources 909a and 909b. Each illumination source illuminates a corresponding region 960a and 960b of the surface 970 of the radiation-curable fluid. The apparatus furthermore comprises two radiation sensors monitoring the region associated with each of the illumination sources 911a and 911b.

Claims

1. An additive manufacturing apparatus (200) for building a product by additive manufacturing, comprising:
   - a vat (201) for holding a radiation-curable fluid to be selectively cured to form the product,
   - a build platform (203) for holding the product, the build platform comprising a platform stage (204) for changing a position of the build platform relative to a surface of the radiation-curable fluid during building of the product, the platform stage (204) being controlled by a platform stage control signal,
   - a curing radiation source (205) configured to receive a curing radiation source control signal and to emit a corresponding two-dimensional curing radiation pattern in a direction towards the surface of the radiation-curable fluid, whereby a corresponding part of the radiation-curable fluid is cured,
   - a radiation sensor (207) configured to produce a sensor signal representing radiation reflected by and/or emitted from the surface of the radiation-curable fluid,
   - a control system (209) configured to:
     i) provide a dynamic characterization of a shape of the surface of the fluid based on the sensor signal during building of the product,
     ii) retrieve a geometry information representing a planned geometry of the product to be built,
     iii) determine a curing radiation pattern and curing radiation intensity to be emitted by the curing radiation source in order to cure the radiation-curable fluid in accordance with the planned geometry, the determining being based at least on the geometry information and the dynamic characterization of the shape of the surface,
     iv) provide a curing radiation source control signal to the curing radiation source corresponding to the determined curing radiation pattern, and

v) provide the platform stage control signal to the platform stage to cause a motion of the build platform during building.

2. An additive manufacturing apparatus in accordance with claim 1, wherein the control system is configured to provide a curing radiation pattern that selectively cures a part of the radiation-curable fluid surface in case said part coincides with a part of the planned geometry of the product.

3. An additive manufacturing apparatus in accordance with claim 1 or 2, wherein the curing radiation source (205) is an orthographic projector.

4. An additive manufacturing apparatus in accordance with one of the preceding claims, wherein the control system is configured to enable the platform stage to move continuously while the curing radiation source is curing radiation-curable fluid.

5. An additive manufacturing apparatus in accordance with one of the preceding claims, wherein the characterization of the shape of the surface includes determining a topography of at least a part of the surface of the radiation-curable fluid.

6. An additive manufacturing apparatus in accordance with claim 5, wherein the topography is determined by recording a plurality of two-dimensional images of reflected and/or emitted radiation from the surface of the radiation-curable fluid and determining surface height variations in the surface based on:

- intensity variations in one or more of the two-dimensional images, and/or
- temporal intensity variations in the two-dimensional images.

7. An additive manufacturing apparatus in accordance with one of the preceding claims, further comprising an illumination source (211) for

providing radiation to be reflected by the surface of the radiation-curable fluid for the dynamic characterization of the shape of the surface.

8. An additive manufacturing apparatus in accordance with claim 7, wherein the illumination source is configured to emit one or more two-dimensional illumination patterns comprising a set of one or more image features, and the control system is configured to determine a topography of the surface of the radiation-curable fluid at least based on how the one or more image features are reflected onto the sensor by the surface of the radiation-curable fluid.

9. An additive manufacturing apparatus in accordance with one of the preceding claims, wherein the characterization of the shape of the surface includes monitoring radiation reflected and/or emitted from a part of the surface, and wherein a motion of the build platform and/or the two-dimensional curing radiation pattern and/or the curing radiation intensity are adjusted in response to changes in the radiation reflected and/or emitted radiation said part of the surface.

10. An additive manufacturing apparatus in accordance with one of the preceding claims, wherein a motion of the build platform and/or the two-dimensional curing radiation pattern and/or the curing radiation intensity are adjusted to ensure that a local flow of radiation-curable fluid onto cured radiation-curable fluid is sufficient for building a further part of the product in accordance with the planned geometry.

11. An additive manufacturing apparatus in accordance with one of the preceding claims, further comprising a second curing radiation source configured to receive a second curing radiation source control signal and to emit a corresponding second two-dimensional curing radiation pattern in a direction towards the surface of the radiation-curable fluid.

12. A method for building a product by additive manufacturing in an additive manufacturing apparatus, the additive manufacturing apparatus comprising:

- a vat for holding a radiation-curable fluid to be selectively cured to form the product,
- a build platform for holding the product, the build platform comprising a platform stage for changing a position of the build platform relative to a surface of the radiation-curable fluid during building of the product, the platform stage being controlled by a platform stage control signal,
- a curing radiation source configured to receive a curing radiation source control signal and to emit a corresponding two-dimensional curing radiation pattern in a direction towards the surface of the radiation-curable fluid, whereby a corresponding part of the radiation-curable fluid is cured,
- a radiation sensor configured to produce a sensor signal representing radiation reflected by and/or emitted from the surface of the radiation-curable fluid,

the method comprising:

- producing, using the radiation sensor, a sensor signal representing radiation reflected by and/or emitted from the surface of the radiation-curable fluid,
- providing a dynamic characterization of a shape of the surface of the fluid based on the sensor signal,
- retrieving a geometry information representing a planned geometry of the product being built,
- determining a curing radiation pattern and curing radiation intensity to be emitted by the curing radiation source in order to cure the radiation-curable fluid in accordance with the planned geometry, the determining being based at least on the geometry information and the dynamic characterization of the shape of the surface, and then providing a corresponding curing radiation source control signal to the curing radiation source, and

- providing the platform stage control signal to the platform stage to cause a motion of the build platform during building of the product.

13. A method in accordance with claim 12, wherein the curing radiation pattern is adapted responsive to the sensor signal to cause curing of a part of the radiation-curable fluid surface in case said part coincides with a part of the planned geometry of the product.

14. Digital computing hardware configured to act as the control system in an additive manufacturing apparatus in accordance with one of claims 1-11.

15. A computer-readable medium comprising instructions which, when executed on suitable computing hardware in an additive manufacturing apparatus in accordance with one of claims 1-11, enable the additive manufacturing apparatus to perform steps i) to v).

Abstract

The present invention provides an additive manufacturing apparatus comprising a vat for holding a radiation-curable fluid to be selectively cured to form the product, a movable build platform for holding the product during building, a curing radiation source configured to receive a curing radiation source control signal and to emit a corresponding two-dimensional curing radiation pattern in a direction towards the surface of the radiation-curable fluid, whereby a corresponding part of the radiation-curable fluid is cured, a radiation sensor configured to produce a sensor signal representing radiation reflected by and/or emitted from the surface of the radiation-curable fluid, and a control system. The control system is configured to provide a dynamic characterization of a shape of the surface and to cause a curing radiation pattern and curing radiation intensity to be adapted when the surface is non-flat, making it possible to manufacture products more quickly and without the staircase artifact known from existing additive manufacturing apparatuses.

(Fig. 2)

Fig. 1a

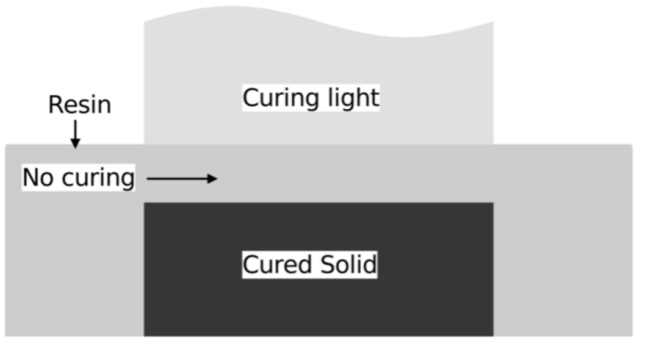

Fig. 1b

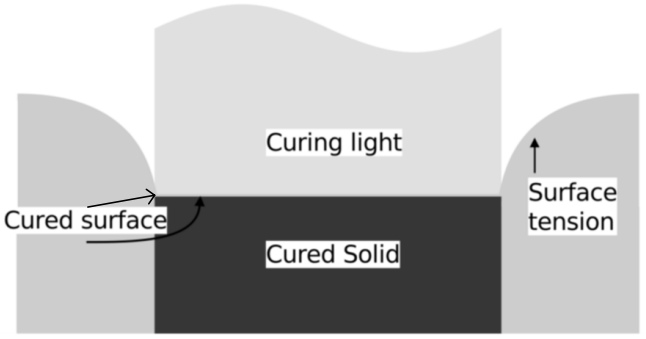

Fig. 1c

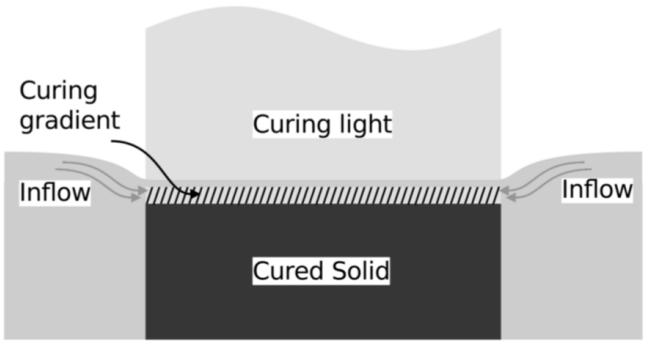

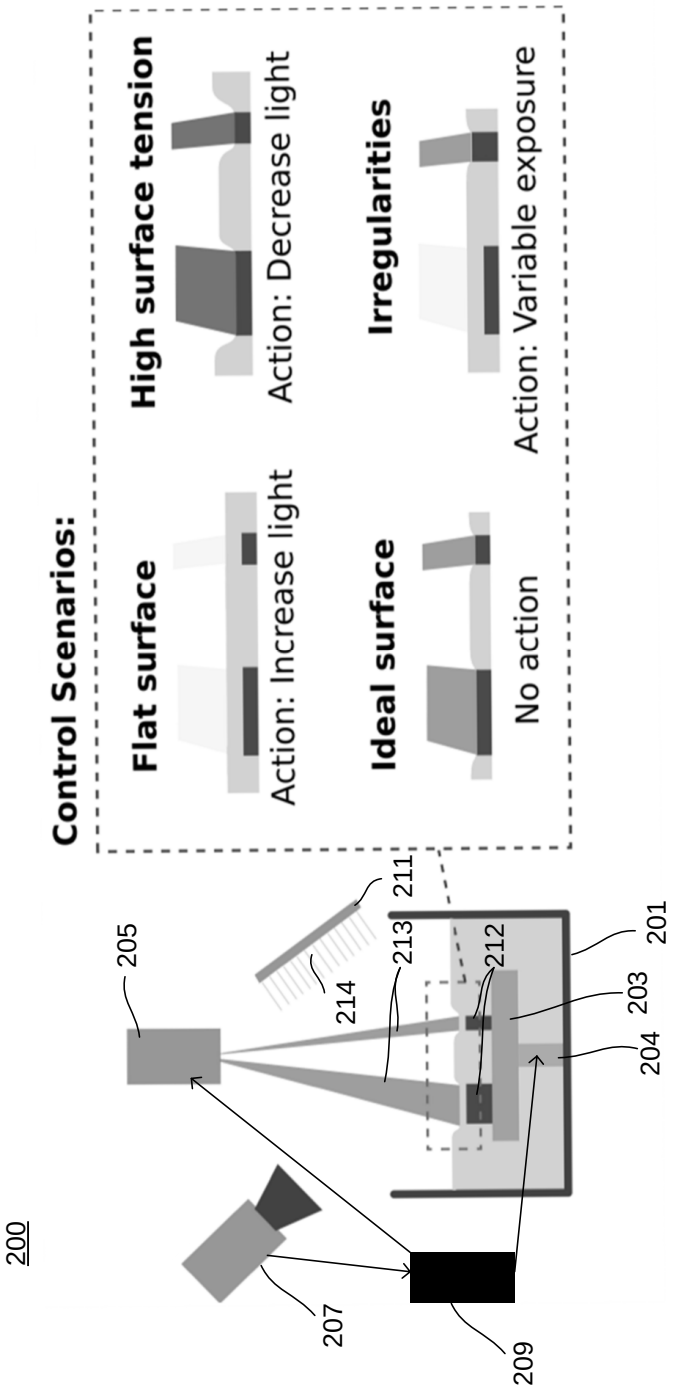
200
205
207
209
211
213
214
212
201
203
204
Control Scenarios:
Flat surface
Action: Increase light
High surface tension
Action: Decrease light
Ideal surface
No action
Irregularities
Action: Variable exposure

Fig. 2

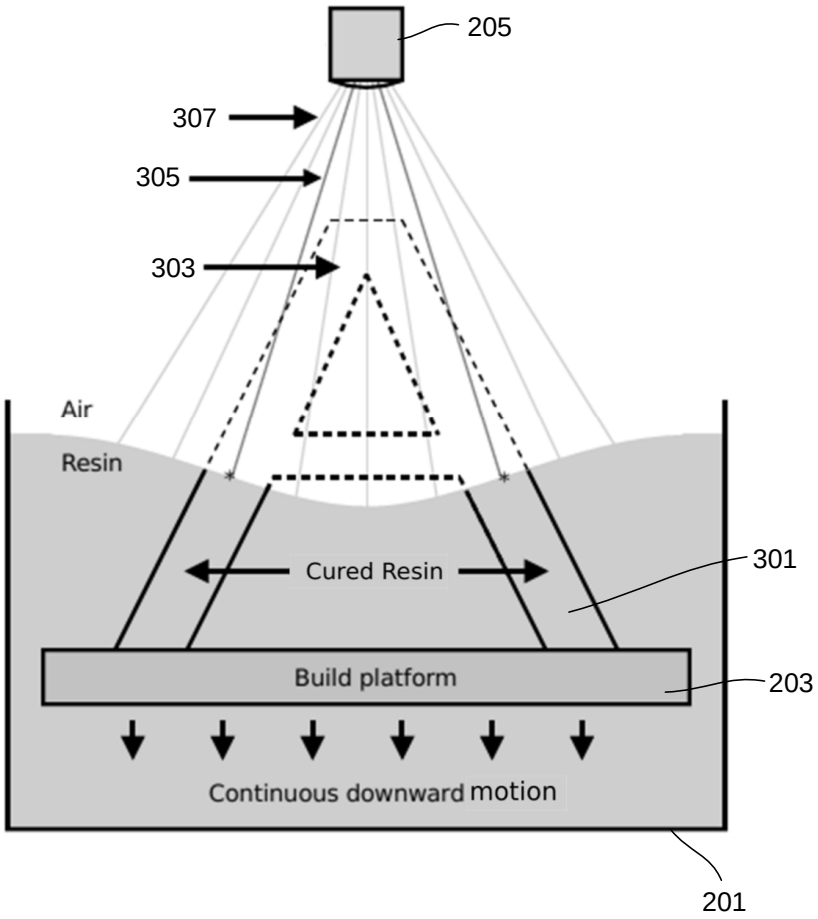
205
307
305
303
Air
Resin
Cured Resin
301
Build platform
203
Continuous downward motion
201

Fig. 3

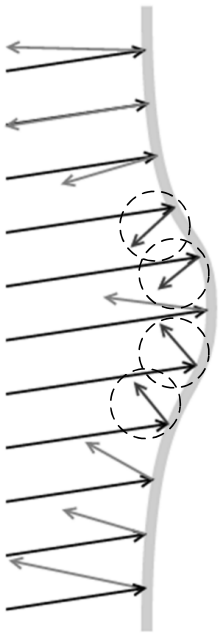

Fig. 4b

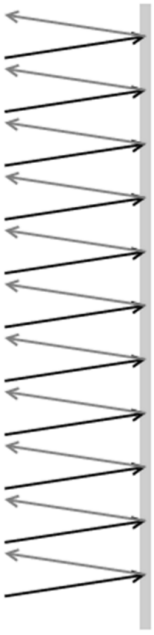

Fig. 4a

Fig. 5

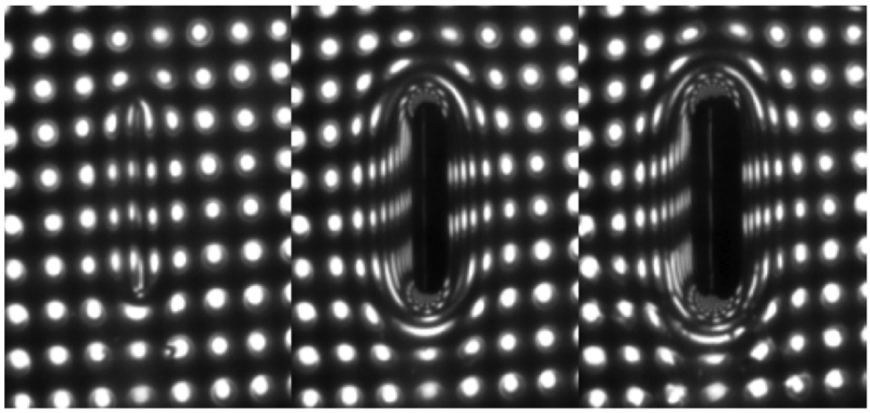

Fig. 6

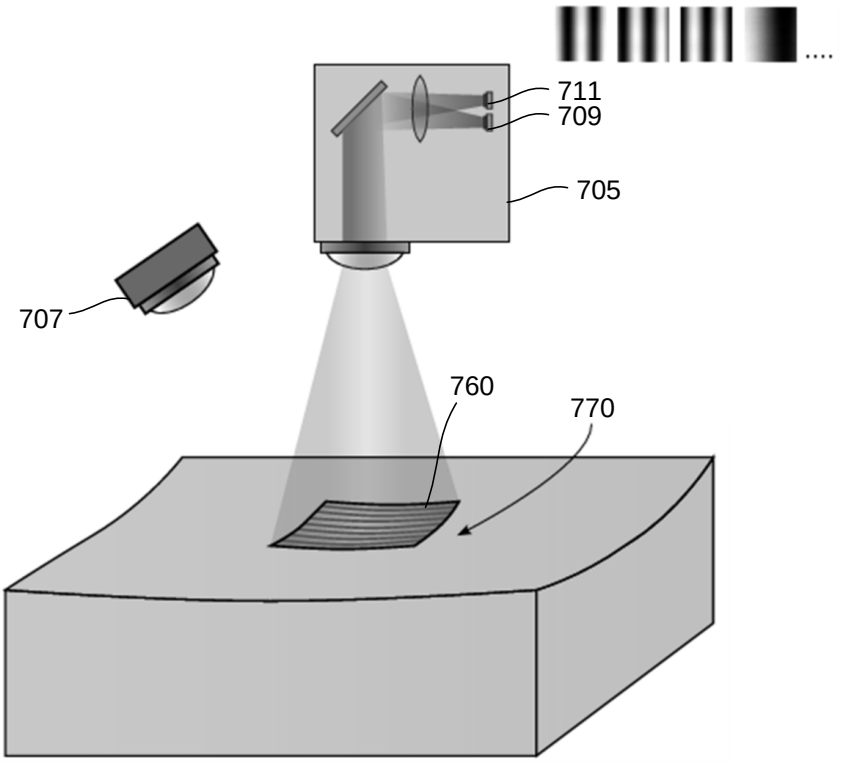

Fig. 7

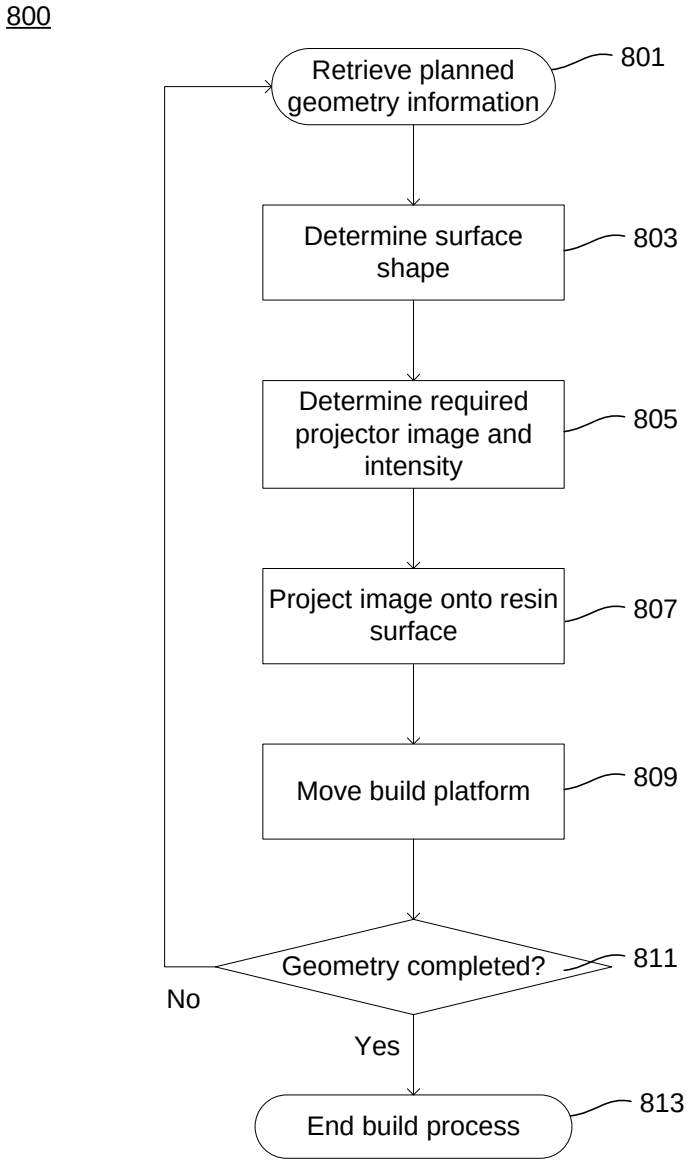
800
Retrieve planned geometry information
801
Determine surface shape
803
Determine required projector image and intensity
805
Project image onto resin surface
807
Move build platform
809
Geometry completed?
811
No
Yes
End build process
813

Fig. 8

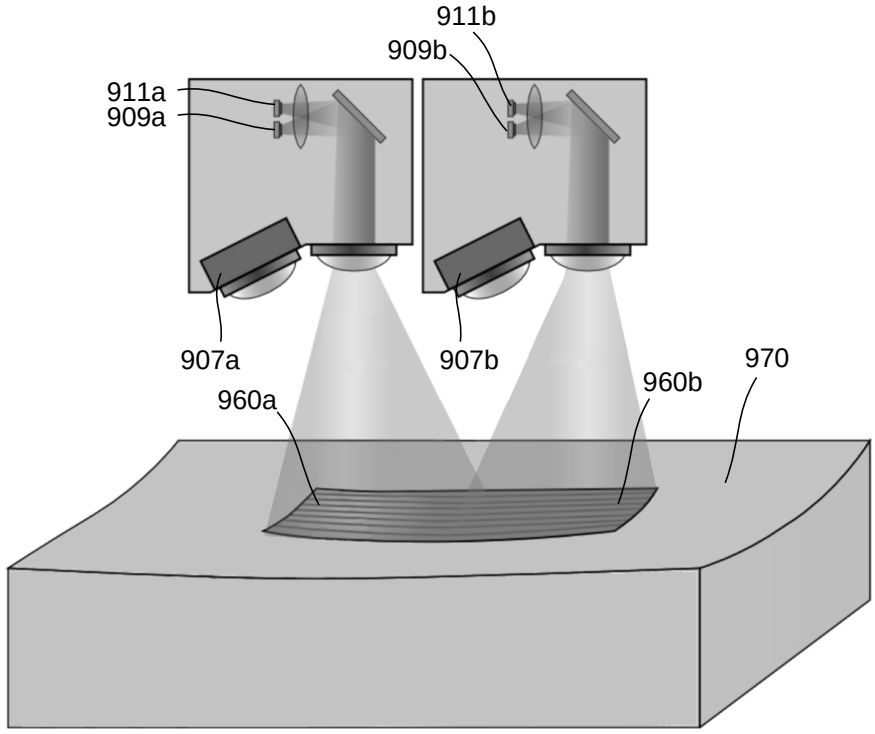

Fig. 9

Contribution I

VirtualTable: A Projection Augmented Reality Game

VirtualTable: a projection augmented reality game

A. Dal Corso M. Olsen K. H. Steenstrup J. Wilm S. Jensen R. Paulsen E. Eiríksson
J. Nielsen J. R. Frisvad G. Einarsson H. M. Kjer

Department of Applied Mathematics and Computer Science, Technical University of Denmark

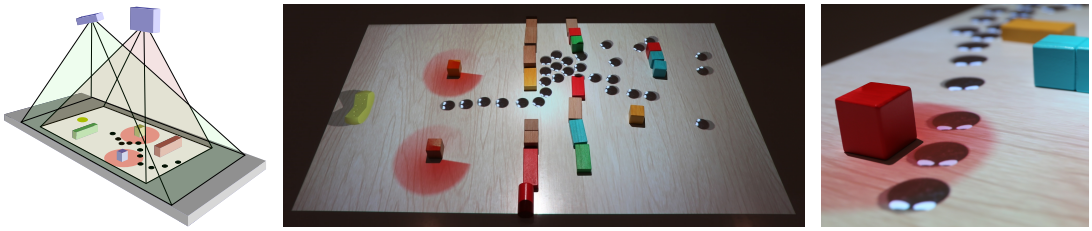

Figure 1: *(left) Our setup using projector (red frustum) and a Kinect camera (green frustum). (middle,right) Pictures of the gameplay.*

VirtualTable is a projection augmented reality installation where users are engaged in an interactive tower defense game.The installation runs continuously and is designed to attract people to a table, which the game is projected onto. Any number of players can join the game for an optional period of time. The goal is to prevent the virtual stylized soot balls, spawning on one side of the table, from reaching the cheese. To stop them, the players can place any kind of object on the table, that then will become part of the game. Depending on the object, it will become either a *wall*, an obstacle for the soot balls, or a *tower*, that eliminates them within a physical range. The number of enemies is dependent on the number of objects in the field, forcing the players to use strategy and collaboration and not the sheer number of objects to win the game.

Our installation is an example of a combination of tangible user interfaces [Shaer and Hornecker 2010] and projection augmented reality [Mine et al. 2012]. Leitner et al. [2008] presented IncreTable, a tabletop game that includes multiple inputs from different devices, including physical objects. Molla and Lepetit [2010] present a similar concept of augmented board game, but in their case the output is shown on a screen and not re-projected on the game. Compared to Leitner et al. [2008], our interaction design can be learned by exploration and thus requires no instructions. This is important in child-computer interaction and in combination with the use of tangibles it empowers the shift from "learning by being told" to "learning by doing" [Hourcade 2008]. We thus believe that our VirtualTable is an excellent concept for development of immersive and engaging learning games for children.

Our approach

VirtualTable uses a computer unit attached to both a Kinect camera and a projector. We first process the input from the Kinect depth camera, then we pass it to the actual game to display the output.

The objects are recognized using the depth camera of the Kinect. We automatically calibrate our software once before the game is actually started, to estimate both a ground depth and the Kinect-projector homography. After the calibration, objects of any significant depth (at least 0.5 cm) can be recognized. The output of the depth camera is used to create a bounding box around the objects. We exclude objects that are connected to the border, to avoid recognizing the players' hands. In Figure 1 (left) we see that the Kinect camera covers an area bigger than the game area, to not accidentally exclude objects lying on the border.

We transmit the identified bounding boxes to the actual game using a custom made protocol. In the virtual game, wall objects are invisible and affect only the behavior of the soot balls. We project a red glow around the towers to distinguish them and give a visual feedback on their range (see Figure 1 (right)). When we update the set of recognized boxes, we compare it with the existing set. Matching boxes have their position updated, interpolating it with their old position to avoid flickering. The remaining boxes are either added or removed to the game accordingly. Objects are distinguished only by shape: elongated objects are walls, square-like objects towers.

The behavior of the soot balls is simulated using Unity Engine's built-in navigation system on navigation meshes. A tower, with a given frequency, shoots bullets to the soot balls within its range, removing them from the game.

The game explores the concept of augmented reality games, combining the tangible sensation of the pieces from board games and the immediate visual feedback from modern computer games.

References

HOURCADE, J. P. 2008. Interaction design and children. *Found. Trends Hum.-Comput. Interact. 1*, 4 (Apr.), 277–392.

LEITNER, J., HALLER, M., YUN, K., WOO, W., SUGIMOTO, M., AND INAMI, M. 2008. IncreTable, a mixed reality tabletop game experience. In *Proceedings of Advances in Computer Entertainment Technology (ACE)*, 9–16.

MINE, M., VAN BAAR, J., GRUNDHOFER, A., ROSE, D., AND YANG, B. 2012. Projection-based augmented reality in Disney theme parks. *Computer 45*, 7 (July), 32–40.

MOLLA, E., AND LEPETIT, V. 2010. Augmented reality for board games. In *Proceedings of the International Symposium on Mixed and Augmented Reality (ISMAR)*.

SHAER, O., AND HORNECKER, E. 2010. Tangible user interfaces: Past, present, and future directions. *Found. Trends Hum.-Comput. Interact. 3*, 1;2 (Jan.), 1–137.

SA'15 Posters, November 02-06, 2015, Kobe, Japan
ACM 978-1-4503-3926-1/15/11.
http://dx.doi.org/10.1145/2820926.2820950

Contribution J

GyroVR: Simulating Inertia in Virtual Reality using Head Worn Flywheels

GyroVR: Simulating Inertia in Virtual Reality using Head Worn Flywheels

Jan Gugenheimer
Ulm University
Ulm, Germany
jan.gugenheimer@uni-ulm.de

Dennis Wolf
Ulm University
Ulm, Germany
dennis.wolf@uni-ulm.de

Eythor R. Eiriksson
DTU Compute
Kgs. Lyngby, Denmark
eruei@dtu.dk

Pattie Maes
MIT Media Lab
Cambridge, MA
pattie@media.mit.edu

Enrico Rukzio
Ulm University
Ulm, Germany
enrico.rukzio@uni-ulm.de

ABSTRACT
We present GyroVR, head worn flywheels designed to render inertia in Virtual Reality (VR). Motions such as flying, diving or floating in outer space generate kinesthetic forces onto our body which impede movement and are currently not represented in VR. We simulate those kinesthetic forces by attaching flywheels to the users head, leveraging the gyroscopic effect of resistance when changing the spinning axis of rotation. GyroVR is an ungrounded, wireless and self contained device allowing the user to freely move inside the virtual environment. The generic shape allows to attach it to different positions on the users body. We evaluated the impact of GyroVR onto different mounting positions on the head (back and front) in terms of immersion, enjoyment and simulator sickness. Our results show, that attaching GyroVR onto the users head (front of the Head Mounted Display (HMD)) resulted in the highest level of immersion and enjoyment and therefore can be built into future VR HMDs, enabling kinesthetic forces in VR.

Author Keywords
gyroVR; haptics; virtual reality; mobile VR, nomadic VR

ACM Classification Keywords
H.5.2. Information Interfaces and Presentation (e.g. HCI): User Interfaces

INTRODUCTION
Virtual Reality HMDs strive to immerse the user inside a virtual environment and are currently mainly targeting the visual sense. Several research projects showed that including the haptic sense inside a virtual environment leads to an increased level of immersion [17].

GyroVR focuses on the kinesthetic part of the haptic perception and mainly on inertia, which occurs when being in fast motion (e.g. flying) or in an altered environment (e.g. underwater). The resistance of the wind, when flying in a wingsuit acts upon the human body as a kinesthetic force, which impedes the movements of the head or limbs similar to when people try to move underwater. This concept of motion is currently one of the most used for Oculus Rift experiences.

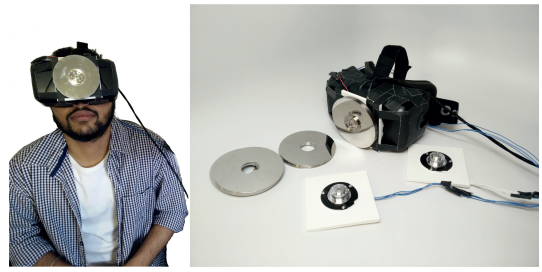

Figure 1. Left: A user wearing a VR HMD with GyroVR attached. Right: A prototype implementation of GyroVR attaching flywheels on the front of an Oculus Rift DK2.

We enable this sensation by attaching flywheels to the human head. These flywheels leverage the gyroscopic effect which occurs when the user tries to rotate his head against the rotational axis of the spinning flywheel. The gyroscopic effect will affect the motion of the users to the perpendicular axis of the motion which is mainly perceived as a resistance [19]. In combination with the visuals of the virtual scene the sensation of inertia is created. We conducted a user study (n=12) to explore how mounting GyroVR to different positions on the human head (back and front) impacts the level of immersion, enjoyment and simulator sickness inside a virtual environment.

Contributions
The main contributions of this work are: (1) the concept of simulating kinesthetic motion forces using head worn flywheels,(2) the implementation of GyroVR, a small, self containing and generic device capable of being attached to the human body, (3) the insights from our study on human perception and the impact of

UIST 2016, October 16–19, 2016, Tokyo, Japan.

DOI: http://dx.doi.org/10.1145/2984511.2984535

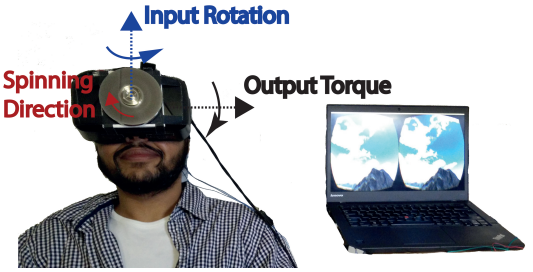

Figure 2. GyroVR is designed to render the simulated force of inertia occurring during movements. The key idea is that the flywheel mounted on the VR HMD impedes the motion of the users. Here the user is experiencing a flying simulation and tries to steer his direction using his head motion (Users' Motion). The rotation speed of GyroVR is correlated with the speed the user has in the virtual environment. GyroVR impedes this motion by generating a perpendicular force creating an experience for the user where it is more difficult to move his head when he is in high motion.

kinesthetic forces by head worn flywheels attached to different locations in terms of immersion, enjoyment and simulator sickness.

GYROVR

GyroVR is designed as an ungrounded haptic feedback device to simulate the kinesthetic force of inertia which fits to different VR experiences (e.g. flying). Ungrounded means that GyroVR has no grounding to counterbalance the output force such as Phantom or HapticMaster [13]. Figure 2 illustrates a setup where the user flies through an environment and depending on his speed perceives a higher or lower level of resistance during his head movements. The concept of GyroVR leverages the effect that the directional force is not perceived precisely enough and more like a general resistance [18]. One important concept of GyroVR is that the force generated does not necessarily have to be realistic (e.g. actual wind resistance). In informal pre-evaluation with colleagues we found that users mostly do not know the exact force which should be acting upon them in most situations but only expect some kind of force which is comprehensible.

Implementation

Similar to [3] we built GyroVR out of desktop computer hard drive components (Western Digital WD 2500). We removed the motor (7200 rpm overclocked to ≈12.000 rpm) and discs from the HDD. For our implementation we used three discs on each motor resulting in a total weight of 96g. We experimented with a different number of discs and found a balance between weight and performance using three. Furthermore, a higher number of discs resulted in the motors to struggle at start-up since they are not used to spin a higher number of discs. To control the three phase HDD motor we used a Hobbyking 30A ESC which receives a PWM signal from an Arduino Nano. After our initial tethered prototype with three motors on the HMD (Figure 6) we built a mobile version (Figure 3) by adding the Bluetooth HC-06 module for the communication between computer and Arduino and adding a 1500mAh Lipo-Battery (from an AR Drone 2.0). The use of off the shelf hardware allows researchers to easily rebuild our implementation.

To experiment with the force on different locations of the human body we built a mobile version (Figure 3 right) where we

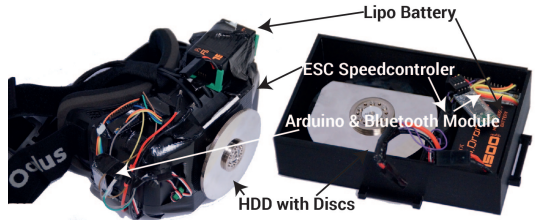

Figure 3. Two implementations of GyroVR. Left: The GyroVR prototype directly attached onto an Oculus Rift DK2. Right: A mobile implementation of GyroVR, built in a generic form factor to be mounted onto the human body.

assembled all components inside a 3D printed case (overall weight 390g). This prototype can be mounted onto the human body using straps (Figure 5). To reduce some of the weight we built a second prototype where we assembled all the components directly onto an Oculus Rift DK2 (Figure 3 left).

Gyroscopic Precession

The force generated by GyroVR is based on Newton's first law of motion which states that objects in motion try to stay in motion. The rotational pendant to this is the gyro effect which states that spinning masses will continue spinning in the same direction around the same axis. Once the user rotates his/her head at a desired angular velocity ω_{in}, a gyroscopic torque τ_out is experienced perpendicular to the head rotation axis. (Figure 4). The relationship is as follows

$$\tau_{out} = \omega_{in} \times L_s = \omega_{in} \times I\omega_s \quad (1)$$

where L_s is the spin angular momentum, I is the moment of inertia and ω_s is the angular velocity of the spinning mass.

By having a double gyroscope setup, sharing the same rotational axis and spinning in the same direction, the angular momentum contribution becomes additive. Effectively doubling the perceived effect and output torque τ_{out}. Figure 4 depicts such a double gyroscope setup where the gyroscopes have been mounted in such a way that they provide a counter balance of weight. Additionally, it illustrates the relationship between head rotation velocity ω_{in} and the gyroscopic torque τ_{out} experienced by the user around the yaw axis.

Mounting Positions

We experimented with several mounting position on the users body using the GyroVR mobile prototype (Figure 5). Our goal was to find mounting positions where users would perceive the force strong enough so it could be used in a user study. Since the force of GyroVR is a reactive force (only perceived if an input force is generated e.g. rotating the head) we experimented with mountings on the human body which are used frequently in motion when inside a virtual environment. The evaluation of the different mounting positions we report here are based on informal pre-evaluations the authors conducted on themselves to pre-select relevant mounting positions for the follow up user study. We evaluated the mounting positions based on *ease of attachment and level of perception*.

Hands: Mounting the device onto the palm (or holding it in the hand) resulted in the strongest perception of the force. This is

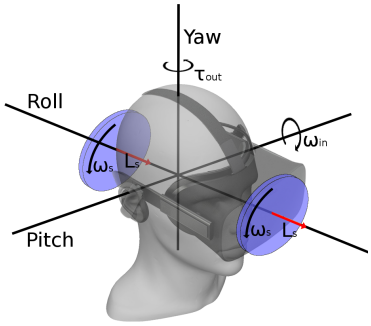

Figure 4. When disks are spun with angular velocity ω_s and the head is rotated around an input axis at angular velocity ω_{in}, the gyroscopic output torque τ_{out} around the yaw axis is experienced by the user.

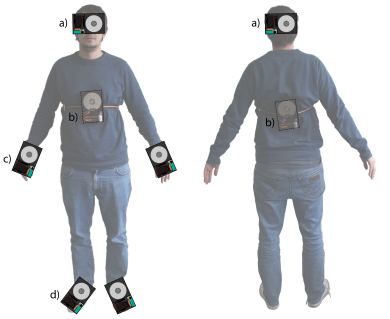

Figure 5. The different mounting positions on the human body which were explored with the mobile implementation of GyroVR.

probably because of the high density of muscle spindles which are responsible for perceiving the kinesthetic force [8]. The mounting onto the hand turned out to be more difficult since the prototype must be rigidly attached and thereby restricted motions of the hand. Furthermore, the size of the prototype lead to occlusion of the fingers which excluded simple hand tracking using the Leap Motion. The best result occurred from holding the prototype in the hand. We excluded that option of holding, since similar results were already reported in prior work [3, 21].

Torso: The least force was perceived when GyroVR was mounted on the torso. We experimented with different mounting locations but did not find a position which resulted in a force which could actually be perceived. As the torsos freedom of motion is by rotating around a vertical axis, the GyroVR must exert an output torque by twisting around the horizontal axis, essentially leveraging the entire body.

Legs/Feet: Attaching GyroVR to the legs resulted similar to the torso location in an easy mounting but low perception of the output force. We also experimented with mounting GyroVR to the feet (similar to a shoe). The force is only perceived when tilting the foot and is only of relevance for room scale VR such as HTC Vive.

Head: Mounting GyroVR onto the head resulted in a high perception of the force since the neck consists of most muscle spindles

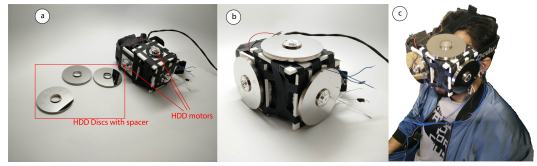

Figure 6. An early prototype of GyroVR on an Oculus Rift DK2 (a) which had a flywheel mounted onto each axis (b). We conducted informal evaluations to asses the output force (c)

[8]. We built one initial prototype (Figure 6) with flywheels on each rotational axis (yaw, pitch and roll). We then experimented with each individual flywheel and its possible combination and ended up with mounting the flywheel to the roll axis as the best result. The reason is that when mounted on the roll axis the gyroscopic effect is perceived when applying a force on the yaw and pitch axis (basically turning the head left/right or up/down). This position benefits from the fact that users explore the virtual environment by rotating the head. Even if the realistic case would be to perceive the force on the whole body, by bundling this haptic feedback with the main source of input (head rotation) the user gets an immediate feedback for an action and accepts the force as part of the immersive experience (see section user study).

APPLICATION EXAMPLES

To explore the design space for GyroVR we implemented three example applications which each create a different mapping of the force and the environment (Figure 7). We used those applications for the user study. For some applications we needed to let the participants generate input (e.g. press button to fly). We used a wireless bluetooth gamepad for this interaction. Applications which depend on virtual forward motion tend to induce simulator sickness (sensory conflict theory). Due to the nature of inertia which mostly appears during motion we took some precautions (e.g. Oculus Guidelines) during the application design to lower simulator sickness. In every scenario we used a different mapping between the virtual environment and the physical rotation to dynamically control the rpm. To generally shorten the ramp up time the flywheels are kept constantly spinning on low rpm (which did not generate enough torque for the participants to feel). All applications were implemented using Unity 3D.

Simulating Forces of Motion - Flying

In the flying game (Figure 7 a) the user can fly over a city. By holding down one button on the gamepad the user can speed up and control his direction by rotating the head. The rotational speed of the flywheel is mapped onto the virtual speed inside the game. For the flying game we used a linear mapping between virtual movement and rotation speed. This allows the user to perceive a higher resistance in turning his head when flying in higher speed. To encourage head rotation we placed stars inside the environment which the user has to collect. The placement is done in such a way that after collecting one star the users has to quickly rotate towards the next target.

Impeded Motion - 3D Shooter

Figure 7 b shows the implementation of the 3D shooter game. The user is located inside a warehouse and has to find two

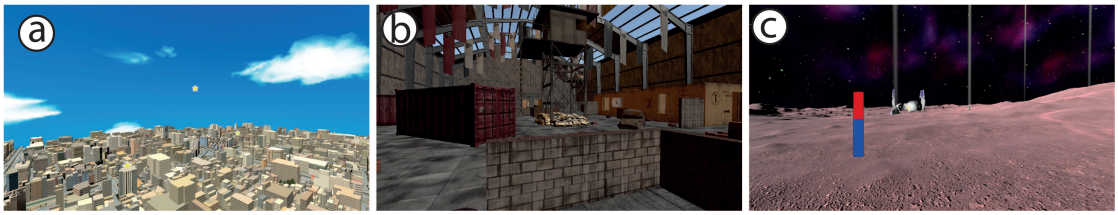

Figure 7. Screenshots of the applications which users experienced in the user study. (a) The flying application showing a star in the distance. (b) A first person view of the warehouse from the 3D Shooter game. (c) The surface of the foreign planet showing the location of several parts which the user has to collect

weapons hidden in random locations. The controls work by having one button to run and a second one to jump. The direction of the running is controlled via head rotation. During the search the users get constantly shot by hidden enemies which they can't find. The more damage the user takes the faster the flywheel spins and the more difficult it becomes to move. At the start of the scene no rotation was used. Every time a user gets hit, the rpm are increased rapidly by a 6th of the maximum rpm. After seven hits the game ends. This allows the user to experience an impeded motion as if he is wounded.

Simulating new Environments - Space Jumper

The last game (Figure 7 c) locates the user on a new planet with new physical forces. The flywheel is constantly spinning at full speed thereby highly restricting head motion and simulating a new form of gravitation. The get off the planet the user has to collect three parts which he needs to repair his spaceship. To move on the planet users are encouraged to jump. To encourage a high head movement, users only have a certain "boost" which they can use to jump that has to be regenerated by shaking their head. The gravitation on the planet is set to almost zero. The user has visually the impression as if he moves in lower gravity, the flywheels generate a force as if he would actually be in an environment with a higher gravitation as earth (since moving the head is difficult). This application beautifully demonstrates the concept of non-realistic forces. Even if that scenario is physically impossible, participants inside our user study ignored this fact and perceived the forces as appropriate, some even calling it "realistic".

RELATED WORK

Our work builds upon the work in the field of ungrounded kinesthetic feedback and virtual reality.

The gyroscopic effect was often used to create an ungrounded kinesthetic force such as the GyroCube [19] which is a handheld gyroscope generating forces along each rotational axis. Sakai et al. evaluated the levels of perception inside the users palm using GyroCube [18]. Badshah et al. applied this concept into the field of HCI by attaching flywheels onto the back of a tablet to generate kinesthetic forces for the user [3]. Several authors presented a concept to make the gyroscopic effect proactive by attaching a flywheel onto a gimbal and control that gimbal [21, 2, 22] to give the user directional cues. Murer et al. presented this concept attached onto a tablet called "TorqueScreen" [16]. By rotating the gimbal with a flywheel attached, the authors could generate kinesthetic feedback allowing the user to feel a virtual ball on the tablet bounce of the edges. The main difference to GyroVR is that all those prototypes were designed to be handheld and not mounted onto the human body.

Figure 8. The study apparatus of GyroVR consisting of a Oculus Rift DK2 with GyroVR attached and a bicycle helmet having a mobile GyroVR prototype attached to the back.

A different direction in the field of ungrounded kinesthetic feedback is work which tries to mount those flywheels onto the human body. Mostly the motivation is to assist human balance [1, 4, 14]. Those prototypes are often quite large to generate a strong enough force and too heavy for casual use. Ando et al. presented a concept for a body worn prototype based on brake change in angular momentum to create a directional force [1]. The prototype built, however, was not wearable but users had to hold it in their hand.

In the field of Virtual Reality, there is a big direction of work focusing on novel input concepts [5] and generating haptic feedback [11, 7, 12, 17, 6]. Early prototypes were used in CAVE environment and were attached to the users limbs using exoskeletons [20] or pulley systems [15]. Both systems are considered to use a grounded force. Recently, Lopes et al. presented a concept for simulating impact in VR using electrical muscular stimulation and a solenoid [11].

To our best knowledge, GyroVR is the first to use head-worn flywheels to simulate kinesthetic feedback in VR.

USER STUDY

To measure the impact of GyroVR onto immersion, engagement, enjoyment and simulator sickness we conducted a user study (n=12). We also evaluated the best position of GyroVR on the users head.

Study Design and Procedure

The study had one independent variable *motor location* with four levels (front, back, both and none). In the *both* condition both flywheels rotated in the same direction along the roll axis to sum up the force. For the user study we used a different apparatus (Figure 8) which consisted of a bicycle helmet which had a GyroVR prototype mounted on it. We used the helmet to ensure

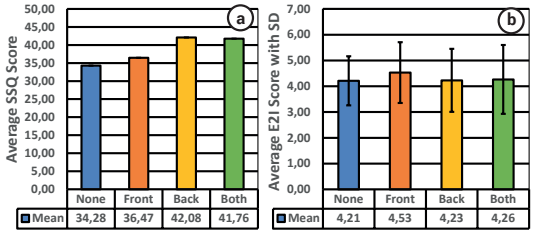

Figure 9. A distribution of the simulator sickness (a) and immersion, engagement and enjoyment questionnaire (b) of the user study.

a sturdy attachment of GyroVR onto the back of the participants' head. To ensure that the force was created equally, both flywheels were equidistant to the users head (≈ 8cm). The *none* condition was used as the baseline. The study took on average 30 minutes and participants received 5 currency. The flywheels generate a small rotation noise which was not heard by the participants due to the use of headphones. To avoid vibration we used hand moldable plastic to press fit a perfectly fitting layer of plastic between the HMD case and the flywheel mount. The battery lasted for at least 2 studies (1h) before charging.

Participants were introduced to the concept of GyroVR and could experience the force. Afterwards they put on the Oculus DK2 and the bicycle helmet and played all three applications (section *Application Examples*) with each of the four conditions of the motor (front, back, both and none). After each motor condition participants were asked to fill out the SSQ (Simulator Sickness Questionnaire) [9] and E^2I questionnaire (immersion, engagement and enjoyment) [10]. At the end participants rated all four conditions as what they perceived as the best experience. Applications and motor conditions were counterbalanced using a Latin-square.

Participants

We randomly recruited 12 participants (3 female) with an average age of 28.5 (range: 25 to 36) from our institution. Six participants had already experience with VR HMDs and all had an academic background.

Results

Quantitative: Figure 9 a shows the distribution of the simulator sickness of all levels of the motor condition. A repeated measures ANOVA revealed no significant differences ($F(3,33)$=.639, n.s.). Even if not significant, the trend shows that the front mount resulted in the lowest level of simulator sickness compared to the other motor levels. Participants in general mentioned that the applications induced a higher level of simulator sickness since they all dependent on virtual movement. The overall ranking of immersion, engagement and enjoyment over all motor levels can be found in Figure 9 b. A repeated measures ANOVA revealed no significant differences ($F(3,33)$=.745, n.s.) between the levels. Nevertheless, the front condition received a slightly higher ranking. This again correlates with the user feedback we received during the study.

Qualitative: In the final feedback after the user study participants comments can be categorized in three topics (*immersion*, *sickness*, *fatigue*): Rapid increase of RPM resulted in a little nudge in a direction and was partially perceived as 'unpleasant' and therefore fitting to increase the level of *immersion* of the 3D Shooter, where a hit from a bullet was simulated by a rapid increase of rpm. Participants said they perceived the front condition as being the strongest in terms of output force. In the final rating of the overall best experience participants preferred having a motor (7) vs having no motor (5). The participants which ranked the "no motor" condition the best mostly experienced an overall high level of *simulator sickness*, which they then correlated with the motor running. In a final ranking participants (6) reported that during the motor conditions, using both motors induced the most level of sickness. Participant 7 mentioned that if GyroVR was not tightly fixed to the head this potentially increased the sickness. High rpm were reported to potentially lead to less head movement due to *fatigue*. Participant 9 suggested to use this effect as a 'punishment' in an attention guidance scenarios. The overall weight of the study apparatus resulted in a certain level of fatigue over the duration of the whole study. However, removing one of the gyros would result in an unbalanced setup (and create an unfair comparison between conditions). Therefore, we decided the leave both gyros on the participants during the whole study. A possible solution to keep the same output force but reducing the weight would be by increasing the rpm. A future prototype which is based around a custom motor with higher rpm would be able to generate the same output force but avoid the high weight and resulting fatigue effects.

DISCUSSION

Our study showed that GyroVR creates an "immersive and realistic" (P3, P5) kinesthetic force which "enhances the experience" (P9). After experiencing a condition with either of the motors and afterwards the *none* condition, participants reported the experience to be "boring without the force" (P10). Overall participants reported they enjoyed the concept despite a certain base level of simulator sickness. Even though the user study did not quantitative show a clear benefit for immersion, engagement and enjoyment when using GyroVR, a possible trend does exist, which warrants further testing with a larger sample size to determine if the trend truly indicates significance.

CONCLUSION

We presented GyroVR, head worn flywheels designed to render inertia in Virtual Reality. These flywheels leverage the gyroscopic effect which impedes users head movement and thereby is perceived as inertia. We presented several implementations and initially explored the mounting positions on the human body. In three example applications we explore the design space and different concept of mapping the force inside of the virtual environment. In a user study we explored the effect of GyroVR attached to the users head on immersion, engagement, enjoyment and simulator sickness. Our results give a first understanding of the implications of attaching a flywheel to the front of a HMD to enable kinesthetic forces of inertia in virtual reality.

ACKNOWLEDGMENTS

We thank whole Fluid Interfaces group at the Media Lab and in particular Tal Achituv for the technical advise. This work was conducted within SFB/TRR 62 Companion-Technology for Cognitive Technical Systems and the Emmy Noether research group Mobile Interaction with Pervasive User Interface both funded by the German Research Foundation (DFG).

REFERENCES

1. Ando, H., Obana, K., Sugimoto, M., and Maeda, T. A wearable force display based on brake change in angular momentum. *Proc Artificial Reality and Telexistence 2002* (2002), 16–21.
2. Antolini, M., Bordegoni, M., and Cugini, U. A haptic direction indicator using the gyro effect. In *World Haptics Conference (WHC), 2011 IEEE*, IEEE (2011), 251–256.
3. Badshah, A., Gupta, S., Morris, D., Patel, S., and Tan, D. Gyrotab: A handheld device that provides reactive torque feedback. In *Proceedings of the SIGCHI Conference on Human Factors in Computing Systems*, CHI '12, ACM (New York, NY, USA, 2012), 3153–3156.
4. Chiu, J., and Goswami, A. Design of a wearable scissored-pair control moment gyroscope (sp-cmg) for human balance assist. In *ASME 2014 International Design Engineering Technical Conferences and Computers and Information in Engineering Conference*, American Society of Mechanical Engineers (2014), V05AT08A023–V05AT08A023.
5. Gugenheimer, J., Dobbelstein, D., Winkler, C., Hass, G., and Rukzio, E. Facetouch: Enabling touch interaction in display fixed uis for mobile virtual reality. In *Conditionally Accepted UIST '16*, UIST '16, ACM (2016).
6. Gugenheimer, J., Wolf, D., Haas, G., Krebs, S., and Rukzio, E. Swivrchair: A motorized swivel chair to nudge users' orientation for 360 degree storytelling in virtual reality. In *Proceedings of the 2016 CHI Conference on Human Factors in Computing Systems*, CHI '16, ACM (New York, NY, USA, 2016), 1996–2000.
7. Hirose, M., Hirota, K., Ogi, T., Yano, H., Kakehi, N., Saito, M., and Nakashige, M. Hapticgear: the development of a wearable force display system for immersive projection displays. In *Virtual Reality, 2001. Proceedings. IEEE*, IEEE (2001), 123–129.
8. Jones, L. A. Kinesthetic sensing. In *in Human and Machine Haptics*, Citeseer (2000).
9. Kennedy, R. S., Lane, N. E., Berbaum, K. S., and Lilienthal, M. G. Simulator sickness questionnaire: An enhanced method for quantifying simulator sickness. *The international journal of aviation psychology 3*, 3 (1993), 203–220.
10. Lin, J. J.-W., Duh, H. B., Parker, D. E., Abi-Rached, H., and Furness, T. A. Effects of field of view on presence, enjoyment, memory, and simulator sickness in a virtual environment. In *Virtual Reality, 2002. Proceedings. IEEE*, IEEE (2002), 164–171.
11. Lopes, P., Ion, A., and Baudisch, P. Impacto: Simulating physical impact by combining tactile stimulation with electrical muscle stimulation. In *Proceedings of the 28th Annual ACM Symposium on User Interface Software & Technology*, UIST '15, ACM (New York, NY, USA, 2015), 11–19.
12. Maeda, T., Ando, H., Amemiya, T., Nagaya, N., Sugimoto, M., and Inami, M. Shaking the world: galvanic vestibular stimulation as a novel sensation interface. In *ACM SIGGRAPH 2005 Emerging technologies*, ACM (2005), 17.
13. Massie, T. H., and Salisbury, J. K. The phantom haptic interface: A device for probing virtual objects. In *Proceedings of the ASME winter annual meeting, symposium on haptic interfaces for virtual environment and teleoperator systems*, vol. 55, Chicago, IL (1994), 295–300.
14. Matsuzaki, R., and Fujimoto, Y. Walking assist device using control moment gyroscopes. In *Industrial Electronics Society, IECON 2013-39th Annual Conference of the IEEE*, IEEE (2013), 6581–6586.
15. Murayama, J., Bougrila, L., Luo, Y., Akahane, K., Hasegawa, S., Hirsbrunner, B., and Sato, M. Spidar g&g: a two-handed haptic interface for bimanual vr interaction. In *Proceedings of EuroHaptics* (2004), 138–146.
16. Murer, M., Maurer, B., Huber, H., Aslan, I., and Tscheligi, M. Torquescreen: Actuated flywheels for ungrounded kinaesthetic feedback in handheld devices. In *Proceedings of the Ninth International Conference on Tangible, Embedded, and Embodied Interaction*, TEI '15, ACM (New York, NY, USA, 2015), 161–164.
17. Ramsamy, P., Haffegee, A., Jamieson, R., and Alexandrov, V. Using haptics to improve immersion in virtual environments. In *Computational Science–ICCS 2006*. Springer, 2006, 603–609.
18. Sakai, M., Fukui, Y., and Nakamura, N. Effective output patterns for torque display'gyrocube'. In *Online Proceeding of the 13th International Conference on Artificial Reality and Telexistence*, vol. 13 (2003), 160–165.
19. Tanaka, Y., Yuka, K., Fukui, Y., Yamashita, J., and Nakamura, N. Mobile torque display and haptic characteristics of human palm. In *Proc. ICAT* (2001), 115–120.
20. Tsetserukou, D., Sato, K., and Tachi, S. Exointerfaces: novel exosceleton haptic interfaces for virtual reality, augmented sport and rehabilitation. In *Proceedings of the 1st Augmented Human International Conference*, ACM (2010), 1.
21. Winfree, K. N., Gewirtz, J., Mather, T., Fiene, J., and Kuchenbecker, K. J. A high fidelity ungrounded torque feedback device: The itorqu 2.0. In *EuroHaptics conference, 2009 and Symposium on Haptic Interfaces for Virtual Environment and Teleoperator Systems. World Haptics 2009. Third Joint*, IEEE (2009), 261–266.
22. Yano, H., Yoshie, M., and Iwata, H. Development of a non-grounded haptic interface using the gyro effect. In *Haptic Interfaces for Virtual Environment and Teleoperator Systems, 2003. HAPTICS 2003. Proceedings. 11th Symposium on*, IEEE (2003), 32–39.

Contribution K

Augmented Reality Interfaces for Additive Manufacturing

Augmented Reality Interfaces for Additive Manufacturing

Eythor R. Eiriksson[1, (✉)], David B. Pedersen[1], Jeppe R. Frisvad[1], Linda Skovmand[1], Valentin Heun[2], Pattie Maes[2], and Henrik Aanæs[1]

[1] Technical University of Denmark, Kgs. Lyngby, Denmark,
[2] MIT Media Lab, Cambridge MA, USA.
eruei@dtu.dk

Abstract. This paper explores potential use cases for using augmented reality (AR) as a tool to operate industrial machines. As a baseline we use an additive manufacturing system, more commonly known as a 3D printer. We implement novel augmented interfaces and controls using readily available open source frameworks and low cost hardware. Our results show that the technology enables richer and more intuitive printer control and performance monitoring than currently available on the market. Therefore, there is a great deal of potential for these types of technologies in future digital factories.

Keywords: 3D Printing, Additive Manufacturing, Augmented Reality

1 Introduction

With recent efforts in industrial digitalization, commonly referred to as 'industry 4.0', the core aim is to realize the factory of the future. These factories are envisioned to be agile and flexible using complex autonomous manufacturing technologies combined with the human skills of reasoning. As the manufacturing technology becomes more and more autonomous the need for intuitive and fluid human-machine interaction becomes necessary. This is in part due to the massive increase in data available to the users. Additionally, it is due to increasing abstraction where complex inter-connectivity between factory elements has become invisible to the operators.

A promising, highly digitized and automated manufacturing technology that frequently comes up in relation to the factory of the future, is additive manufacturing (AM), commonly known as 3D printing. For large scale manufacturing using not only several AM systems but also other highly automated machine tools, the need for a larger control framework is required. Managing multiple machinery as well as monitoring their performance often cannot easily be achieved through their conventional physical user interfaces. However, these interfaces can be dynamically scaled in an augmented reality control interface. With such an interface, it can be evolved and iteratively tailored towards the specific use cases at any given time. As an example, multiple machines can be controlled using a single AR user interface.

In this paper, we focus on the integration of an augmented reality based human-machine interface that substitutes a conventional user interface on an additive manufacturing (AM) machine tool. This is achieved using readily available open source frameworks, web technologies and low cost mobile hardware.

2 Related Work

Mobile embedded systems such as smartphones, tablets and head mounted displays (HMD) [1, 2] now have enough computing power to enable augmented reality applications at a low cost. In an industrial scenario, applications such as remote technical support [3], worker training [4] and design [5], can be achieved.

In the context of AR industrial machine control and visualization, Zhang et al. [6] performed augmented cutting simulations on a industrial milling machine, as well as provided an interface control panel using a camera and high end processing computer. Olwal et al. demonstrated an industrial AR projection system that augments machine information onto a transparent display [7]. Both examples above, classify as tethered solutions that do not offer the flexibility achievable with a mobile device. Kollatsch et al. [8] presented a mobile implementation using a Windows tablet PC that displayed machine status parameters when presented with an AR marker, however no machine control was possible.

Our method takes advantage of recent advancement in high performance mobile technology that enables use of both consumer tablets and smartphones. Using open source systems we have implemented bi-directional AR interfaces that both monitor and control a 3D printer, in such a way that any changes made on the printer from external sources are reflected in the AR interface and vice versa.

3 Method

As consumer mobile tablet devices have already made their way into the industrial environment, we use a traditional iPad Mini 3 for this study. It is responsible for both displaying augmented interfaces as well as performing the computer vision necessary to identify and pose estimate unique optical markers that are placed on relevant locations on the machine.

For this study, we employ the Ultimaker Original [9] desktop 3D printer to represent an industrial AM machine tool on a factory floor. It is connected to a laptop via a USB-serial interface, where the control and readout takes place. For this implementation, any device capable of running the `node.js` JavaScript runtime environment [10] could be used to handle the printer communication. This includes popular devices such as the Raspberry Pi, Arduino Yún as well as many industry standard embedded systems built on ARM technology. Thus it is entirely feasible for several machines to be equipped with AR functionality at a very low cost. Both the tablet, and laptop, are connected to a common wireless network (WIFI). The laptop runs a `node.js` web server that communicates to both tablet and printer.

3.1 Additive Manufacturing Machine Tool

The Ultimaker Original is entirely open source and belongs to the class of extrusion based printers. Its construction is cartesian with a motorized horizontal X-Y carriage system. It is used to trace 2D cross-sectional slices of 3D objects, whilst simultaneously extruding melted thermoplastic material through a heated extruder nozzle. The vertical Z-axis, that translates the build plate, is then moved downward. Typically in sub-mm increments for each new layer to be produced. The printer belongs to a large family of numerically controlled (NC) devices following the G-code standard [11]. It is possible to control the machine tool through its USB hardware interfaces which presents itself as a standard serial port when connected to a computer. The printer can then be operated using G-code commands which are conventionally used in computer-aided manufacturing to control automated technologies (CAx). It is thus possible to set and query all features of the printer ranging from motion control to tooling settings.

3.2 Open Hybrid

Open hybrid [12] is a highly customizable open source platform from the MIT Media Lab, that enables flexible interactions between physical objects through augmented user interfaces. Objects or systems powered by Open Hybrid enable the possibility of inter-connectivity between each one. Such that the underlying input- and output connectivity routing between objects can be dynamically altered though simple drag and drop gestures. The augmentation system is enabled by web standards, and as such each object is set up solely in standardized protocols through a simple Application Programming Interface (API).

3.3 Reality Editor

The Reality Editor [13] is a publicly available mobile iOS app that functions as a digital window and multi-tool for Open Hybrid objects. Allowing the user to connect and manipulate the functional behavior of any physical object that is enabled by the Open Hybrid platform. As a mobile device (tablet or phone) is pointed toward an object AR marker, the Reality Editor recognizes it and performs camera pose estimation in real time. It then proceeds to augment and display the corresponding user interface on the mobile device with the correct perspective transformation. Physical buttons, indicator lights and sensors may be shown as nodes between which relationships can be defined through gestures. Once configured, the object will retain its state until the mobile tool is used again to alter the previously defined relations.

3.4 Object Markers

Throughout this study we use a novel type of quick response (QR) codes called Human Readable Quick Response Codes [14] (HRQR). The marker consist of high contrast visual features that allow for robust marker detection and pose estimation. Furthermore, as the marker is readable by humans, its text will give an indication to what type of interface is to be expected.

4 Use Cases

The following sections describe use cases implemented in this study. We identified these cases based on common interactions for this type of printer and how they might be improved using AR.

4.1 Print Visualization

In a manufacturing setting, the ability to see what object is being produced per machine can be beneficial. Giving the user a overview on the current status on the production floor. Such functionality can be provided by AR interface. Currently, there are two ways of identifying the object under print. One is by visual inspection of the actual part and secondly by its filename, which is usually displayed on the printers graphical display. For the latter, special care must be taken in naming the files accordingly, especially when dealing with different versions of the same part. Throughout a print process it can be unclear what model is being printed. This also holds true when parts are being printed that vary only slightly in form. That being said, there could be cases where it is non-trivial what part is being printed. To address the above, we implemented a use case where the entire print bed consists of an AR marker. When the marker is observed using the Reality Editor, the 3D model being printed is augmented on the print platform itself. As the AR interface supports standard web technologies, we use the `three.js` Javascript 3D library for loading and rendering the mesh geometry. Camera pose estimation is obtained each frame by observing the AR marker, and the mesh is perspectively transformed accordingly. See Figure 1.

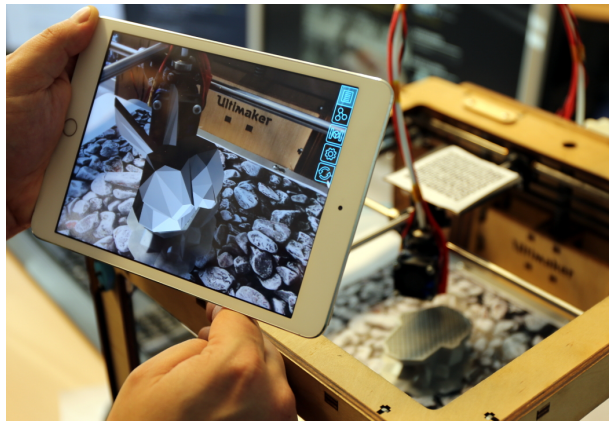

Fig. 1. Print visualization example. A 3D model (Bunny) is augmented whilst printing.

In line with our previous work on pre-visualization of printed parts prior to printing [15, 16]. Further efforts were made in order to make the rendering more visually accurate. We render the triangle mesh using a pixel shader with standard Phong lighting [17] and shadow mapping [18]. To add the staircase effect often observed in layered manufacturing [19], we customize our shader by adding procedural normal mapping. Having the Z-axis as the printing direction, our procedure for normal mapping is to find the layer index i of the surface fragment observed in the pixel, calculate the distance t to the intersection of the eye ray with the next layer, and use this to modify the Z-coordinate of the normal. In mathematical terms,

$$i = \left\lfloor \frac{p_z}{\ell} \right\rfloor + H(\omega_z) \quad , \quad t = \frac{i\,\ell - p_z}{\omega_z} \quad , \quad \boldsymbol{n}^* = (n_x, n_y, H(\ell - t)\,\mathrm{sign}(n_z))$$

where $\boldsymbol{n}$ is the unit length surface normal, $\boldsymbol{p}$ is the world space fragment position, $\boldsymbol{\omega}$ is the unit length direction vector from the camera position toward $\boldsymbol{p}$, ℓ is the layer thickness, $H(x)$ is the Heaviside step function (which is 1 for $x \geq 0$ and 0 otherwise), and $\boldsymbol{n}^*$ is the modified normal that produces the staircase effect. See Figure 2 for an example.

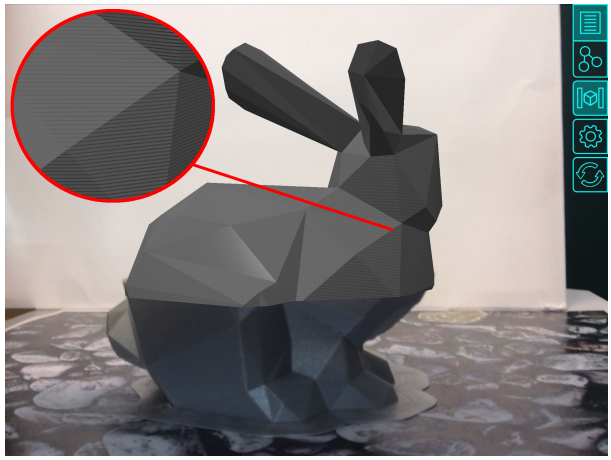

Fig. 2. Reality Editor screenshot showing model augmentation using the staircase effect shader. Due to high performance AR marker tracking, obscured viewing angles such as this can be achieved. Note: Only the part of the model that is missing is augmented.

The sharp edges in our staircase normal mapping produce aliasing artifacts in excess. We anti-alias our renderings by sampling $N = 50$ positions $\boldsymbol{p}$ in an area of 2 by 2 pixels around the original fragment position. We use a linear congruential generator with the same seed in all pixels to generate a pseudo-random distribution of window space positions without expensive texture look-ups. Still in the pixel shader, we invert the graphics pipeline transformations to get the world space coordinates of the sampled positions. For every sampled position, we then compute the normal using the given procedure and evaluate the lighting. The final pixel value is the mean of these N lighting evaluations. By reducing the number of samples ($N = 25$), we can trade render quality for performance. Very thin layers (small ℓ) introduce Moiré patterns in the renderings.

4.2 Nozzle Thermal Control

Thermal control of the nozzle that extrudes liquid plastic, is one of the most frequently operated settings on the Ultimaker. Currently, users have to perform five menu operations to reach this setting. We propose to tie the relevant parameters to a simple AR interface that is accesses through an AR marker on the print tool-head. There, the user can instantaneously monitor the current temperature, as well as easily change the set temperature through an intuitive slider. Figure 3 shows the interface under use.

Fig. 3. A minimal augmented interface showing the target and current temperatures of the heated print nozzle. Additionally a slider is included for easy manual operation.

4.3 3D Model Selection

The work flow for setting up a print job is conventionally by pre-processing a 3D geometry in a standalone software that generates a G-code print job. However, in a manufacturing setting, more often than not, the same set of models will be printed repeatedly. For most printers, these job files are stored on an on-board memory but cannot be pre-visualized or identified, other than by its filename. To improve upon this, we propose a print job selector, that allows the user to preview available models and select which should be printed. Allowing for very rapid job selections. The interface may be seen in Figure 4.

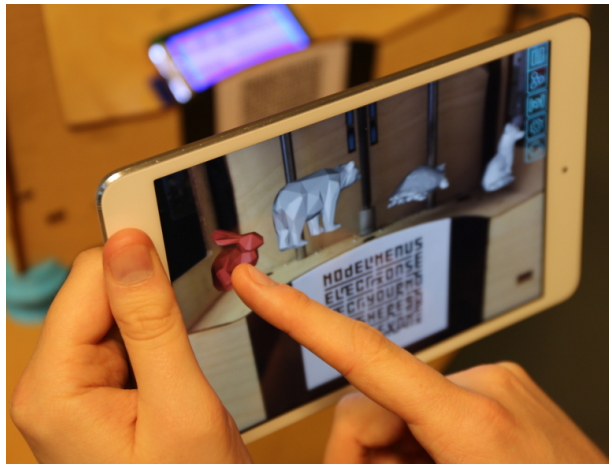

Fig. 4. Our implemented selection interface for easy selection of parts to be printed. To select a job, the user simply presses on the responding augmented model.

4.4 Carriage Motion Control

Frequently, the X-Y carriage of the printer is moved for maintenance. To do this, only one axis can be jogged at a time through a cumbersome menu system on the printers current interface. For some systems, the implementation is non-direct. Then by pressing a button, the axis starts by moving slowly. However, the speed of the axis increases the longer the button is pressed. This non-direct implementation results in less controlled motion by the user. We have implemented direct augmented control of the carriage that allows it to be moved using the AR interface. Enabling a more precise motion control tool that follows the speed of the user. The implementation can be seen in Figure 5. When a user touches

the augmented joystick, we record the markers `(u,v)` screen coordinates on the display device. Then the user can proceed to pan the device, which updates the markers coordinates on the screen. This causes a disparity which is the used as a control signal for the X and Y motors. The greater the disparity, the faster the carriage will move. In practice, the absolute scale of the AR marker could be used as control for the Z-axis. This Z-axis control was however not implemented.

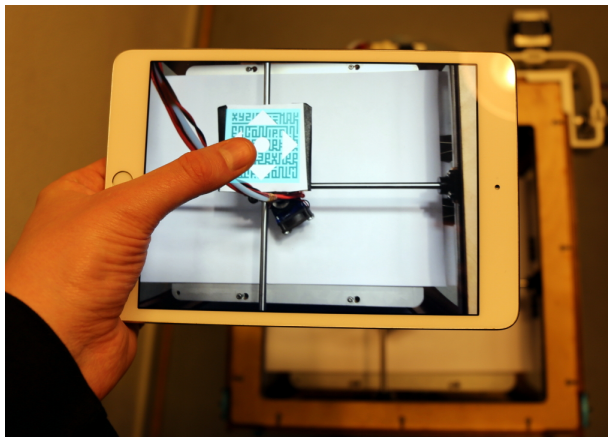

Fig. 5. Example interaction of intuitive carriage motion control.

5 Future Work

For future interfaces we envision the following:

Extrusion control that enables users to change plastic feed-rates, as well as the initiation of extrusion.

Model placement on the build plate to be used to position one or more 3D objects in an intuitive fashion. Object collision or out of bounds events may be visualized by changing the objects color. Additionally, dimensional scaling of the geometries could be performed through common zoom pinching gestures.

Printer-to-printer interactions are possible as more printers are enabled by the Open Hybrid platform. This could allow for 'drag and drop' of 3D models between printers such that high demand geometry easily can be placed in a print

queue. This allows for agile production ramp up of parts. An implementation could allow various types of printer technologies to interact, as the de-facto standard fileformat is based upon wireframe meshes.

Drag and dropping of models directly from community driven services such as `thingiverse.com` could be made possible. The back-end AR server would then be responsible for downloading the `STL` geometry, slicing the model and generating the machine code.

Layer by layer visualization could be implemented, where tool planning and support structures are shown. In addition, model areas lacking support structures could be highlighted.

Drawing shapes on the build plate, as well as simple sculpting operations can be supported. Drawing modes could for example include manual drawing of support structures.

6 Discussion and Conclusion

In this paper, we have explored and touched upon possible use cases for augmented reality systems in a manufacturing environment. This was done as an effort to explore how augmented reality can be used as a seamless interface for the factory of the future. In this spirit, the implementation has been realized on the next-gen manufacturing method of 3D printing. However, it is important to note the presented augmented reality interfaces are not limited to this specific family of manufacturing technologies. In fact, similar augmented interfaces can be implemented on any kind of manufacturing tools and machinery such as CNC machine tools, water jet- and laser cutters, injection moulding machines, forging presses etc. Any modern conventional manufacturing process chain can readily be set up as an Open Hybrid object and monitored and/or controlled through means presented in this paper.

With the rapidly increasing amounts of data produced by modern machine tools, AR can serve as a medium that provides operators with context related data on demand. Thus bridging a gap that may be created as content complexity increases. The scalability enabled by AR interfaces has the potential to be an enabling technology for modular production platforms, rapid product development and hyperflexible automation. By using constantly evolving bi-directional interfaces and the ability to instantaneously switch between them, it is possible to rapidly adapt to changes in production, bring products to market faster and small series production platforms can be set up quickly.

With few limits and near endless possibilities we have demonstrated the importance of embracing augmented reality in manufacturing engineering such that advanced manufacturing processes and process chains can be interfaced in a simple and intuitive manner.

References

1. "Microsoft HoloLens." https://www.microsoft.com/microsoft-hololens/en-us. Accessed: 2017-01-05.
2. "DAQRI Smart Helmet." https://daqri.com/products/smart-helmet/. Accessed: 2017-01-05.
3. M. Billinghurst and H. Kato, "Collaborative augmented reality," *Communications of the ACM*, vol. 45, no. 7, pp. 64–70, 2002.
4. S. Webel, U. Bockholt, T. Engelke, N. Gavish, M. Olbrich, and C. Preusche, "An augmented reality training platform for assembly and maintenance skills," *Robotics and Autonomous Systems*, vol. 61, no. 4, pp. 398–403, 2013.
5. A. Nee, S. Ong, G. Chryssolouris, and D. Mourtzis, "Augmented reality applications in design and manufacturing," *CIRP Annals-Manufacturing Technology*, vol. 61, no. 2, pp. 657–679, 2012.
6. J. Zhang, S. Ong, and A. Nee, "A volumetric model-based CNC simulation and monitoring system in augmented environments," in *Cyberworlds, 2006. CW'06. International Conference on*, pp. 33–42, IEEE, 2006.
7. A. Olwal, J. Gustafsson, and C. Lindfors, "Spatial augmented reality on industrial CNC-machines," in *Electronic Imaging 2008*, International Society for Optics and Photonics, 2008.
8. C. Kollatsch, M. Schumann, P. Klimant, V. Wittstock, and M. Putz, "Mobile augmented reality based monitoring of assembly lines," *Procedia CIRP*, vol. 23, pp. 246–251, 2014.
9. "Ultimaker Original, BOM and parts." github.com/Ultimaker/UltimakerOriginal. Accessed: 2017-01-05.
10. "Node.js." https://nodejs.org/en/. Accessed: 2017-01-09.
11. "ISO 6983-1:2009. Automation systems and integration – Numerical control of machines – Program format and definitions of address words – Part 1: Data format for positioning, line motion and contouring control systems.," standard, International Organization for Standardization, Geneva, CH, Dec. 2009.
12. "Open Hybrid: Platform for interaction with everyday objects.." http://openhybrid.org/. Accessed: 2017-01-05.
13. V. Heun, J. Hobin, and P. Maes, "Reality editor: Programming smarter objects," in *Proceedings of the 2013 ACM conference on Pervasive and ubiquitous computing adjunct publication*, pp. 307–310, ACM, 2013.
14. "HRQR: Human Readable Quick Response Code." http://hrqr.org/. Accessed: 2017-01-05.
15. E. R. Eiríksson, D. B. Pedersen, and H. Aanaes, "Predicting color output of additive manufactured parts," in *ASPE 2015 Spring Topical Meeting*, pp. 95–99, 2015.
16. E. R. Eiriksson, A. Luongo, J. R. Frisvad, D. B. Pedersen, and H. Aanaes, "Designing for color in additive manufacturing," in *Proceedings of the Aspe/euspen 2016 Summer Topical Meeting on Dimensional Accuracy and Surface Finish in Additive Manufacturing*, ASPE–The American Society for Precision Engineering, 2016.
17. B. T. Phong, "Illumination for computer generated pictures," *Communications of the ACM*, vol. 18, pp. 311–317, June 1975.
18. L. Williams, "Casting curved shadows on curved surfaces," *Computer Graphics (Proceedings of SIGGRAPH 78)*, vol. 12, pp. 270–274, August 1978.
19. Y. He, G. huai Xue, and J. zhong Fu, "Fabrication of low cost soft tissue prostheses with the desktop 3D printer," *Scientific reports*, vol. 4, no. 6973, 2014.

Bibliography

[ABTU15] Can Ates Arikan, Alan Brunton, Tejas Madan Tanksale, and Philipp Urban. Color-managed 3d printing with highly translucent printing materials. In *SPIE/IS&T Electronic Imaging*, pages 93980S–93980S. International Society for Optics and Photonics, 2015.

[ADP12] Henrik Aanæs, Anders Lindbjerg Dahl, and Kim Steenstrup Pedersen. Interesting interest points. *International Journal of Computer Vision*, 97(1):18–35, 2012.

[APHN13] Ulrik Vølcker Andersen, David Bue Pedersen, Hans Nørgaard Hansen, and Jakob Skov Nielsen. In-process 3d geometry reconstruction of objects produced by direct light projection. *International Journal of Advanced Manufacturing Technology*, 68(1-4):565–573, 2013.

[ART17] ARToolKit. Open Source Augmented Reality SDK. https://artoolkit.org/, 2017. [Online; accessed 1-Mar-2017].

[AWL15] Miika Aittala, Tim Weyrich, and Jaakko Lehtinen. Two-shot SVBRDF capture for stationary materials. *ACM Transactions on Graphics (Proceedings of SIGGRAPH 2015)*, 34(4):110, 2015.

[Azu97] Ronald T Azuma. A survey of augmented reality. *Presence: Teleoperators and virtual environments*, 6(4):355–385, 1997.

[B+00] Gary Bradski et al. The opencv library. *Doctor Dobbs Journal*, 25(11):120–126, 2000.

[BAH11] D Brackett, I Ashcroft, and R Hague. Topology optimization for additive manufacturing. In *Proceedings of the solid freeform fabrication symposium, Austin, TX*, pages 348–362, 2011.

[BAU15] Alan Brunton, Can Ates Arikan, and Philipp Urban. Pushing the limits of 3d color printing: Error diffusion with translucent materials. *ACM Transactions on Graphics (TOG)*, 35(1):4, 2015.

[Ber12] Barry Berman. 3-d printing: The new industrial revolution. *Business horizons*, 55(2):155–162, 2012.

[BETVG08] Herbert Bay, Andreas Ess, Tinne Tuytelaars, and Luc Van Gool. Speeded-up robust features (surf). *Computer vision and image understanding*, 110(3):346–359, 2008.

[BFKR14] Malte Brettel, Niklas Friederichsen, Michael Keller, and Marius Rosenberg. How virtualization, decentralization and network building change the manufacturing landscape: An industry 4.0 perspective. *International Journal of Mechanical, Industrial Science and Engineering*, 8(1):37–44, 2014.

[BK02] Mark Billinghurst and Hirokazu Kato. Collaborative augmented reality. *Communications of the ACM*, 45(7):64–70, 2002.

[Bou] Jean-Yves Bouguet. Camera Calibration Toolbox for Matlab. http://www.vision.caltech.edu/bouguetj/calib_doc/. [Online; accessed 6-Mar-2017].

[BP88] Roy S Berns and Kelvin H Petersen. Empirical modeling of systematic spectrophotometric errors. *Color Research & Application*, 13(4):243–256, 1988.

[BS13] Martin Philip Bendsoe and Ole Sigmund. *Topology optimization: theory, methods, and applications*. Springer Science & Business Media, 2013.

[BZ15] Philipp Brauner and Martina Ziefle. Human factors in production systems. In *Advances in production technology*, pages 187–199. Springer, 2015.

[C+10] International Color Consortium et al. Specification ICC. 1: 2010 (Profile version 4.3. 0.0) Image technology colour management–Architecture, profile format, and data structure, 2010.

[Car] Carbon3d. Carbon M1. http://www.carbon3d.com/. [Online; accessed 6-Mar-2017].

[CB97] Rikk Carey and Gavin Bell. *The annotated VRML 2.0 reference manual*. Addison-Wesley, 1997.

[CBG12] Ian Campbell, David Bourell, and Ian Gibson. Additive manufacturing: rapid prototyping comes of age. *Rapid prototyping journal*, 18(4):255–258, 2012.

[DAQ17] DAQRI. Smart Helmet. https://daqri.com/products/smart-helmet/, 2017. [Online; accessed 1-Mar-2017].

[DCHM05] Leonardo De Chiffre, Hans Nørgaard Hansen, and Renata Erica Morace. Comparison of coordinate measuring machines using an optomechanical hole plate. *CIRP Annals-Manufacturing Technology*, 54(1):479–482, 2005.

[DCHM06] L De Chiffre, HN Hansen, and RE Morace. Metrological validation of an optomechanical hole plate for the verification of optical and multiprobing coordinate measuring machines. In *Proc. of the 6th euspen Int. Conference, Baden*, pages 528–531, 2006.

[Dec97] Carl R Deckard. Apparatus for producing parts by selective sintering, January 28 1997. US Patent 5,597,589.

[DNRP14] Greta D'Angelo, Jakob Skov Nielsen, Jeppe Rasmussen, and David Bue Pedersen. A comparative performance analysis of fdm machines based on a calibration artefact. In *Proceedings of the 29th Annual Meeting of the American Society for Precision Engineering*, 2014.

[DOS+15] Alessandro Dal Corso, Mikkel Damgaard Olsen, Kasper Hornbak Steenstrup, Jakob Wilm, Sebastian Hoppe Nesgaard Jensen, Rasmus Reinhold Paulsen, Eyþór Rúnar Eiríksson, Jannik Boll Nielsen, Jeppe Revall Frisvad, Gudmundur Einarsson, and Hans Martin Kjer. *VirtualTable: a projection augmented reality game*. Association for Computing Machinery, 2015.

[Dua71] C Brown Duane. Close-range camera calibration. *Photogramm. Eng*, 37(8):855–866, 1971.

[EHS+16] Sarah K Everton, Matthias Hirsch, Petros Stravroulakis, Richard K Leach, and Adam T Clare. Review of in-situ process monitoring and in-situ metrology for metal additive manufacturing. *Materials & Design*, 95:431–445, 2016.

[ELF+16] Eyþór Rúnar Eiríksson, Andrea Luongo, Jeppe Revall Frisvad, David Bue Pedersen, and Henrik Aanæs. *Designing for Color in Additive Manufacturing*, pages 98–102. ASPE – The American Society for Precision Engineering, 2016.

[Enl12] Altair Enlighten. Topology Optimization Joins the Mile High Club. http://altairenlighten.com/opinion/topology-optimization-joins-the-mile-high-club/, 2012. [Online; accessed 25-Feb-2017].

[EPA15] Eyþór Rúnar Eiríksson, David Bue Pedersen, and Henrik Aanæs. *Predicting Color Output of Additive Manufactured Parts*, volume 60, pages 95–99. ASPE – The American Society for Precision Engineering, 2015.

[Evi13] Jake Evill. Cortex. Exoskeleton protecting the internal skeleton. http://www.evilldesign.com/cortex, 2013. [Online; accessed 25-Feb-2017].

[EWPA16] Eyþór Rúnar Eiríksson, Jakob Wilm, David Bue Pedersen, and Henrik Aanæs. Precision and accuracy parameters in structured light 3-d scanning. *International Archives of the Photogrammetry, Remote Sensing and Spatial Information Sciences*, Volume XL-5/W8:7–15, 2016. The Archives are open access publications, they are published under the Creative Common Attribution 3.0 License.

[FdSB16] Mauricio A Frigo, Ethel CC da Silva, and Gustavo F Barbosa. Augmented reality in aerospace manufacturing: A review. *Journal of Industrial and Intelligent Information Vol*, 4(2), 2016.

[FMH15] Graham D Finlayson, Michal Mackiewicz, and Anya Hurlbert. Color correction using root-polynomial regression. *IEEE Transactions on Image Processing*, 24(5):1460–1470, 2015.

[Fra95] FJ Francis. Quality as influenced by color. *Food quality and preference*, 6(3):149–155, 1995.

[GAVN13] Mohit Gupta, Amit Agrawal, Ashok Veeraraghavan, and Srinivasa G Narasimhan. A practical approach to 3d scanning in the presence of interreflections, subsurface scattering and defocus. *International journal of computer vision*, 102(1-3):33–55, 2013.

[Gen11] Jason Geng. Structured-light 3d surface imaging: a tutorial. *Advances in Optics and Photonics*, 3(2):128–160, 2011.

[GHTC03] Xiao-Shan Gao, Xiao-Rong Hou, Jianliang Tang, and Hang-Fei Cheng. Complete solution classification for the perspective-three-point problem. *IEEE transactions on pattern analysis and machine intelligence*, 25(8):930–943, 2003.

[GJMSMCMJ14] Sergio Garrido-Jurado, Rafael Muñoz-Salinas, Francisco José Madrid-Cuevas, and Manuel Jesús Marín-Jiménez. Automatic generation and detection of highly reliable fiducial markers under occlusion. *Pattern Recognition*, 47(6):2280–2292, 2014.

[GM98] Edward J Giorgianni and Thomas E Madden. *Digital color management: encoding solutions*. Addison-Wesley Longman Publishing Co., Inc., 1998.

[GM11] Phil Green and Lindsay MacDonald. *Colour engineering: achieving device independent colour*, volume 30. John Wiley & Sons, 2011.

[GSLZ14] Dominic Gorecky, Mathias Schmitt, Matthias Loskyll, and Detlef Zühlke. Human-machine-interaction in the industry 4.0 era. In *Industrial Informatics (INDIN), 2014 12th IEEE International Conference on*, pages 289–294. IEEE, 2014.

[Gui32] John Guild. The colorimetric properties of the spectrum. *Philosophical Transactions of the Royal Society of London. Series A, Containing Papers of a Mathematical or Physical Character*, 230:149–187, 1932.

[GWE+16] Jan Gugenheimer, Dennis Wolf, Eyþór Rúnar Eiríksson, Pattie Maes, and Enrico Rukzio. *GyroVR: Simulating Inertia in Virtual Reality using Head Worn Flywheels*, pages 227–232. Association for Computing Machinery, 2016.

[GZR+15] Wei Gao, Yunbo Zhang, Devarajan Ramanujan, Karthik Ramani, Yong Chen, Christopher B Williams, Charlie CL Wang, Yung C Shin, Song Zhang, and Pablo D Zavattieri. The status, challenges, and future of additive manufacturing in engineering. *Computer-Aided Design*, 69:65–89, 2015.

[Har01] Jon Y Hardeberg. *Acquisition and reproduction of color images: colorimetric and multispectral approaches*. Universal-Publishers, 2001.

[HCHDC06] Hans Nørgaard Hansen, Kim Carneiro, Han Haitjema, and Leonardo De Chiffre. Dimensional micro and nano metrology. *CIRP Annals-Manufacturing Technology*, 55(2):721–743, 2006.

[HDC97] Hans Nørgaard Hansen and Leonardo De Chiffre. A combined optical and mechanical reference artefact for coordinate measuring machines. *CIRP Annals-Manufacturing Technology*, 46(1):467–470, 1997.

[HEM17] Valentin Heun, Eyþór Rúnar Eiríksson, and Pattie Maes. *HRQR: A Human and Machine Decodable Matrix Code.* In review at the 16th IEEE International Symposium on Mixed and Augmented Reality (ISMAR), 2017.

[HH12] Timothy J Horn and Ola LA Harrysson. Overview of current additive manufacturing technologies and selected applications. *Science progress*, 95(3):255–282, 2012.

[HLMD15] Yong Huang, Ming C Leu, Jyoti Mazumder, and Alkan Donmez. Additive manufacturing: current state, future potential, gaps and needs, and recommendations. *Journal of Manufacturing Science and Engineering*, 137(1):014001, 2015.

[HLMH13] Samuel H Huang, Peng Liu, Abhiram Mokasdar, and Liang Hou. Additive manufacturing and its societal impact: a literature review. *The International Journal of Advanced Manufacturing Technology*, 67(5-8):1191–1203, 2013.

[HNRP14] Hans Nørgaard Hansen, Jakob Skov Nielsen, Jakob Rasmussen, and David Bue Pedersen. Performance verification of 3d printers. In *Proceedings of ASPE 2014 Spring Topical Meeting*, pages 104–108. American Society for Precision Engineering, 2014.

[Hor91] Larry J Hornbeck. Spatial light modulator and method, October 29 1991. US Patent 5,061,049.

[HP11a] Hans Nørgaard Hansen and David Bue Pedersen. Absolute 3d geometry reconstruction of complex additive manufactured parts using layered mesh generation. In *16th European Forum on Rapid Prototyping and Manufacturing*, 2011.

[HP11b] Robert William Gainer Hunt and Michael R Pointer. *Measuring colour*. John Wiley & Sons, 2011.

[HRV97] Bernhard Hill, Th Roger, and Friedrich Wilhelm Vorhagen. Comparative analysis of the quantization of color spaces on the basis of the cielab color-difference formula. *ACM Transactions on Graphics (TOG)*, 16(2):109–154, 1997.

[HS97] Janne Heikkila and Olli Silven. A four-step camera calibration procedure with implicit image correction. In *Computer Vision and Pattern Recognition, 1997. Proceedings., 1997 IEEE Computer Society Conference on*, pages 1106–1112. IEEE, 1997.

[Hul86] Charles W Hull. Apparatus for production of three-dimensional objects by stereolithography, March 11 1986. US Patent 4,575,330.

[Hul96] Charles W Hull. Method and apparatus for production of three-dimensional objects by stereolithography, September 10 1996. US Patent 5,554,336.

[Hun67] Robert William Gainer Hunt. The reproduction of colour. 1967.

[Hun93] Po-Chieh Hung. Colorimetric calibration in electronic imaging devices using a look-up-table model and interpolations. *J. Electronic Imaging*, 2(1):53–61, 1993.

[HXF14] Yong He, Guang-huai Xue, and Jian-zhong Fu. Fabrication of low cost soft tissue prostheses with the desktop 3d printer. *Scientific reports*, 4:6973, 2014.

[HZ03] Richard Hartley and Andrew Zisserman. *Multiple view geometry in computer vision*. Cambridge university press, 2003.

[IKL+08] Ivo Ihrke, Kiriakos N Kutulakos, Hendrik PA Lensch, Marcus Magnor, and Wolfgang Heidrich. State of the art in transparent and specular object reconstruction. In *EUROGRAPHICS 2008 STAR–STATE OF THE ART REPORT*. Citeseer, 2008.

[ISO08] ISO 11664-4:2008. Colorimetry – Part 4: CIE 1976 L*a*b* Colour space. Standard, International Organization for Standardization, Geneva, CH, November 2008.

[ISO10] ISO 15076-1:2010. Image technology colour management – Architecture, profile format and data structure – Part 1: Based on ICC.1:2010. Standard, International Organization for Standardization, Geneva, CH, December 2010.

[ISO15] ISO/ASTM 52900:2015. Additive manufacturing – General principles – Terminology. Standard, International Organization for Standardization, Geneva, CH, December 2015.

[ISO16] ISO/ASTM 52915:2016. Specification for additive manufacturing file format (AMF) Version 1.2. Standard, International Organization for Standardization, Geneva, CH, February 2016.

[KBC+11] Jean Pierre Kruth, Markus Bartscher, Simone Carmignato, Robert Schmitt, Leonardo De Chiffre, and Albert Weckenmann. Computed tomography for dimensional metrology. *CIRP Annals-Manufacturing Technology*, 60(2):821–842, 2011.

[KHHW13] Henning Kagermann, Johannes Helbig, Ariane Hellinger, and Wolfgang Wahlster. *Recommendations for Implementing the strategic initiative INDUSTRIE 4.0: securing the future of German manufacturing industry; final report of the Industrie 4.0 working group.* Forschungsunion, 2013.

[KPH14] Siavash H Khajavi, Jouni Partanen, and Jan Holmström. Additive manufacturing in the spare parts supply chain. *Computers in industry*, 65(1):50–63, 2014.

[L+77] Edwin H Land et al. *The retinex theory of color vision.* Citeseer, 1977.

[LA08] Jing Li and Nigel M Allinson. A comprehensive review of current local features for computer vision. *Neurocomputing*, 71(10):1771–1787, 2008.

[LCR01] M Ronnier Luo, Guihua Cui, and B Rigg. The development of the cie 2000 colour-difference formula: Ciede2000. *Color Research & Application*, 26(5):340–350, 2001.

[LH10] Harry T Lawless and Hildegarde Heymann. Color and appearance. In *Sensory Evaluation of Food*, pages 283–301. Springer, 2010.

[LK+81] Bruce D Lucas, Takeo Kanade, et al. An iterative image registration technique with an application to stereo vision. 1981.

[Low99] David G Lowe. Object recognition from local scale-invariant features. In *Computer vision, 1999. The proceedings of the seventh IEEE international conference on*, volume 2, pages 1150–1157. Ieee, 1999.

[LZZD15] William S Land, Bin Zhang, John Ziegert, and Angela Davies. In-situ metrology system for laser powder bed fusion additive process. *Procedia Manufacturing*, 1:393–403, 2015.

[Mat] Mathworks. MATLAB: Computer Vision System Toolboxk. http://www.mathworks.com/help/vision. [Online; accessed 6-Mar-2017].

[McL76] K McLaren. Xiii—the development of the cie 1976 (l* a* b*) uniform colour space and colour-difference formula. *Coloration Technology*, 92(9):338–341, 1976.

[MEO94] Marc Mahy, L Eycken, and André Oosterlinck. Evaluation of uniform color spaces developed after the adoption of cielab and cieluv. *Color Research & Application*, 19(2):105–121, 1994.

[Mic17] Microsoft. Microsoft HoloLens. https://www.microsoft.com/microsoft-hololens/en-us, 2017. [Online; accessed 1-Mar-2017].

[MLD+15] Mahesh Mani, Brandon Lane, Alkan Donmez, Shaw Feng, Shawn Moylan, and Ronnie Fesperman. Measurement science needs for real-time control of additive manufacturing powder bed fusion processes. *National Institute of Standards and Technology, Gaithersburg, MD, Standard No. NISTIR*, 8036, 2015.

[MS95] Roderick McDonald and Kenneth J Smith. Cie94-a new colour-difference formula. *Coloration Technology*, 111(12):376–379, 1995.

[MTN+17] Michael Mischkot, Guido Tosello, Daniel K. Y. Nielsen, David Bue Pedersen, Yang Zhang, Thomas Hofstätter, Lucas Herbin, and Hans Nørgaard Hansen. Injection moulding pilot production: Performance assessment of tooling process chains based on tool inserts made from brass and a 3d printed photopolymer. In *75th Annual Technical Conference and Exhibition of the Society of Plastics Engineers, SPE ANTEC Anaheim*, 2017.

[MVR05] J Murray and W Van Ryper. Wavefront obj file format summary, 2005.

[MWE+17] Dolores Messer, Jakob Wilm, Eyþór Rúnar Eiríksson, Vedrana Andersen Dahl, and Anders Bjorholm Dahl. *Image-Based Alignment of 3D Scans.* In review, 2017.

[NAFC16] Jannik Boll Nielsen, Henrik Aanæs, Jeppe Revall Frisvad, and Knut Conradsen. *On Practical Sampling of Bidirectional Reflectance.* PhD thesis, 2016.

[NEK+15] Jannik Boll Nielsen, Eyþór Rúnar Eiríksson, Rasmus Lyngby Kristensen, Jakob Wilm, Jeppe Revall Frisvad, Knut Conradsen, and Henrik Aanæs. *Quality Assurance Based on Descriptive and Parsimonious Appearance Models.* Eurographics, 2015.

[NOCM12] AYC Nee, SK Ong, G Chryssolouris, and D Mourtzis. Augmented reality applications in design and manufacturing. *CIRP Annals-Manufacturing Technology*, 61(2):657–679, 2012.

[Obe05] Hartmut Obendorf. The making of the palm pilot–reflections on a minimal information appliance. In *CHI: Conference on Human Factors in Computing Systems*, 2005.

[ON13] Soh K Ong and Andrew Yeh Chris Nee. *Virtual and augmented reality applications in manufacturing.* Springer Science & Business Media, 2013.

[Ope17] OpenHybrid. Open Hybrid: A platform for interaction with everyday objects. http://openhybrid.org/, 2017. [Online; accessed 1-Mar-2017].

[oS] Web of Science. Web of Science Core Collection Home. http://apps.webofknowledge.com. [Online; accessed 20-Feb-2017].

[PDH13] David Bue Pedersen, Leonardo De Chiffre, and Hans Nørgaard Hansen. *Additive Manufacturing: Multi Material Processing and Part Quality Control.* PhD thesis, 2013.

[PEAH16] David Bue Pedersen, Eyþór Rúnar Eiríksson, Henrik Aanæs, and Hans Nørgaard Hansen. *In-Situ Monitoring in Additive Manufacturing Using Contact Image Sensors*, pages 114–118. ASPE – The American Society for Precision Engineering, 2016.

[PEHN16] David Bue Pedersen, Eyþór Rúnar Eiríksson, Hans Nørgaard Hansen, and Jakob Skov Nielsen. A self-calibrating robot based upon a virtual machine model of parallel kinematics. *Virtual and Physical Prototyping (Online)*, 11(3):227–234, 2016.

[PH14] David B. Pedersen and Hans N. Hansen. Comparability of the performance of in-line computer vision for geometrical verification of parts, produced by additive manufacturing. In *Proceedings of the 2014 ASPE Spring Topical Meeting*, pages 179–183. American Society for Precision Engineering, 2014.

[PHE15] David Bue Pedersen, Hans Nørgaard Hansen, and Eyþór Rúnar Eiríksson. *Spatial Accuracy of Embedded Surface Coloring in Color 3D Printing*, volume 60, pages 147–150. ASPE – The American Society for Precision Engineering, 2015.

[PHN10] David Bue Pedersen, Hans Nørgaard Hansen, and Jakob Skov Nielsen. In-line monitoring and reverse 3d model reconstruction in additive manufacturing. In *The 7th International Workshop On Microfactories*, pages 1–7, 2010.

[PWRH08] Carinna Parraman, Peter Walters, Brendan Reid, and David Huson. Specifying colour and maintaining colour accuracy for 3d printing. In *Electronic Imaging 2008*, pages 68050L–68050L. International Society for Optics and Photonics, 2008.

[PZNH16] David Bue Pedersen, Yang Zhang, Jakob Skov Nielsen, and Hans Nørgaard Hansen. Adaptive layer height during dlp materials processing. In Chua Chee Kai, Yeong Wai Yee, Tan Ming Jen, and Liu Er Jia, editors, *Proceedings of the 2nd International Conference on Progress in Additive Manufacturing*, pages 246–251. Research Publishing Services, 2016.

[QL99] Long Quan and Zhongdan Lan. Linear n-point camera pose determination. *IEEE Transactions on pattern analysis and machine intelligence*, 21(8):774–780, 1999.

[R+88] LE Roscoe et al. Stereolithography interface specification. *America-3D Systems Inc*, page 27, 1988.

[RAB+99] David B Russell, Timothy Anderson, James F Bredt, Michael J Vogel, Martin Seymour, Walter J Bornhorst, and Marina I Hatsopoulos. Method and apparatus for prototyping a three-dimensional object, December 28 1999. US Patent 6,007,318.

[RGG07] Lars-Erik Rännar, Anders Glad, and Claes-Göran Gustafson. Efficient cooling with tool inserts manufactured by electron beam melting. *Rapid Prototyping Journal*, 13(3):128–135, 2007.

[RWS+11] Peiran Ren, Jiaping Wang, John Snyder, Xin Tong, and Baining Guo. Pocket reflectometry. *ACM Transactions on Graphics (Proceedings of SIGGRAPH 2011)*, 30(4):45, 2011.

[SB02] Gaurav Sharma and Raja Bala. *Digital color imaging handbook*. CRC press, 2002.

[SCB87] Michael W Schwarz, William B Cowan, and John C Beatty. An experimental comparison of rgb, yiq, lab, hsv, and opponent color models. *ACM Transactions on Graphics (TOG)*, 6(2):123–158, 1987.

[SDCS07] Enrico Savio, Leonardo De Chiffre, and Robert Schmitt. Metrology of freeform shaped parts. *CIRP Annals-Manufacturing Technology*, 56(2):810–835, 2007.

[SDO+17] Jonathan Dyssel Stets, Alessandro Dal Corso, Jannik Boll Olsen, Nielsen, Rasmus Ahrenkiel Lyngby, Sebastian Hoppe Nesgaard Jensen, Jakob Wilm, Mads Emil Brix Doest, Eyþór Rúnar Carsten Gundlach, Eiríksson, Knut Conradsen, Jakob Andreas Bærentzen, Jeppe Revall Frisvad, and Henrik Aanæs. *Heterogeneous Scenes and Evaluating the Pipeline Using Photorealistic Rendering.* In review, 2017.

[SFPL10] Joaquim Salvi, Sergio Fernandez, Tomislav Pribanic, and Xavier Llado. A state of the art in structured light patterns for surface profilometry. *Pattern recognition*, 43(8):2666–2680, 2010.

[SG31] Thomas Smith and John Guild. The cie colorimetric standards and their use. *Transactions of the Optical Society*, 33(3):73, 1931.

[SL16] PI Stavroulakis and RK Leach. Invited review article: Review of post-process optical form metrology for industrial-grade metal additive manufactured parts. *Review of Scientific Instruments*, 87(4):041101, 2016.

[SLGS12] Maja Stanic, Branka Lozo, and Diana Gregor Svetec. Colorimetric properties and stability of 3d prints. *Rapid Prototyping Journal*, 18(2):120–128, 2012.

[SLM+08] Maja Stanić, Branka Lozo, Tadeja Muck, Sonja Jamnicki, and Rahela Kulčar. Color measurements of three-dimensional inkjet prints. In *NIP & Digital Fabrication Conference*, volume 2008, pages 623–626. Society for Imaging Science and Technology, 2008.

[SLW10] Maja Stanić, Branka Lozo, and Peter Walters. Reproduction in three-dimensional ink jet printing. *Journal of Imaging Science and Technology*, 54(6):60201–1, 2010.

[SPB04] Joaquim Salvi, Jordi Pages, and Joan Batlle. Pattern codification strategies in structured light systems. *Pattern recognition*, 37(4):827–849, 2004.

[Sta10] Maja Stanić. *Structure, Surface and Permanence Properties of Three Dimensional Printing Materials*. PhD thesis, Grafički fakultet, Sveučilište u Zagrebu, 2010.

[Str16] Stratasys. Stratasys J750. http://www.stratasys.com/3d-printers/production-series/stratasys-j750, 2016. [Online; accessed 26-Feb-2017].

[Str17a] Stratasys. 3D Printing Solutions for Digital Dentistry. http://www.stratasys.com/en/Dental, 2017. [Online; accessed 25-Feb-2017].

[Str17b] Stratasys. Trek Color, Multi-Material Prototypes. http://www.stratasys.com/resources/case-studies/consumer-goods/trek-color-multi-material, 2017. [Online; accessed 25-Feb-2017].

[SVM+97] Dennis R Smalley, Thomas J Vorgitch, Chris R Manners, Charles W Hull, Stacie L VanDorin, et al. Simultaneous multiple layer curing in stereolithography, January 28 1997. US Patent 5,597,520.

[SWD05] Gaurav Sharma, Wencheng Wu, and Edul N Dalal. The ciede2000 color-difference formula: Implementation notes, supplementary test data, and mathematical observations. *Color Research & Application*, 30(1):21–30, 2005.

[Tar05] Albert Tarantola. *Inverse problem theory and methods for model parameter estimation*. SIAM, 2005.

[TDG+16] Camilla Himmelstrup Trinderup, Vedrana Andersen Dahl, Kristian Murphy Gregersen, Ludovic Antoine Alexandre Orlando, and Anders Bjorholm Dahl. *The Traveling Optical Scanner – Case Study on 3D Shape Models of Ancient Brazilian Skulls*, pages 398–405. Springer International Publishing, Cham, 2016.

[TDJ+15] Camilla H Trinderup, Anders Dahl, Kirsten Jensen, Jens Michael Carstensen, and Knut Conradsen. Comparison of a multispectral vision system and a colorimeter for the assessment of meat color. *Meat science*, 102:1–7, 2015.

[TE14] Gustavo Tapia and Alaa Elwany. A review on process monitoring and control in metal-based additive manufacturing. *Journal of Manufacturing Science and Engineering*, 136(6):060801, 2014.

[TM11] Matthew Tomlin and Jonathan Meyer. Topology optimization of an additive layer manufactured (alm) aerospace part. In *Proceeding of the 7th Altair CAE technology conference*, pages 1–9, 2011.

[TSB+16] Andrew Townsend, N Senin, Liam Blunt, RK Leach, and JS Taylor. Surface texture metrology for metal additive manufacturing: a review. *Precision Engineering*, 46:34–47, 2016.

[VDI00] 2634 VDI/VDE. Optical 3d measuring systems. *VDI/VDE guideline*, 2000.

[Vuf16] Vuforia. VuMark. https://library.vuforia.com/articles/Training/VuMark, 2016. [Online; accessed 1-Mar-2017].

[Vuf17] Vuforia. Vuforia. https://www.vuforia.com/, 2017. [Online; accessed 1-Mar-2017].

[WALP16] Jakob Wilm, Henrik Aanæs, Rasmus Larsen, and Rasmus Reinhold Paulsen. *Real Time Structured Light and Applications*. PhD thesis, 2016.

[WBE+13] Sabine Webel, Uli Bockholt, Timo Engelke, Nirit Gavish, Manuel Olbrich, and Carsten Preusche. An augmented reality training platform for assembly and maintenance skills. *Robotics and Autonomous Systems*, 61(4):398–403, 2013.

[WG16] Terry Wohlers and Tim Gornet. History of additive manufacturing. *Wohlers Report*, 2016.

[WHPS09] Peter Walters, David Huson, Carinna Parraman, and M Stanić. 3d printing in colour: Technical evaluation and creative applications. In *Impact 6 International Printmaking Conference*, 2009.

[Wid17] Widex. In-the-ear hearing aids (ITE): How they work. http://blog.widex.com/post/81668566088/ite-hearing-aids-how-they-work, 2017. [Online; accessed 25-Feb-2017].

[Woh16] Terry T Wohlers. *Wohlers report 2016: 3D printing and additive manufacturing state of the industry. Annual worldwide progress report*. Wohlers Associates, 2016.

[WOL14] Jakob Wilm, Oline V Olesen, and Rasmus Larsen. Slstudio: Open-source framework for real-time structured light. In *Image Processing Theory, Tools and Applications (IPTA), 2014 4th International Conference on*, pages 1–4. IEEE, 2014.

[Wri29] William David Wright. A re-determination of the trichromatic coefficients of the spectral colours. *Transactions of the Optical Society*, 30(4):141, 1929.

[WS82] Gunter Wyszecki and Walter Stanley Stiles. *Color science*, volume 8. Wiley New York, 1982.

[XZvNY14] Kaida Xiao, Faraedon Zardawi, Richard van Noort, and Julian M Yates. Developing a 3d colour image reproduction system for additive manufacturing of facial prostheses. *The International Journal of Advanced Manufacturing Technology*, 70(9-12):2043–2049, 2014.

[ZBL+15] Guenter Zenzinger, Joachim Bamberg, Alexander Ladewig, Thomas Hess, Benjamin Henkel, Wilhelm Satzger, Dale E Chimenti, and Leonard J Bond. Process monitoring of additive manufacturing by using optical tomography. In *AIP Conference Proceedings*, volume 1650, pages 164–170. AIP, 2015.

[Zha99] Zhengyou Zhang. Flexible camera calibration by viewing a plane from unknown orientations. In *Computer Vision, 1999. The Proceedings of the Seventh IEEE International Conference on*, volume 1, pages 666–673. Ieee, 1999.

[ZZFD16] Bin Zhang, John Ziegert, Faramarz Farahi, and Angela Davies. In situ surface topography of laser powder bed fusion using fringe projection. *Additive Manufacturing*, 12:100–107, 2016.